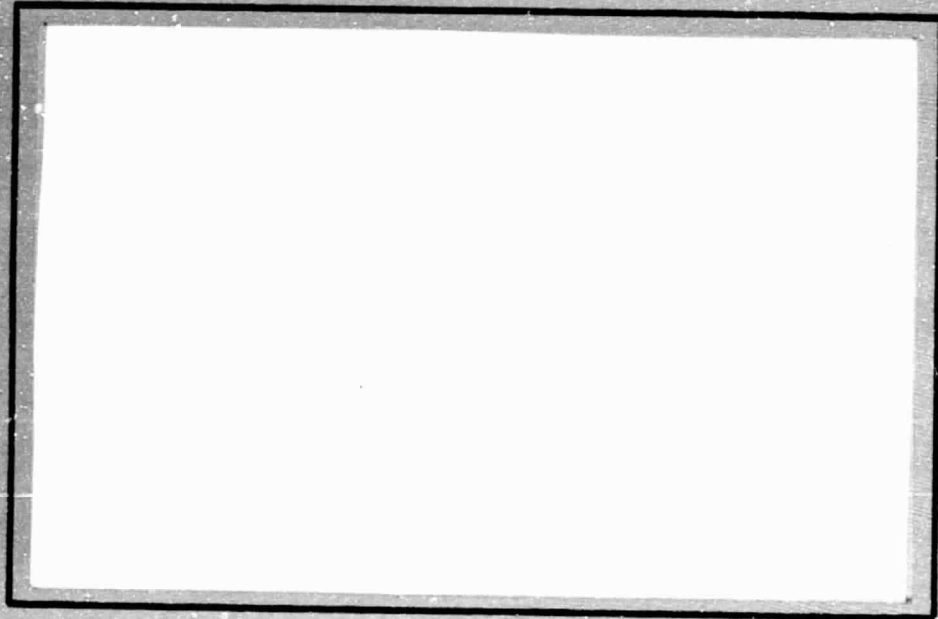# N O T I C E

THIS DOCUMENT HAS BEEN REPRODUCED FROM MICROFICHE. ALTHOUGH IT IS RECOGNIZED THAT CERTAIN PORTIONS ARE ILLEGIBLE, IT IS BEING RELEASED IN THE INTEREST OF MAKING AVAILABLE AS MUCH INFORMATION AS POSSIBLE

COLLEGE

OF ENGINEERING

VIRGINIA
POLYTECHNIC
INSTITUTE AND
STATE
UNIVERSITY

BLACKSBURG,
VIRGINIA

VPI-E-79-23   June 1979

THE STRUCTURAL BEHAVIOR OF A GRAPHITE-POLYIMIDE
HONEYCOMB SANDWICH PANEL WITH QUASI-ISOTROPIC
FACE SHEETS AND AN ORTHOTROPIC CORE

By

Michael W. Hyer[1]

and

Jane A. Hagaman[2]

[1] Assistant Professor, Department of Engineering Science and Mechanics, Virginia Polytechnic Institute and State University, Blacksburg, VA 24061.

[2] Research Assistant, Old Dominion University Research Foundation, P. O. Box 6369, Norfolk, VA 23508.

BIBLIOGRAPHIC DATA SHEET	1. Report No. VPI-E-79-23	2.	3. Recipient's Accession No.
4. Title and Subtitle THE STRUCTURAL BEHAVIOR OF A GRAPHITE-POLYIMIDE HONEYCOMB SANDWICH PANEL WITH QUASI-ISOTROPIC FACE SHEETS AND AN ORTHOTROPIC CORE			5. Report Date June 1979
			6.
7. Author(s) Michael W. Hyer (VPI&SU) and Jane A. Hagaman (ODU)			8. Performing Organization Rept. No.
9. Performing Organization Name and Address Old Dominion University Research Foundation P. O. Box 6369 Norfolk, VA 23508			10. Project/Task/Work Unit No. 802-068-1 (VPI&SU/ODU)
			11. Contract/Grant No. NSG-1167 (ODU/NASA)
12. Sponsoring Organization Name and Address National Aeronautics and Space Administration Langley Research Center Hampton, VA 23665			13. Type of Report & Period Covered Final Report 6/1/78 to 3/15/79
			14.

15. Supplementary Notes ~~The grantee for this project is the Old Dominion University Research Foundation.~~ (grant NSG 1167 with NASA/Langley Research Center); Dr. Hyer is now affiliated with Virginia Polytechnic Institute and State University, Blacksburg, Va 24061.

16. Abstracts This report presents the results of testing a series of graphite-polyimide honeycomb sandwich panels. The panels were 1.22-m long, 0.508-m wide, and approximately 13.3-mm thick (48.0 × 20.0 × 0.511 in.). The face sheets were a T-300/PMR-15 fabric in a (0°/90°/45°/-45°) layup and were 0.279-mm (0.011-in.) thick. The core was Hexcel HRH 327-3/16 - 4.0 glass-reinforced polyimide honeycomb, 12.7-mm (0.50-in.) thick. Three panels were used in the test: one was cut into smaller pieces for testing as beam, compression, and shear specimens; a second panel was used for plate bending tests, while the third panel was used for in-plane stability tests. Presented are the experimental results of four-point bending tests, short-block compression tests, core transverse shear modulus, three-point bending tests, vibration tests, plate bending tests and panel stability tests. The results of the first three tests are used to predict the results of some of the other tests. The predictions and experimental results are compared, and the agreement is quite good.

17. Key Words and Document Analysis. 17a. Descriptors

Honeycomb panels
Quasi-isotropic panels
Sandwich panels
Buckling of sandwich panels
Shear modulus of honeycomb
Graphite-polyimide

17b. Identifiers/Open-Ended Terms

17c. COSATI Field/Group

18. Availability Statement	19. Security Class (This Report) UNCLASSIFIED	21. No. of Pages 125
	20. Security Class (This Page) UNCLASSIFIED	22. Price

TABLE OF CONTENTS

LIST OF TABLES

LIST OF TABLES (CONCL'D)

LIST OF FIGURES

LIST OF FIGURES (CONT'D)

LIST OF FIGURES (CONCL'D)

ABSTRACT

This report presents the results of testing a series of graphite-polyimide honeycomb sandwich panels. The panels were 1.22-m long, 0.508-m wide, and approximately 13.3-mm thick (48.0   20.0   0.511 in.). The face sheets were a T-300/PMR-15 fabric in a (0°/90°/45°/-45°) layup and were 0.279-mm (0.011-in.) thick. The core was Hexcel HRH 327-3/16 - 4.0 glass-reinforced polyimide honeycomb, 12.7-mm (0.50-in.) thick. Three panels were used in the test: one was cut into smaller pieces for testing as beam, compression, and shear specimens; a second panel was used for plate bending tests, while the third panel was used for in-plane stability tests. Presented are the experimental results of four-point bending tests, short-block compression tests, core transverse shear modulus, three-point bending tests, vibration tests, plate bending tests and panel stability tests. The results of the first three tests are used to predict the results of some of the other tests. The predictions and experimental results are compared, and the agreement is quite good.

THE STRUCTURAL BEHAVIOR OF A GRAPHITE-POLYIMIDE HONEYCOMB SANDWICH PANEL WITH QUASI-ISOTROPIC FACE SHEETS AND AN ORTHOTROPIC CORE

By

Michael W. Hyer[1] and Jane A. Hagaman[2]

INTRODUCTION

As is well known, fiber-reinforced composite materials offer substantial weight savings in aerospace structural applications, and the use of these materials is increasing. Military aircraft, such as the F-16, routinely use fiber-reinforced composites as a structural material. Currently, commercial aircraft programs are being conducted to evaluate the use of composites for both primary and secondary structures. As a further example, payload-bay doors of the baseline space shuttle design are fabricated from graphite-epoxy. For the above-mentioned applications, the thermal environments are not too severe and the strength of the composite material is not appreciably affected by heating. However, when temperatures exceed 120 to 150° C (250-300° F), the strength of the epoxy-matrix composites decreases. Recently polyimide-matrix composites have been developed which maintain their strength properties up to 315° C (600° F). One application for such a material is on the space shuttle. Graphite-polyimide is a candidate material for replacing aluminum on the body flap of the orbiter. The flap, located on the lower aft end of the orbiter, is basically an aerodynamic control surface. It is approximately 6.4-m (21-ft) long, 2-m (6.7-ft) wide and tapers linearly from 0.4 m (1.3 in.), at the shuttle body, to zero at the trailing edge of the flap. The flap is hinged at the body. The flap is a spar-stringer-skin construction, and the proposed design, using graphite-polyimide, calls for the skin to be a sandwich panel. The panels use thin, orthotropic face sheets and a honeycomb core. The exact materials to be used in a final design are not yet completely determined. In addition, the fabrication process has not be finalized. However, in a step toward finalizing

---

[1] Assistant Professor, Department of Engineering Science and Mechanics, Virginia Polytechnic Institute and State University, Blacksburg, Virginia 24061.

[2] Research Assistant, Old Dominion University Research Foundation, P.O. Box 6369 Norfolk, Virginia 23508.

the design of the flap, Rockwell International, under contract with the NASA
Langley Research Center, fabricated three panels. using a woven T-300/PMR-15
fabric for the face sheets and an HRH 327-3/16 - 4.0 Hexcel glass-reinforced poly-
imide honeycomb core. The panels were then tested for structural properties at
NASA/LaRC. The results of that testing are the subject of this report. For a
complete description of the panel fabrication process, see reference 1.

PANEL DESCRIPTION

Figure 1 illustrates the panel geometry. Three such panels were fabricated.
Each face sheet consists of two layers of $0°/90°$ woven fabric arranged to have a
quasi-isotropic layup, i.e., $0°/90°/+45°/-45°$. Since there were only four layers
and a quasi-isotropic layup was desired, the face sheets themselves were an unsym-
metric layup. However, since the face sheets were woven fabric, they did not have
the usual properties associated with unsymmetric layups. The face sheets were
approximately 0.28-mm (0.011-in.) thick. The honeycomb core was 12.7-mm (0.5-in.)
thick and had a cell size of 4.76 mm (0.1875 in.). The 1.22 m × 0.5 m (48 in. ×
20 in.) panel represented the size of the unsupported area of skin between the
spar and stringer framework. On the actual flap, the four edges of the panel will
be attached, either with adhesives or mechanical fasteners, to the flap framework.

TESTS CONDUCTED

To determine the structural properties of the panels, seven tests were
conducted. The test were

> four-point beam bending
> short-block compression
> transverse shear modulus
> three-point beam bending
> vibration tests
> plate bending
> panel stability

The first three tests were designed to provide data to predict the panel response
of the next three tests. To have panel specimens for all the tests, one of the
three panels was cut into beams of various lengths. In addition, to test the
quasi-isotropic properties, replicate specimens were cut at 0°, 22.5°, 45°,

2

and 90° orientations relative to the long dimension of the panel. Comparison of the responses in the four directions, for a given test, would then indicate the degree of isotropy of the panel. It should be pointed out that in addition to the face sheets being orthotropic, the core was also orthotropic due to the manner in which honeycomb is manufactured. The second panel was used for the stability experiments, and the third panel was used for static plate bending experiments.

There was a definite relation among the seven tests. Basically the four-point bending tests provided an effective EI for the panel, and the transverse shear modulus test provided a value of G for the core material. The results of these two tests were then used to predict the results of the three-point bending tests. The results of the four-point bending tests, along with the mass data, were also used to predict the natural vibration frequencies. The short-block compression tests were used to determine the effective in-plane E, ν and the compressive strength of the panel. The data from the first three tests could be used to predict the results of the plate bending and plate stability tests.

Figure 2 shows the orientation and nomenclature for the various specimens cut from one of the panels. Specimens AA, AB, AC, and AD were beam specimens used for the three- and four-point bending tests and the vibration tests. Specimens BA, BB, BC, and BD were for transverse shear tests. Specimens DA, DB, DC, and DD were used for the short-block compression tests while specimens CA and CD were cut for future in-plane shear testing. Note: in the nomenclature scheme, the second letter, e.g. D in AD, refers to the orientation of the specimen in the original panel, A being the 0° (the long direction), B being the 90°, C the 45°, and D the 22.5° specimens. By the nature of the geometry, the beam specimens were all of different length.

What follows is a description of each test setup, a presentation of data from the tests, and a comparison of experimental results with theoretical calculations.

Four-Point Bending Tests

The four-point bending test is a classic test for determining the effective EI of a beam. If E or I is known, the other quantity can be determined. However, since in many problems of interest E and I appear together as a product, the value of the product rather than the individual quantities is generally

sufficient. Typically in the four-point bending test. the loading is applied through knife-edge or roller devices to minimize the area over which the load is applied. Since on these honeycomb panels the thin face sheet was to bear the load of the four supports, rollers and rounded knife edges were used. Figure 3 illustrates the setup. The beam specimen rested on two rounded metal knife-edge supports which were part of the support fixture. The horizontal distance between the lower supports could be adjusted and spans of different length tested. The loads were transmitted into the top of the beam from a second stiffback metal beam via rollers. The load was applied to the stiffback with the deadweight hanger/arm mechanism shown. The response of the two longer beams was measured with three dial gages, one at the center, and one each under the upper load application points (under the rollers). Only one gage was used for the shorter beams. Figure 4 shows the loading nomenclature for the tests with L_s denoting the distance between the lower supports and e denoting the distance between the lower support and the upper load application point.

The longest beam, AA, was tested with L_s = 0.737 m (29.0 in.) and e = 76.2 mm (3.00 in.) while all 4 beams were tested with L_s = 0.406 m (16.0 in.) and e = 76.2 mm (3.00 in.). Each beam was tested twice: once with one face sheet up and once with the other face sheet up. This double testing would indicate any thicknesswise dissymmetries in panel construction.

Figure 5 shows the force-deflection measurements for beam AA with L_s = 0.737 m (29.0 in.) and e = 76.2 mm (3.00 in.) in both face sheet orientations. For orientation purposes, the faces are referred to as side A and side B. Plotted in figure 5 is the difference in the midspan deflection and the average of the two deflections measured under the load application points. The figure then shows the response of a simply supported beam of length L, where $L = L_s - 2e$, with moment M = Pe/2 applied at the ends. Using the formula for the bending deflection, W, at the center of a simply supported beam of length L under a pure bending moment, i.e.

$$W = \frac{ML^2}{8EI}$$ (1)

the effective EI can be computed. The slope of the W-P relation in figure 5 is 20.2 × 10^{-6} m/N (0.00354 in./lb), and using L = 0.584 m (23.0 in.) and M =

4

0.169 P N-m (1.50 P in.-lb) leads to an effective EI of 1.27 kN-m^2 (11.2 kip-in.^{2}) per unit width of beam. The slope in figure 5, as in all subsequent plots, was determined by least-squares fitting of the data, from sides A and B, to a straight line. There doesn't seem to be any significant difference in side A and side B data.

Figure 6 shows similar results for all four beam specimens at a span of L_s = 0.406 m (16.0 in.) and e = 76.2 mm (3.00 in.). Side B "D of beam AC seemed softer than the other beam tests, but among the for $\checkmark$ $\checkmark$ the data scatter was quite uniform. Of particular interest was the 2$\checkmark$ beam, beam AD, which has no fibers in the bending direction. The data for this specimen appeared to be quite similar to the data from the other specimens. Specifically, the effective EI's, measured on the 0.406-m (16.0-in.) span and based on a beam of unit width, are listed in table 1. The numbers in table 1 are based on a least-squares straight line passing through the side A and side B data for the specific beams in figure 6. The straight line in figure 6 is the least-squares line passing through all of the data for all of the beams. Comparison of the 5 values of effective EI's indicates the 22.5° beam behaves no differently than the other 4 beams, nor is the 0.406-m (16.0-in.) span data different than the 0.737-m (29.0-in.) span data. Because of the uniformity of the tests, the value of EI for the beams, based on a unit width was taken to be the average of the 5 tests, namely 1.30 kN-m^2 (11.5 kip-in.^{2}).

Short-Block Compression Tests

To determine compressive material properties of the panel and, in particular, the face sheet properties, specimens short enough to prevent buckling were loaded in in-plane compression. The specimens, whose dimensions are shown in figure 2, were potted in an epoxy-based compound to form flats on which to load the specimens. Figure 7 shows the four specimens, DA, DB, DC, and DD, and figure 8 shows a closeup of specimen DB. The numerial "1" following "DB" on the specimen indicates side 1 and was used for orientation purposes. Each specimen was gaged with two back-to-back pairs of strain gages. One pair was aligned with the load direction, to measure the effective in-plane E, while the other pair was mounted to measure the effective Poisson's ratio. A direct-current displacement transducer (DCDT) was used to measure the change in distance between the loading heads as the load was applied. The specimens were loaded until failure.

Figures 9 to 12 show the axial strain versus load for the four specimens while figures 13 to 16 show the bending strains versus load; figures 17 to 20 show the lateral strain versus axial strain, and figures 21 to 24 show the change in head distance versus load. The 22.5° specimen failed at a much lower load than the other 3 specimens. Comparisons of the 4 bending strain relations show the 22.5° specimen experienced considerably more bending than did the other 3. However, in all cases, the bending strains were at least an order of magnitude less than the axial strains and did not contribute to the failure. It appears the 22.5° specimen was not as strong as the other 3 specimens.

Assuming Young's modulus of the core to be three orders of magnitude less than Young's modulus of the face sheets*, the slope of the load versus axial strain data can be used to determine Young's modulus of the face sheets. In addition, Poisson's ratio for the face sheet material can be computed using the lateral strain data. Finally, assuming the face sheets absorb all the load, estimates of the face sheet ultimate strength can be computed.

Tables 2 to 4 present the material properties of the face sheets based on the data in figures 9 to 20 and the geometry of the specimens. From the tables, the average value of in-plane E is seen to be 43.6 GPa (6.32 × 10^6 psi), and Poisson's ratio is 0.271. For the fiber direction, the compressive strength is 353 GPa (51.2 ksi), based on an average of DA, DB, and DC. In the 22.5° direction, the compressive strength is 211 GPa (30.6 ksi).

Transverse Shear Modulus Test

For sandwich panels, in certain loading conditions, the shear deformations in the core can become important. For the higher vibration modes, for example, shear deformations tend to drastically reduce the natural frequencies, even for homogeneous beams. When the length of the beam becomes less than 10 times its thickness, shear deformations of homogeneous beams become an important factor in beam response computations. For sandwich beams, depending on the value of the core shear modulus, with a beam length-to-thickness ratio of 10:1, shear deformations can substantially affect calculations. To determine the value of the shear modulus used in the sandwich panel, a double-lap shear

---

* Even though Young's modulus of the core is less than the modulus for the face sheets, the thickness ratio is $10^2/2$ (= 50), hence the 10^{-3} requirement on the ratios of E's.

fixture was constructed with the honeycomb core bonded between the laps. Figure 25 shows the fixture with the honeycomb in place. Rather than using specimens cut from the panel, i.e. specimens BA, BB, BC and BD, a piece of honeycomb with no face sheets was used in the tests. Two DCDT's were used to measure the relative displacement between the inner and outer laps. Since the fixture was longer than the DCDT cores, threaded rods were used to transmit the displacement of the inner lap to the DCDT cores. The ends of the threaded rods were cupped to serve as a seat for the DCDT core. In the photograph, steel pins can be seen holding the three laps from moving in shear relative to each other. These pins were kept in place unitl the testing was to begin in order to avoid inadvertently stressing the honeycomb and risking possible danger. The laps were loaded via the holes in the ends of the fixture. To keep the two outer laps from spreading apart or squeezing together when the tensile load was applied, a spacer and clamping mechanism (not shown) were used on the double-lapped end. In this particular setup, the section of the honeycomb being tested was 152 × 50.8 mm (6.00 × 2.00 in.). Also, only one test was conducted on the honeycomb and that was in the ribbon direction. This gave an upper bound on the core transverse shear modulus.

During the test, despite precautions to avoid it, a dissymmetry developed in the loading. As a result, the double-lap fixture pulled to one side causing one DCDT core to jump out of the cupped seat in the threaded extension rod.* After that point, the data from the test was useless. However, by averaging the output of the two DCDT's until that point, the bending effects could be accounted for and the data used to determine the shear modulus of the core. Using the slope of the axial force versus relative displacement of the laps, $\Delta F/\Delta d$, the core thickness, t_c (t_c = 12.7 mm (0.50 in.)), and the core area, A (A = 7740 mm^2 (12.0 in.^{2})), the transverse shear modulus, G_t, could be determined by

$$G_t = \frac{\Delta F}{\Delta d} \frac{t_c}{2A} \qquad (2)$$

Results of the test are shown in figures 26 and 27. Figure 26 shows the force versus the average of the two DCDT readings and figure 27 shows the force versus the difference of the two DCDT readings. The initial low load

---

* The ASTM type test fixture avoids this problem by using a single-lap. However, that particular fixture requires extensive machining and, in the interest of time, was not used.

level data, which was irregular due to the slack in the fixture, has been eliminated from the plots. The nonzero average in figure 27 indicates the tendency of the fixture to pull slightly to one side. Using the slope of figure 26 and equation (2), the value of G_t was determined to be 56 MPa (8.12 ksi).

Three-Point Bending Tests

The three-point bending test is also a classic test in strength of materials. Using the test, the effect of shear can be assessed. The setup for the three-point tests was similiar to the four-point bending setup except no stiffback beam was used. The load was applied directly through the deadweight hanger and, to avoid crushing the thin face sheet, the load was transmitted through a deformable rubber sphere. This tended to spread the deadweight load with the spread area proportional to the load. Figure 28 shows the setup, and figure 29 shows the loading nomenclature. Three dial gages, one at the center and one near each end, were used as a measure of beam response. Five lengths between supports were tested, the lengths ranging from 0.152 to 0.711 m (6.00 to 28.0 in.). It was expected the longer span lengths would not be affected by shear deformations of the core whereas the shorter span lengths would.

Figure 30 shows the load-deflection curves for beam AA, side A and side B, for a 0.711-m (28.0-in.) span. Although the deflections were symmetric about the center of the beam, there was a significant difference between side A and side B deflections. The slope of the load versus midspan deflection using both side A and side B data was 0.113 m/N (19.8×10^{-3} in./lb). Using Euler beam theory, thus neglecting shear deformations, the load-deflection relation (P-W) for the center of the beam is

$$W = \frac{PL^3}{48EI} \qquad \cdot \qquad \text{(3)}$$

In equation (3), using 1.30 kN-m^2 (11.5 kip-in.^{2}) from the 4 point bending tests as the value of EI per unit width of beam results in a slope of 0.0908 m/N (15.9×10^{-3} in./lb).

Figure 31 shows the load-deflection data for beam AC with a 0.508-m (20.0-in.) span. There does not seem to be as large a difference between side A and side B data for this beam and span as there was for the first three-point

8

bending test. The slope of the load-deflection data at midspan is 0.0395 m/N (6.91×10^{-3} in./lb) while equation (3) yields 0.033 m/N (5.97×10^{-3} in./lb) for this span.

Figures 32, 33, and 34 show the force-deflection data for all 4 beams at a span of 0.410 m (16.0 in.), 0.254 m (10.0 in.) and 0.152 m (6.00 in.), respectively. To check the degree of isotropy of the beams, the least-squares load-midspan deflection slopes for each beam and span length were compared. The midspan least-squares lines are indicated in figures 30 to 34. A comparison of the data from each beam showed beams AA and AC were slightly softer but not significantly so. Thus it was concluded the original panel was, to a good first approximation, isotropic. The least-squares load-deflection slopes to both sides A and B for all the three-point bending tests are summarized in table 5. Table 4 also shows the average of sides A and B as well as the average of all four beams for a particular span length.

For the shorter span three-point bending tests, shear deformations can be important. If shear deformations are taken into account, the load deflection relation for the center of the beam is*

$$ W = \frac{PL^3}{48EI} \left\{ 1 + \frac{12EI}{G_t t_c bL^2} \right\} \tag{4} $$

In this expression, t_c is the thickness of the core and b is the width of the beam. In the case at hand, t_c = 12.7 mm (0.500 in.), b = 63.5 mm (2.50 in.), EI = 0.082 kN-m^2 (28.8 kip-in.^{2}), and G_t = 5.60 MPa (8.12 ksi). To determine the importance of shear deformations, the experimental load-deflection slope and the load-deflection slopes as predicted by equations (3) and (4) were compared. These three quantities as a function of length are presented in table 6. The experimental number is the average of the results for all four beams at a given span and is taken from the last column of table 5. Including the effects of shear deformation definitely leads to closer predictions for the shorter spans. However, it can be shown by energy methods that theories always overpredict the stiffness of a system, and thus it is surprising to see the experimental load-deflection slopes less than the predictions in several cases. In particular, this reversal of theoretical and experiment stiffnesses occured

---

* Equation (4) is obtained by reducing the plate equations, presented in a subsequent section, to beam equations, solving the resulting differential equations, and applying the proper boundary conditions.

for the shorter spans. For the shorter spans, the three-point beam was quite stiff, and large forces were required to generate substantial deflections. Not wanting to inadvertently damage the beam specimens, the forces were kept the same magnitude as for the longer span tests. Consequently the deflections were small, and any errors in reading the dial gages, span length measurements, etc., contributed more to the experimental results than they did for the longer spans. This perhaps accounts for what appears to be reversals of classical trends of the data in table 6.

Vibration Tests

The vibration facility at NASA/LaRC, Structural Dynamics Division, was used to determine the natural frequencies and damping characteristics of the panel. Specifically, the four beams were tested in the free-free condition using the impulse technique to excite the beams and accelerometers to measure the response. To simulate free-free boundary conditions (actually boundaries with zero stiffness), the beams were supported horizontally at each end by laying the beam across two taut rubber bands. The appendix contains the raw data for the vibration tests. Table 7 condenses the information and presents natural frequencies and modal damping factors for the four beams.

Using the EI from the four-point bending tests and the masses of the beams, the free-free bending frequencies, based on Euler beam theory, can be predicted. A theory which takes into account the shear deformations could be developed, but that was not done here. Basically, the beams were weighed and, using the average mass per unit length, the length and the effective EI, frequency predictions were made.

Table 8 presents the weights of the individual beams. The average weight of the beams was 0.151 N/m (8.65×10^{-3} lb/in.). The vibration frequencies for a Euler beam are given by reference 2 as

$$f_n = \frac{\left(\beta_n L\right)^2}{2\pi} \sqrt{\frac{EI}{mL^4}} \tag{5}$$

where f_n is the natural frequency, in hertz, of the n-th mode, m is the mass of the beam per unit length, and E, I, and L have their usual definitions. The quantity $(\beta_n L)$ depends on mode number and the boundary conditions for the beam. The first three values are

10

Mode No.	$(\beta_n L)$
1	4.7300
2	7.8532
3	10.996

Table 9 shows the predicted and experimental natural frequencies for the beams. Again it can be shown theoretical predictions are always higher than experimental results due to the overconstraining tendencies of theoretical kinematic assumptions. Euler beam theory assumes infinite shear rigidity and, in spite of this, the theoretical and predicted results are close. At the higher modes, and for the shorter beams at the lower modes, shear effects will lower the frequency. Also, the mass of the accelerometers mounted on the beam, to measure its response, will always lower the experimentally observed frequencies.

Plate-Bending Test

The equations describing the static bending of a sandwich panel with thin orthotropic face sheets and an orthotropic core are given by (ref. 3)*

$$D_{11}\left\{\frac{\partial^2 \beta_x}{\partial x^2} + \nu_{xy} \frac{\partial^2 \beta_y}{\partial x \partial y}\right\} + D_{66}\left\{\frac{\partial^2 \beta_x}{\partial y^2} + \frac{\partial^2 \beta_y}{\partial y \partial x}\right\} - Q^c_{xz} = 0 \tag{6}$$

$$D_{22}\left\{\frac{\partial^2 \beta_y}{\partial y^2} + \nu_{xy} \frac{\partial^2 \beta_x}{\partial y \partial x}\right\} + D_{66}\left\{\frac{\partial^2 \beta_y}{\partial x^2} + \frac{\partial^2 \beta_x}{\partial y \partial x}\right\} - Q^c_{yz} = 0 \tag{7}$$

$$\frac{\partial Q^c_{xz}}{\partial x} + \frac{\partial Q^c_{yz}}{\partial y} = - q(x,y) \tag{8}$$

with

$$Q^c_{xz} = G^c_{xz} \, c \left(\beta_x + \frac{\partial w}{\partial x}\right) \tag{9}$$

* There are sign errors in reference 3.

11

$$Q_{yz}^c = G_{yz}^c c \left(\beta_y + \frac{\partial w}{\partial y} \right) \tag{10}$$

where

x,y = coordinates in the plane of the plate; z is perpendicular to the plate;

β_x = plate cross-sectional rotation in x-direction (due to bending and shear deformation);

β_y = plate cross-sectional rotation in y-direction (due to bending and shear deformation);

w = plate lateral deflection (due to bending and shear deformation);

G_{xz}^c = transverse shear modulus of core in the x-direction;

G_{yz}^c = transverse shear modulus of core in the y-direction;

$q(x,y)$ = transverse loading per unit area;

Q_{xz}^c = shear force on an x-face of plate cross section;

Q_{yz}^c = shear force on a y-face of plate cross section;

ν_{xy}, ν_{yx} = Poisson's ratios;

$$D_{11} = \frac{(c + t_f)^2}{2} \frac{E_x^f t_f}{1 - \nu_{xy} \nu_{yx}} ;$$

$$D_{22} = \frac{(c + t_f)^2}{2} \frac{E_y^f t_f}{1 - \nu_{xy} \nu_{yz}} ;$$

$$D_{66} = \frac{(c + t_f)^2}{2} G_{xy}^c t_f + \frac{G_{xy}^c c^3}{12} ;$$

c = core thickness;

t_f = face sheet thickness;

E_x^f = Young's modulus of the face sheet material in the x-direction;

E_y^f = Young's modulus of the face sheet material in the y-direction;

G_{xy}^f = in-plane shear modulus of the face sheet material; and

G_{xy}^c = in-plane shear modulus of the core material.

The plate bending experiment is shown in figure 35. The plate was supported at the 4 corners by vertical steel dowels, 2.54 cm (1.00 in.) in diameter and rounded at the tops. The distance between supports along the long sides was 1.17 m (46.0 in.), while the distance between supports along the short side was 0.457 m (18.0 in.). The plate was loaded at the center with the arm-deadweight mechanism shown. The response of the panel was measured with back-to-back strain gage pairs, to measure bending, and dial gages, to measure deflections. The locations of the strain gages are shown in figure 36, and the locations of the dial gages are shown in figure 37. Strain gage 9 was directly under the load application point, and dial gage 5 was slightly to one side of center to avoid contact with the strain gage. Dial gage 5 essentially measured the center deflection of the panel, but it was felt local loading effects might have an influence on strain gage 9 and it would not accurately measure global bending effects in the lengthwise direction.

The load-deflection characteristics of the plate at the various dial-gage locations are shown in figures 38 to 42. The straight line in each figure is the least-squares line for all the data in the figure. Comparison of the deflection response of the panel at dial gage locations 3, 4, 5, 8, and 9 (figures 38, 39, and 40) indicates the panel deflection at midspan was quite uniform across the width. Thus the panel was behaving like a long, wide beam. Equation (3), then, essentially governs the load-deflection behavior at the center of the beam. In equation (3), using a length of L = 1.17 m (46 in.), a width of 0.457 m (20 in.), and an effective EI per unit width

of 1.30 kN-m (11500 lb-in.), leads to a load-midpanel deflection relation of
0.0503 mm/N (0.00882 m/lb). The experimental load-midpanel deflection relation
from figure 38 is 0.0550 mm/N (0.00965 in./lb), the experimental result showing
9.4 percent more flexibility.

Table 10 summarizes the slopes of the load-deflection behavior for the
data shown in figures 38 to 42.

Figures 43 to 47 show the load versus bending strain for the various strain
gage locations. Except for strain gage 9, the side A and side B responses of
the gage were quite similar, and the symmetrically placed gage pairs (e.g. 5/12
and 1/16) were also similar. The straight line in each figure is a least-squares
fit of all the data on the figure. Using the idea of a wide, simply supported
beam, the bending strains can be computed in a straightforward manner. Measuring
the x-coordinate lengthwise from the center of the panel, the expression for
the bending moment in the "beam" is

$$M(x) = \frac{PL}{4} \left[1 - 2\left(\frac{x}{L}\right) \right] \tag{11}$$

The bending strain is given by

$$\varepsilon(x) = \frac{M(x) \ c}{EI} \tag{12}$$

where c is the distance to the outer fibers or strain gage locations from the
centerplane, or neutral plane, of the panel. In this case, c = 6.63 mm (0.261
in.). Using L = 1.17 m (46.0 in.), an effective EI per unit width of 1.30 kN-m
(11.5 kip) and a width of 0.457 m (20.0 in.) results in a load-strain relation
at midspan (x = 0) of

$$\Delta\varepsilon/\Delta P = 2.93 \times 10^{-6} \text{ mm/mm/N}$$
$$\tag{13}$$
$$\Delta c/\Delta P = 13.0 \times 10^{-6} \text{ in./in./lb}$$

The slope of the load-bending strain relation from gage 9 (fig. 43) is

$$\Delta\varepsilon/\Delta P = 4.04 \times 10^{-6} \text{ mm/mm/N}$$
$$\tag{14}$$
$$\Delta\varepsilon/\Delta P = 18.0 \times 10^{-6} \text{ in./in./lb}$$

14

This experimental load-bending strain relationship is substantially different than the one predicted. Still at centerspan but away from the load application point, strain gages 1, 5, 12, and 16 (fig. 45) give a load-bending strain relation of

$$\Delta\varepsilon/\Delta P = 3.04 \times 10^{-6} \text{ mm/mm/N}$$

$$\Delta\varepsilon/\Delta P = 13.5 \times 10^{-6} \text{ in./in./lb} \tag{15}$$

Although the deflections of the plate were uniform across the width at midspan, it was expected there would be some widthwise variation in the bending strains. However, it was not expected to be substantial, and the theoretical predictions at the center of the plate should compare reasonably well with experimental results at any position across the width. Comparison of equations (13) and (15) confirms this, and it is felt the differences between equations (13) and (14) are due to local loading effects on the strain gage at the center of the plate. In addition, equations (11) and (12) predict the bending strain at strain gage locations 4, 8, 11, and 15 to be two-thirds of the values at midspan. From figure 44, the slope of the load-bending strain relation is

$$\Delta\varepsilon/\Delta P = 2.02 \times 10^{-6} \text{ mm/mm/N}$$

$$\Delta\varepsilon/\Delta P = 9.01 \times 10^{-6} \text{ in./in./lb} \tag{16}$$

or 66 percent of the value at midspan!

The data from the plate bending tests is remarkably consistent except for the relation between gages at right angles to each other. Since gages 4, 8, 11, and 15 are at right angles to gages 3, 7, 10 and 14 and since the panel behaved as a wide beam, it was expected the ratio of these gage readings would be close to Poisson's ratio. This was not the case, nor was it the case for gages 1, 5, 12, 16 and 2, 6, 13 and 17. For the former pairs the average ratio is 0.124, while for the latter pair the ratio is 0.135, which is substantially different than the value of 0.271 computed for Poisson's ratio from the short-block compression tests. This indicates some widthwise bending of the panel

Table 11 summarizes the slopes of the load-bending strain relationships for all the gages.

Panel stability with respect to in-plane loads was studied with two tests. In the first test, the 0.51-mm (20.0-in.) ends were potted in an epoxy compound in a manner similar to the short-block compression specimens shown in figure 7. The long sides were not supported, and the load was applied parallel to the long sides. In this configuration the panel was essentially a wide Euler column with fixed ends. The panel deformations were measured with DCDT's, strain gages, and shadow Moiré fringes. Two DCDT's were used: one to measure the change in the distance between the heads of the loading machine, i.e., shortening of the panel due to compression, and the other to measure out-of-plane deflections at the center of the panel. The strain gages were located at L/2, L/4 and L/8, L being the long dimension, and were primarily mounted to measure strains in the lengthwise, L, direction. One set of gages was mounted to measure in-plane shear deformations. The panel was painted white to enhance the shadow Moiré measurements. Figure 48 shows the panel in the loading machine, while figure 49 indicates the strain gage locations and nomenclature. Seen in figure 48 is the frame for the Moiré master grid, a grid with 19.6 lines/cm (50 lines/in.) in the vertical direction in the figure.

In the second test, the long sides of the panel were constrained between knife edges. The knife edges were not rigidly attached to anything, but were merely clamped on the sides to enforce a zero-curvature condition. This setup simulated a condition of simple supports on the long sides.

For the case with the free long edge, test 1, the critical load, P_{cr}, is given by

$$P_{cr} = \frac{4\pi^2 EI}{L^2} \tag{17}$$

Using an EI per unit width of panel at 1.30 kN-m (11.5 kip-in.), a 0.51-m (20.0-in.) width and an L of 1.22 m (48 in.), the critical load was predicted to be 17.5 kN (3.94 kips).

Figure 50 shows the fringe pattern of the free-edge panel in the no-load condition. Visible are the strain gage wires running vertically along the centerline of the panel. The no-load fringe pattern is due to initial out-of-plane warping of the panel, and the dissymmetry of the pattern is indicative of the dissymmetry at the initial warping. This warping is due to slight

16

differences in the thermal expansion and mechanical properties of the panel material throughout the panel. As the panel is cooled from its curing temperature, these nonuniformities in material properties lead to an out-of-plane displacement at room temperature.

Figure 51 shows the relative out-of-plane displacement at midpan.. (zero displacement equals the no-load condition), as measured with the DCDT, versus applied load. The initial shallow sloped portion of this curve and similar initial irregularities on other load-response plots are due to initial clearances in the loading fixture closing up as the load is increased from zero. Since the panel was to be used in the second test, it was not loaded to failure. Figure 52 shows the fringe pattern just prior to unloading. The fringe count at the maximum load correlates well with the out-of-plane displacement indicated by the DCDT measurement of figure 51. Figure 53 shows the in-plane shortening versus applied load; figure 54 shows the axial strains versus load along the panel, and figure 55 shows the bending strains along the panel. Indicated on the strain response plots are the various strain gage pairs.

With the potted ends, it was expected the panel would behave like a fixed-end column with inflection points at L/4 and a reverse of curvature along the panel. This appeared to be the case since the strain gage pairs 6-13 and 1-8, located at L/4 from the ends, showed relatively little strain, and gage pair 7-14 indicated bend strains opposite in sign to the bending strains at 5-12 and 3-10. The shear strains, shown in figure 56, were insignificant. The axial strain versus load data was consistent with the value of E established in the short-block compression tests (table 2), and the in-plane shortening was consistent with the axial strains. The asymptote for the out-of-plane displacement versus load relation appeared to be approximately 15.6 kN (3.30 kips), slightly lower than the prediction of 17.5 kN (3.94 kips).

Panel Stability, Test 2

For a homogeneous isotropic plate with two opposite sides simply supported, the other two sides clamped, and loaded parallel to the simply supported sides, the critical load is given by (ref. 4):

$$P_{cr} = K \frac{\pi^2 D}{b} \tag{18}$$

where b is the panel dimension along the loaded side; $D = Eh^3/12$, h being the panel thickness, and K is a function of the panel aspect ratio. For the aspect ratio of these panels Y is approximately 4.50. Using a D of 1.30 kN-m (11.5 kip-in.^{2}), b = 0.51 m (20.0 in.), and the value of P_{cr} is 113 kN (25.2 kips). Assuming only the 0.279-mm (0.011-in.) thick face sheets react the in-plane load, the compressive face-sheet stress at the critical load is 400 MPa (58.0 ksi). This is greater than the compressive strength of the face sheet as computed from the short-block compression tests (table 4). Thus, failure of the face sheet was expected before the panel buckled. This was indeed the case. However, face sheet failure occurred at a load of 58.3 kN (13.1 kips), well below the load of 100 kN (22.5 kips), based on table 4, required for face sheet failure. The panel failed near the potted end at the top. Figure 57 shows an overall view of the failure. The failure was mainly face sheet cracking, at the upper left corner, and localized buckling at the upper right side. Figure 58 shows details of the cracking/buckling area, and figure 59 shows damage to the honeycomb which was visible in the upper right-hand corner of the panel. It is difficult to say exactly where the failure began, but it is not surprising the failure occurred at the potted end. First, to allow for in-plane shortening of the panel, there had to be a 6.25-mm (0.250-in.) gap between one end of the knife edge and the potting. In this case, the gap was at the top, and this produced a short unsupported section of edge. Any curvature that was to develop as the load was applied developed in the short gap. Second, there was most likely a mismatch of Poisson's ratios between the panel and the potting compound. This could have led to a region of high stresses at the ends of the panel. An attempt to remedy the first problem during testing of isogrid panels is discussed in reference 5; however, the mismatch in Poisson's ratios can be a problem whenever a potting compound is used. Since the short block compression specimens did not fail at the potted ends, it is felt the 0.51-m (20.0 in.) length at the potted edge contributed to the problem with the panels.

The bending strains, shear strains, and out-of-plane displacements were quite small compared to the axial strains since the panel did nothing except shorten in-plane. Figure 60 shows the axial compressive strains versus load, and figure 61 shows the in-plane shortening of the panel. The strain gage pairs are identified on figure 60, and both the axial strain and the in-plane shortening are consistent with each other and the value of in-plane E estab-

18

lished in the short-block compression tests. For completeness the bending strains, out-of-plane displacements, and shear strains are shown in figures 62, 63, and 64, respectively.

CONCLUDING REMARKS

Based on the results of the three-point bending tests, the vibration tests, and the various plate tests, the structural response of the panel seems quite predictable. The data from the four-point bending tests, the short-block compression tests, and the core transverse shear modulus test, when used in simple theories, predicted the plate response with reasonable accuracy. In addition, the panel behaved very much like an isotropic plate despite the orthotropic nature of the face sheets and core. It should be remembered the correlation was best for what might be considered long wavelength responses. Had plate vibration tests been conducted, for example, for 10 vibration modes, it would be expected that equations (6) to (10) would have to have been solved to determine the response rather than using an equivalent Euler plate. However, it is important to know fundamental equations of structural mechanics and strength of materials can be used to obtain good estimates of response for certain types of loadings.

PRECEDING PAGE BLANK NOT FILMED

APPENDIX

National Aeronautics and
Space Administration

Langley Research Center
Hampton, Virginia
23665

NASA

August 14, 1978

MEMORANDUM

TO: ODU/Michael Hyer

FROM: 230/Aero-Space Technologist, Structural Mechanics Branch,
            SDD
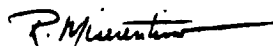
SUBJECT: Carbon-Cloth Honeycomb Beam Models

The four carbon-cloth honeycomb beam models were tested August 11, 1978
as you had requested.

A copy of the raw data was transmitted to you and a summary of the test
results is below.

Free-free Beam Results for Model

Mode Number	AA Natural Freq. Hz	AA Damping Factor %	AB Nat. Freq. Hz	AB Damp Fact. %	AC Nat. Freq. Hz	AC Damp. Fact. %	AD Nat. Freq. Hz	AD Damp Fact. %
1	134	.7	364	.7	257	.6	412	1.6
2	356	.4	972	.6	689	.4	1078	.5
3	650	.3	1767	.5	1248	.5	1900	.7
4	1024	.2			1882	.9		
5	1409	.4						
6	1829	.7						
7	2253	1.2						

R. Miserentino
2817

cc:
230/SMB
230/Miserentino

REFERENCES

1. Frost, R.K.: Evaluation of Graphite/Polyimide Fabric Structures for Application to Space Shuttle Orbiter. Final Report, NASA Contract NAS1-14131, Nov. 1977.

2. Thomson, W.T.: Theory of Vibration with Applications. Prentice-Hall, Inc. (Englewood Cliffs, N.J.), p. 435, 1972.

3. Advanced Composite Design Guide. 3rd Edition, Vol. 1, Design, Structures Division, Air Force Materials Laboratory, Sept. 1976, p. 2.2.2. 32, Section 2.2.2.2.5,

4. Timoshenko, S.P.; and Gere, J.M.: Theory of Elastic Stability. 2nd Edition, McGraw-Hill (New York, N.Y.) pp. 385-386, section 9.8, 1961.

5. Hyer, M.W.; and Douglas, D.O.: Results of Graphite-Polyimide Isogrid Panel Tests. Progress Report, NASA Grant NSG 1167, June 1977.

Table 1. Effective EI of beams.*

Specimen	EI $(kN - m^2)$	EI $(kip - in.^2)$
AA	1.30	11.5
AB	1.35	11.9
AC	1.24	11.0
AD	1.34	11.8
Average	1.31	11.6

* Based on a beam of unit width and an average of side A
  and side B data.

Table 2. Young's modulus for face sheet as computed from short-block compression tests.

Specimen	E (GPa)	E (psi)
DA	45.4	6.58×10^6
DB	45.4	6.59
DC	39.0	5.66
DD	44.5	6.45
Average	43.6	6.32

Table 3. Poisson's ratio for face sheet as computed from short-block compression tests.

Specimen	ν
DA	0.240
DB	0.247
DC	0.273
DD	0.324
Average	0.271

28

Table 4. Ultimate compressive strength of face-sheet material as computed from short-block compression tests.

Specimen	σ_c^u (GPa)	σ_c^u (ksi)
DA	345	50.0
DB	345	50.0
DC	370	53.7
DD	211	30.6

Table 5. Slopes of load-midspan deflection data, three-point bending tests, m/N × 10³ (in./lb × 10³).

Span m (in.)	BEAM AA			BEAM AB			BEAM AC			BEAM AD			Avg.
	Side A	Size B	Avg.	Side A	Side B	Avg.	Side A	Side B	Avg.	Side A	Side B	Avg.	
0.711 (28.0)	101 (17.7)	124 (21.8)	113 (19.8)	not tested			not tested			not tested			113 (19.8)
0.508 (20.0)	not tested			not tested			39.8 (6.97)	39.1 (6.85)	39.4 (6.91)	not tested			39.4 (6.91)
0.406 (16.0)	20.1 (3.52)	20.3 (3.56)	20.2 (3.54)	17.6 (1.08)	18.6 (3.26)	18.1 (3.17)	22.0 (3.85)	21.9 (3.83)	21.9 (3.84)	18.3 (3.20)	19.0 (3.32)	18.6 (3.26)	19.7 (3.45)
0.254 (10.0)	5.62 (0.984)	5.53 (0.969)	5.57 (0.976)	4.48 (0.837)	4.78 (0.838)	4.78 (0.838)	5.61 (0.983)	5.54 (0.970)	5.57 (0.976)	4.84 (0.847)	4.93 (0.864)	4.89 (0.856)	5.21 (0.912)
0.152 (6.00)	1.70 (0.297)	1.60 (0.281)	1.65 (0.289)	1.70 (0.297)	1.60 (0.281)	1.65 (0.289)	1.66 (0.291)	1.58 (0.276)	1.62 (0.284)	1.42 (0.249)	1.31 (0.230)	1.37 (0.240)	1.58 (0.276)

30

Table 6. Comparison between experimental and theoretical slopes of the
load-deflection relations for the three-point bending tests;
$m/N \times 10^{-3}$ (in./lb $\times 10^3$).

Span m (in.)	Experiment Average from Table 5	Predictions from eq. (3)	%* Difference	Predictions from eq. (4)	%* Difference
0.711 (28.0)	113 (19.8)	90.8 (15.9)	19.7	94.8 (16.6)	16.2
0.508 (20.0)	39.4 (6.91)	33.1 (5.80)	16.1	35.9 (6.29)	8.9
0.406 (16.0)	19.7 (3.45)	17.0 (2.97)	13.9	19.2 (3.36)	2.5
0.254 (10.0)	5.21 (0.912)	4.14 (0.725)	20.5	5.54 (0.971)	- 6.5
0.152 (6.00)	1.58 (0.276)	0.891 (0.156)	44.5	1.74 (0.304)	-10.1

* % Diff = (Exp - Theory)/Exp

31

Table 7. Frequencies and damping factors for vibration tests of free-free beams.

Mode No.	Beam AA		Beam AB		Beam AC		Beam AD	
	Natural Frequency (hz)	Damping Factor (%)	Natural Frequency (hz)	Damping Factor (%)	Natural Frequency (hz)	Damping Factor (%)	Natural Frequency (hz)	Damping Factor (%)
1	134	0.7	364	0.7	257	0.6	412	1.6
2	356	0.4	972	0.6	689	0.4	1078	0.5
3	650	0.3	1767	0.5	1248	0.5	1900	0.7
4	1024	0.2			1882	0.9		
5	1409	0.4						
6	1829	0.7						
7	2253	1.2						

Table 8.   Beam weights.

Specimen	Wt (N)	Wt (lb)
AA	1.156	0.260
AB	0.645	0.145
AC	0.800	0.180
AD	0.712	0.160

Table 9. Comparison between experimental and theoretical natural frequencies for free-free beam (Euler beam theory).

Mode No.	BEAM AA			BEAM AB			BEAM AC			BEAM AD		
	Exp	Theory	% Diff*	Exp	Theory	% Diff	Exp	Theory	% Diff	Exp	Theory	% Diff
1	134	142	- 6	364	394	- 8	257	289	-12	412	441	- 7
2	356	391	-10	972	1090	-12	689	798	-16	1080	1220	-13
3	650	766	-18	1770	2130	-20	1250	1560	-25	1900	2390	-26

* % Diff = (Exp - Theory)/Exp.

Table 10. Slopes of load-deflection data from the plate bending tests (refer to figure 37 for dial gage locations).

Dial Gage Location	Figure No.	Slope	
		mm/N	in./lb
5	38	0.0551	0.00964
3, 8	39	0.0549	0.00961
4, 9	40	0.0559	0.00979
2, 6	41	0.0249	0.00436
1, 7	42	0.0016	0.00028

Table 11. Slopes of load-bending strain data from the plate bending
tests (refer to figure 36 for strain gage locations).

Strain Gage Location	Figure No.	Slope	
		μmm/mm/N	uin./in./lb
9	43	4.04	18.0
4, 8, 11, 15	44	2.02	9.01
1, 5, 12, 16	45	3.04	13.5
2, 6, 13, 17	46	0.41	1.82
3, 7, 10, 14	47	0.25	1.11

BOTH FACE SHEETS
IDENTICAL LAYUP

FACE SHEET MATERIAL:
T-300/PMR-15 FABRIC

0.50 m
(20.0 in.)

1.22 m
(48.0 in.)

0°
45°
90°
-45°

HONEYCOMB CORE CELL
SIZE = 4.76 mm (0.188 in.)
Hexcel HRH 327 - 3/16 - 4.0

0.28 mm (0.011 in.)

12.7 mm (0.50 in.)

Figure 1. Panel geometry.

Specimen	Dimensions mm	(in.)
AA	762 × 63.5	(30.0 × 2.50)
AB	457 × 63.5	(18.0 × 2.50)
AC	533 × 63.5	(21.0 × 2.50)
AD	432 × 63.5	(17.0 × 2.50)
BA	152 × 50.8	(6.00 × 2.00)
BB	152 × 50.8	(6.00 × 2.00)
BC	152 × 50.8	(6.00 × 2.00)

Specimen	Dimensions mm	(in.)
BD	152 × 50.8	(6.00 × 2.00)
CA	228 × 228	(9.00 × 9.00)
CB	228 × 228	(9.00 × 9.00)
DA	102 × 50.8	(4.00 × 2.00)
DB	102 × 50.8	(4.00 × 2.00)
DC	102 × 50.8	(4.00 × 2.00)
DD	102 × 50.8	(4.00 × 2.00)

Figure 2. Orientation and nomenclature of specimens cut from panel.
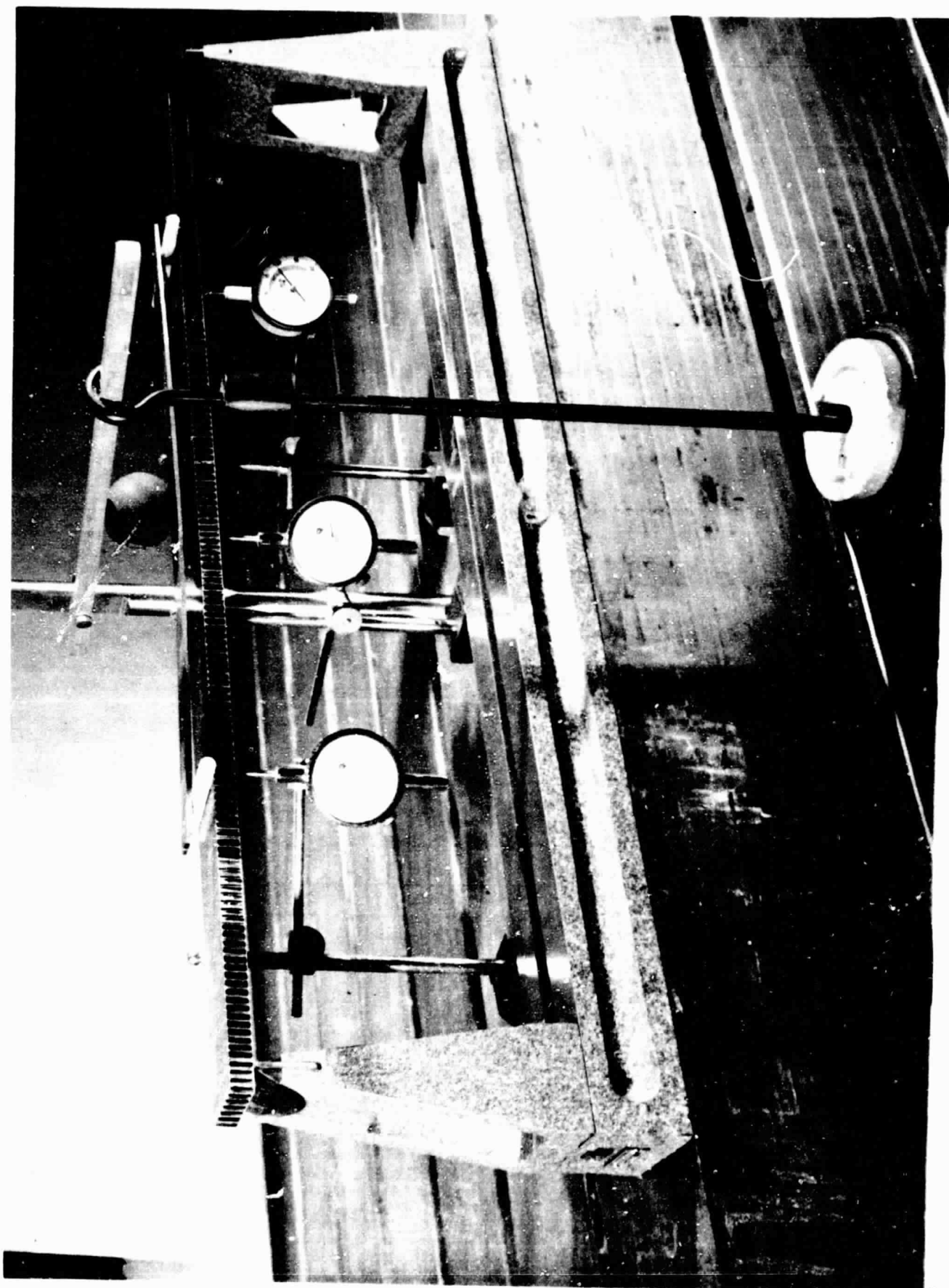
Figure 3. Four-point bending test setup.
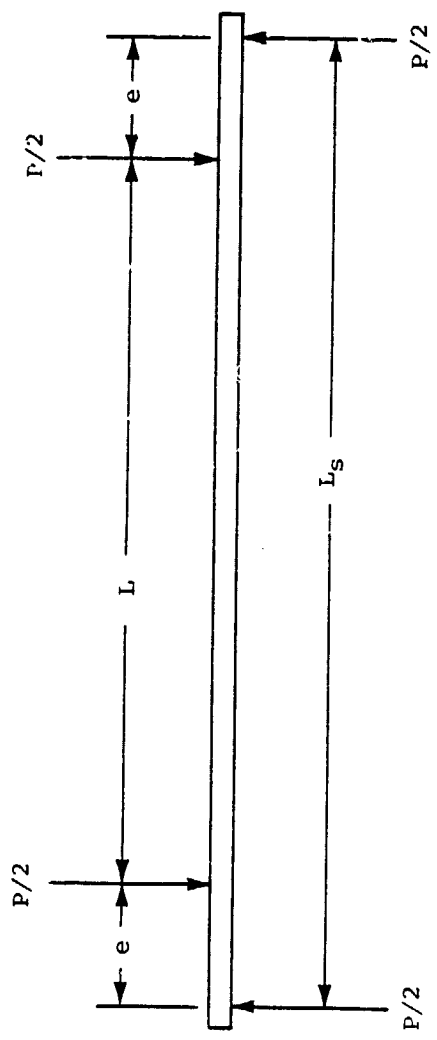
P   =   load

e   =   distance between load application points

L_S =   distance between supports

L   =   effective length of beam

M   =   moment in midsection = Pe/2

Figure 4.   Loading nomenclature for four-point bending tests.
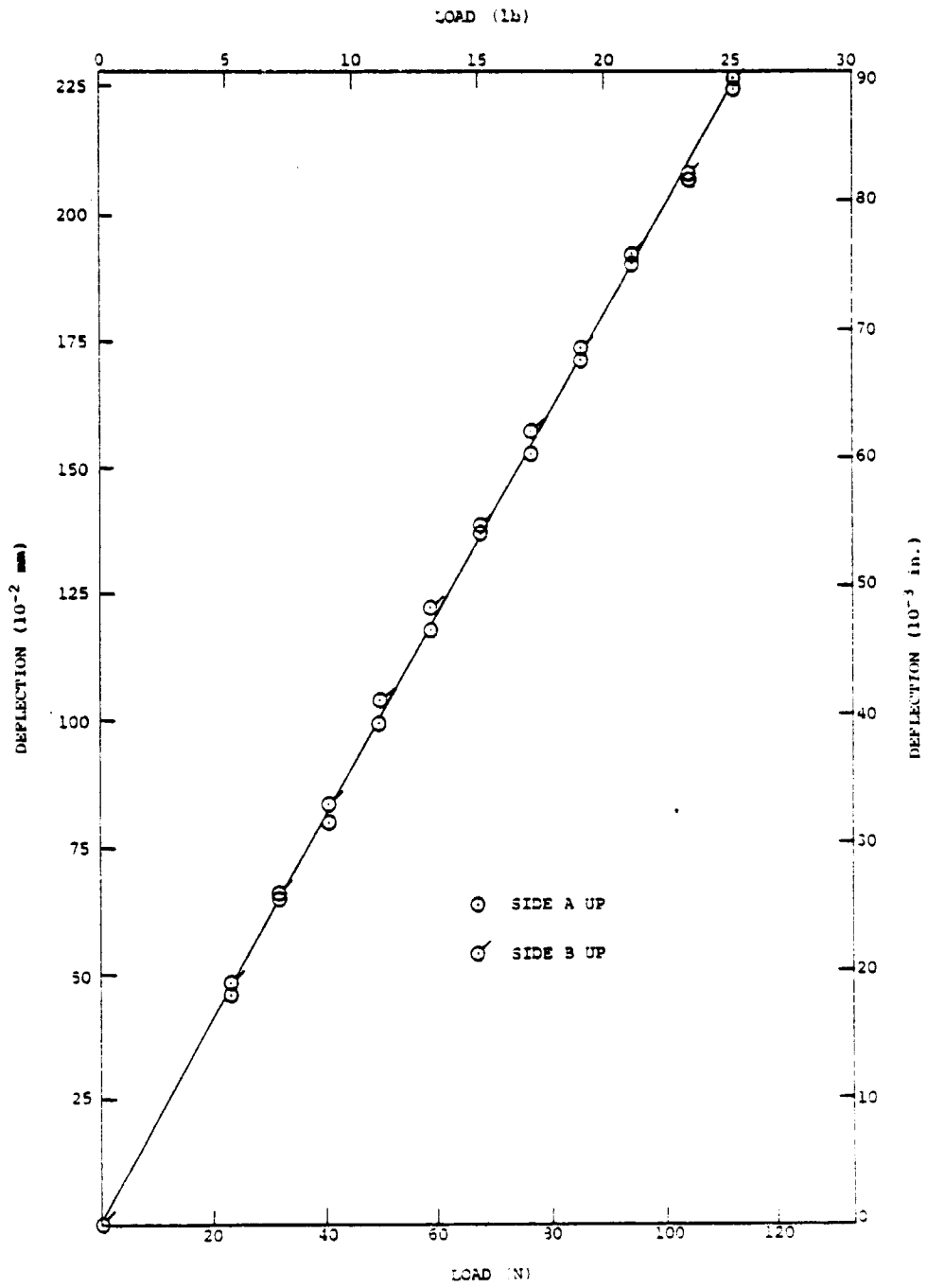
Figure 5.   Load-deflection characteristics for four-point bending test of
beam AA, L_S = 0.737 m (29.0 in.), e = 76.2 m (3.00 in.).

42
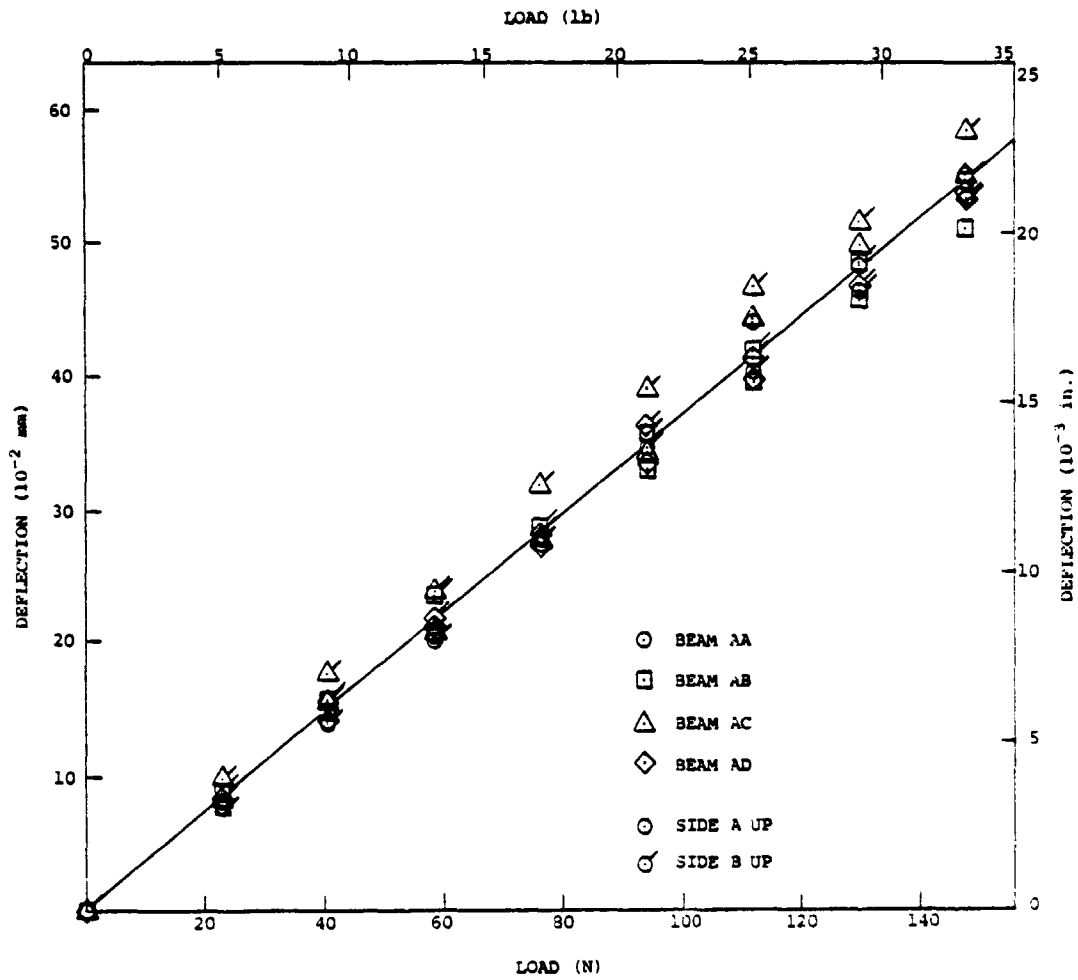
Figure 6. Load-deflection characteristics for four-point bending tests, all beams, $L_s = 0.406$ m (16.0 in.), $e = 76.2$ mm (3.00 in.).
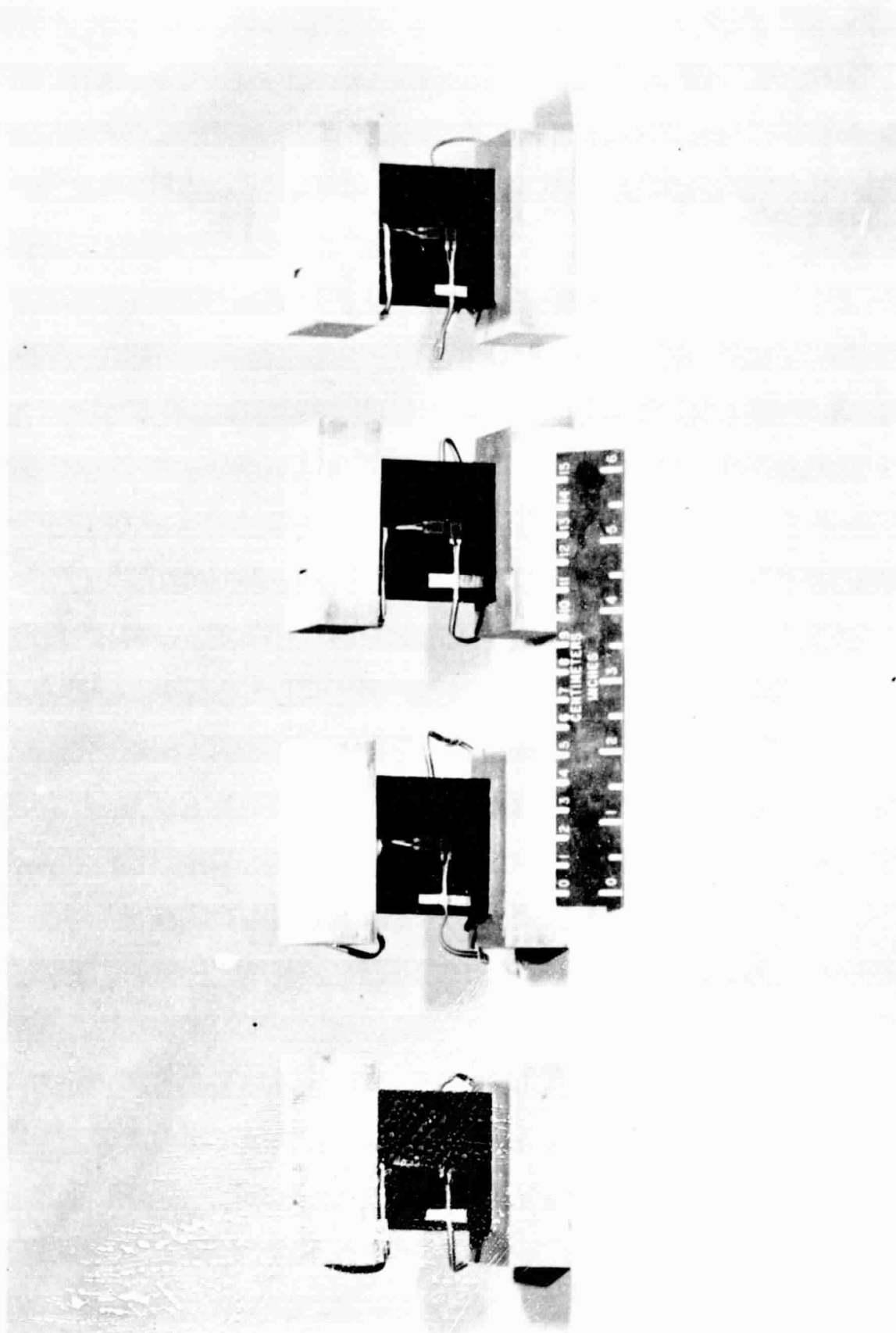
Figure 7. Short-block compression specimens.
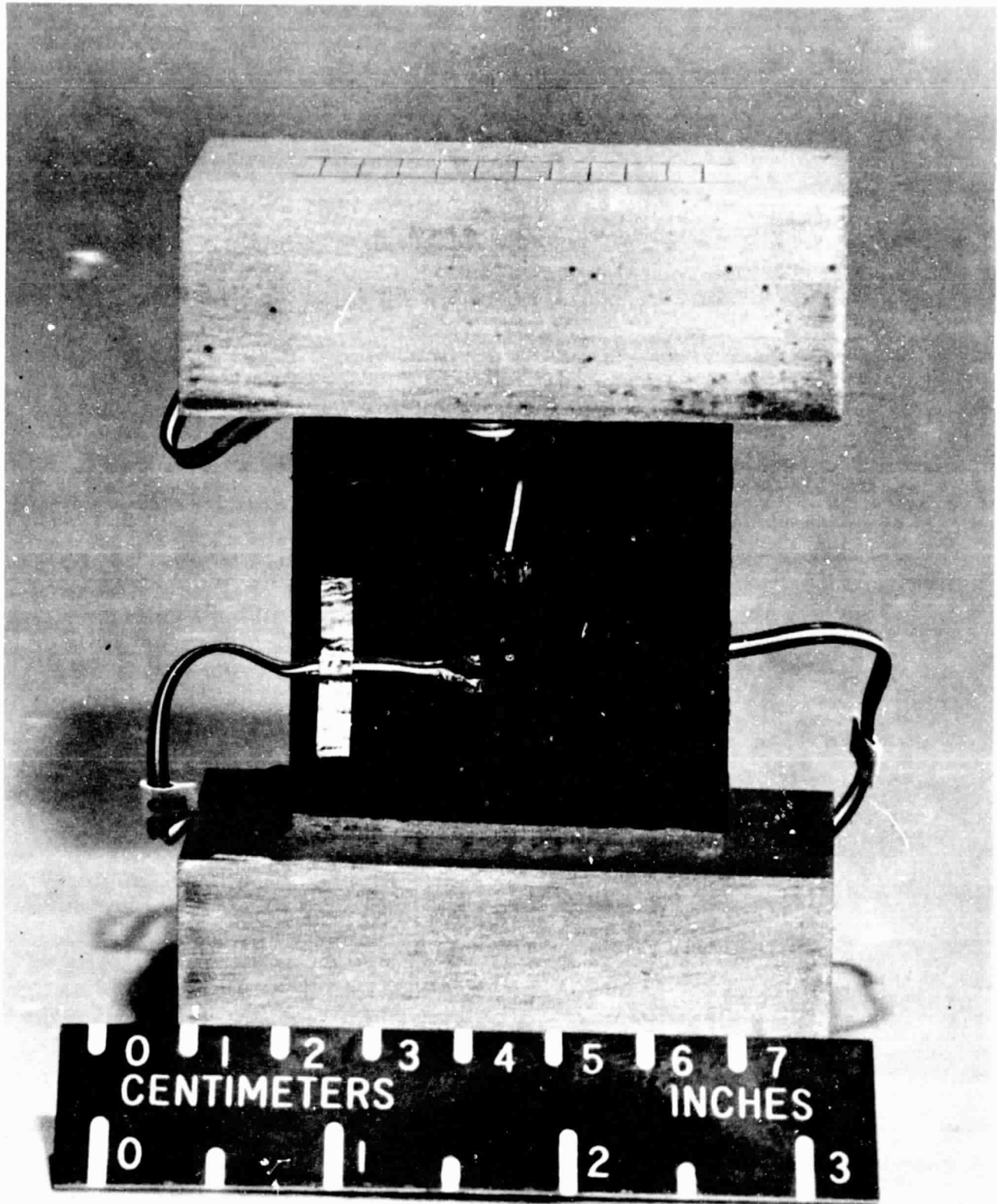
Figure 8.   Closeup of short-block compression specimen.
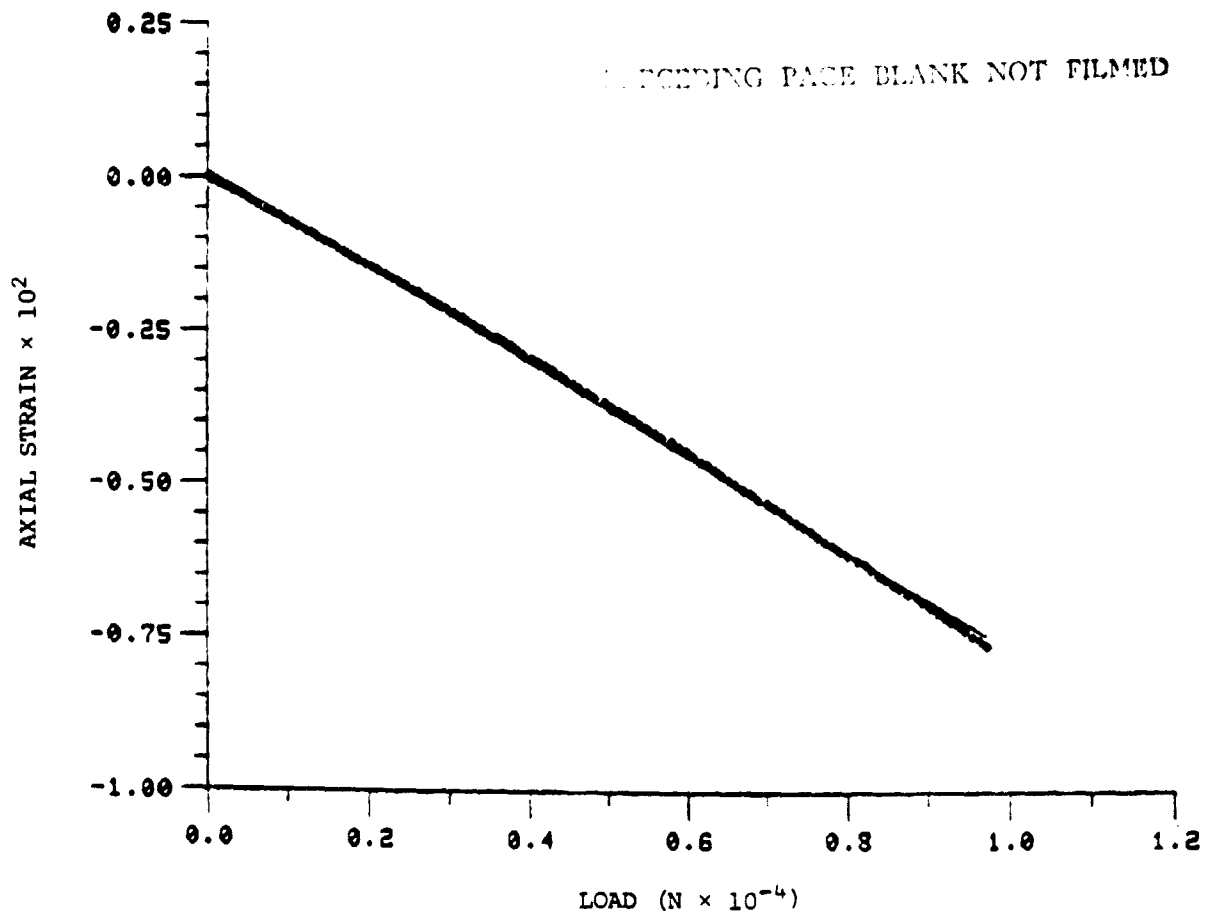
Figure 9. Load-axial strain response of short-block specimen DA (0°).
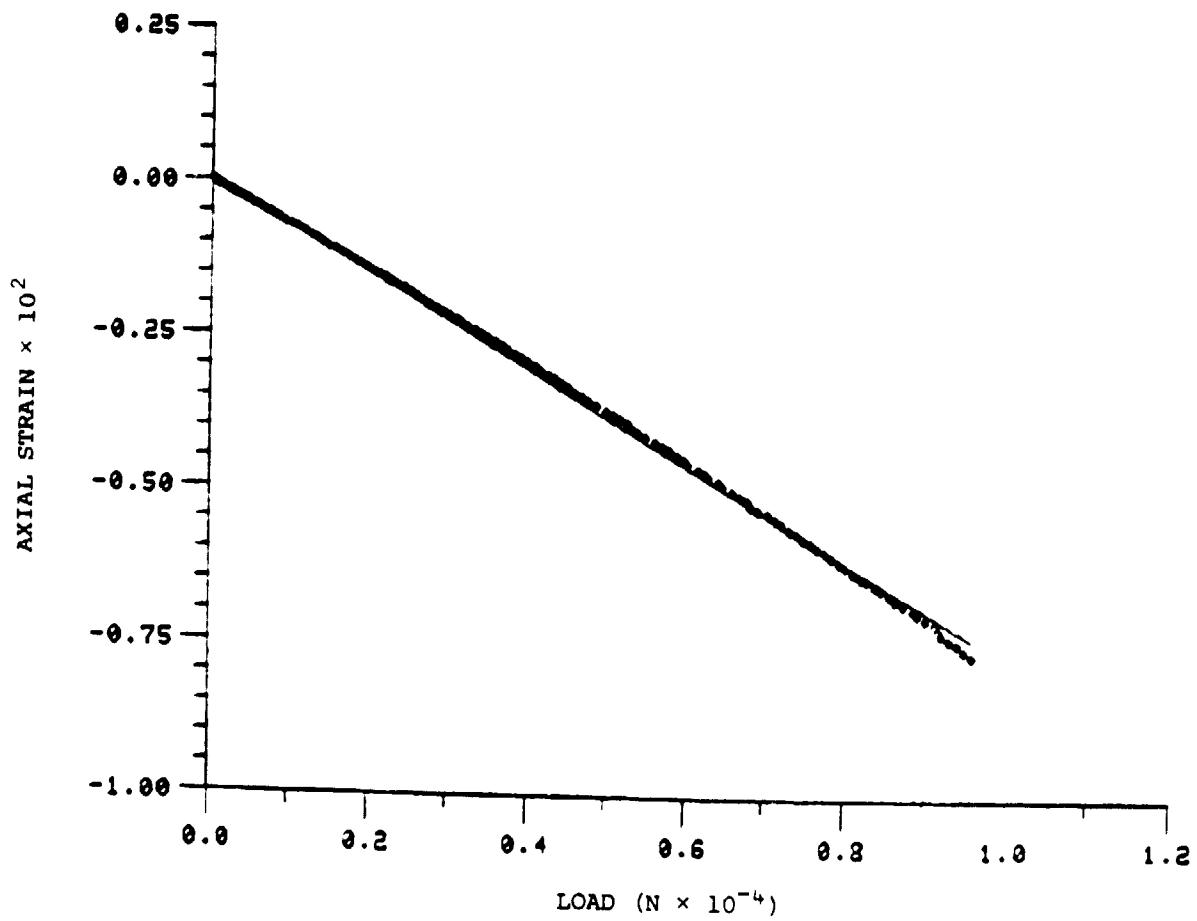
Figure 10. Load-axial strain response of short-block specimen DB (90°).
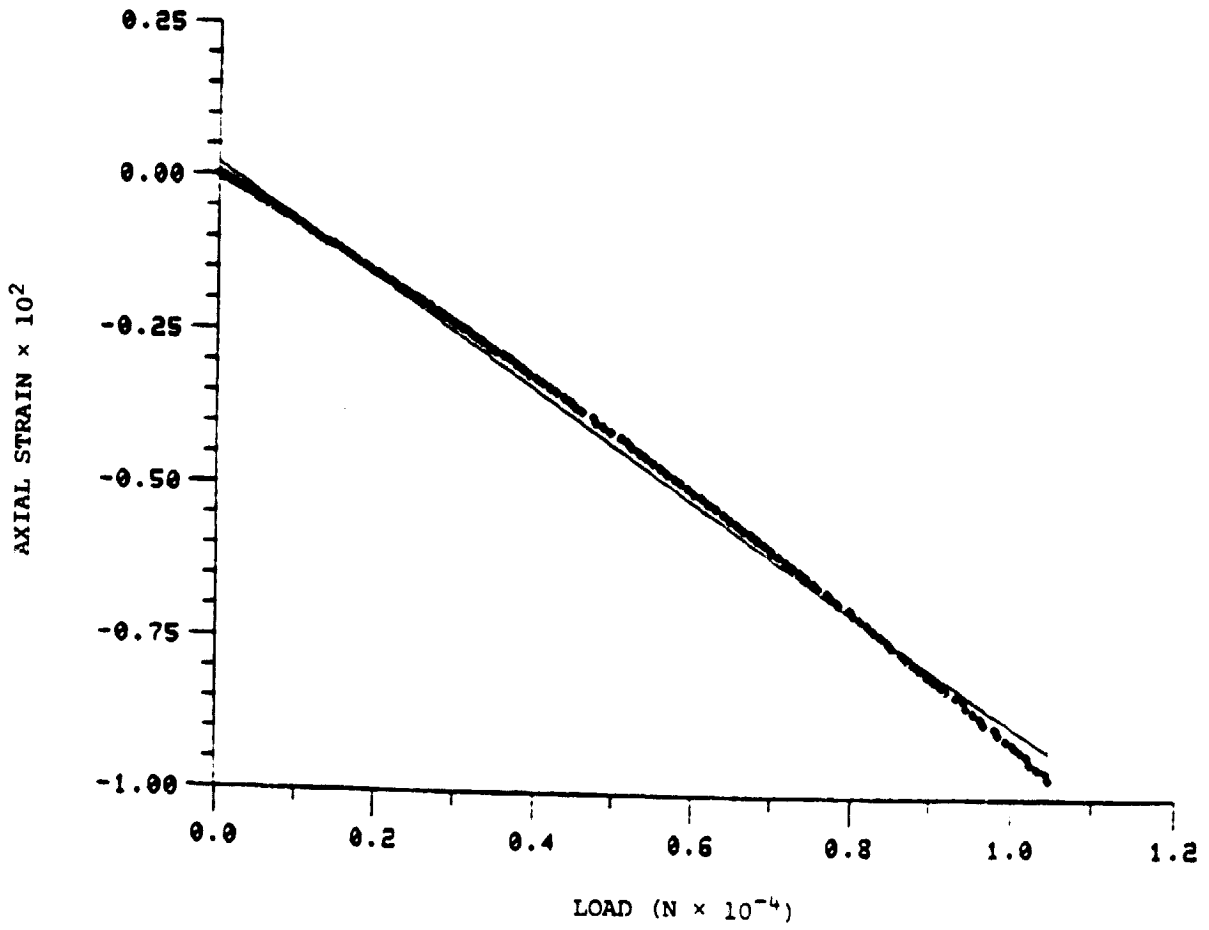
Figure 11. Load-axial strain response of short-block specimen DC (45°).
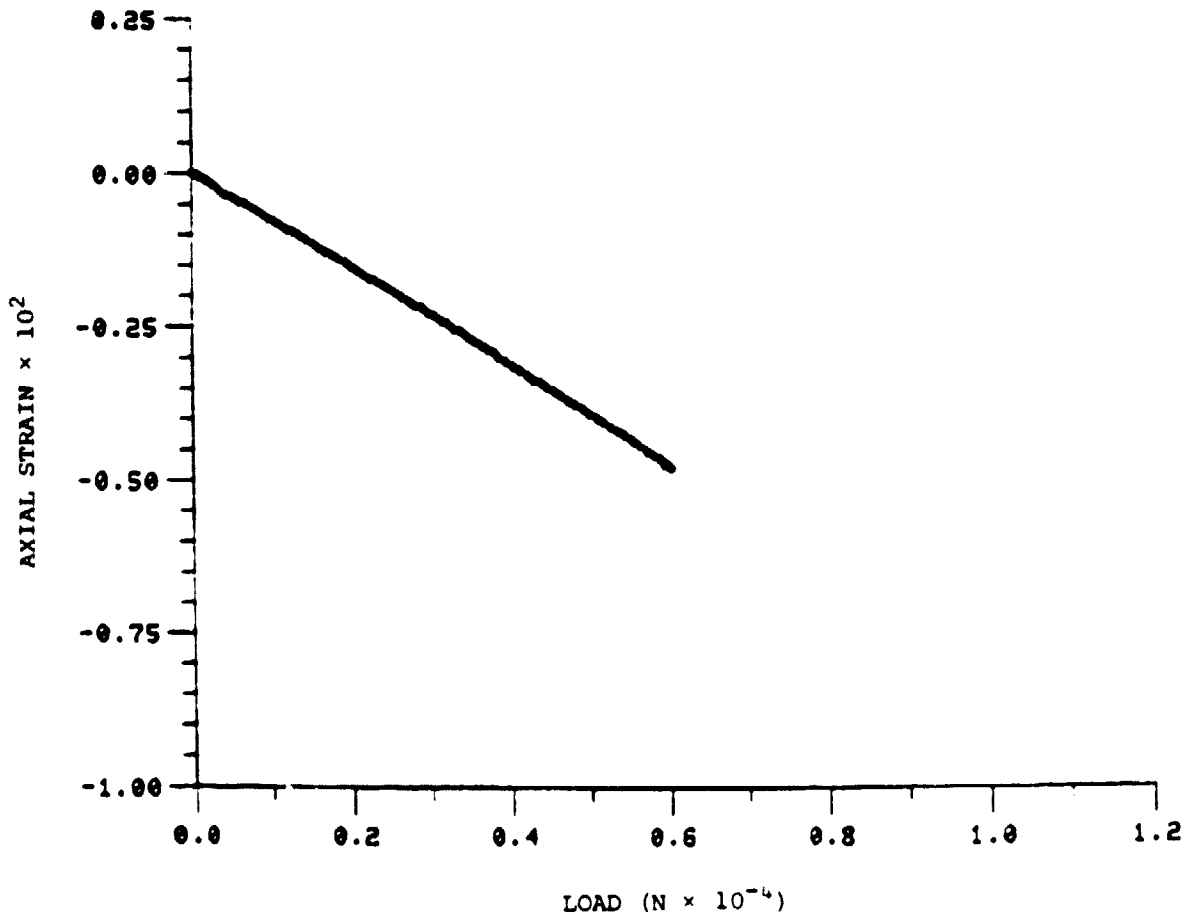
Figure 12. Load-axial strain response of short-block specimen DD (22.5°).
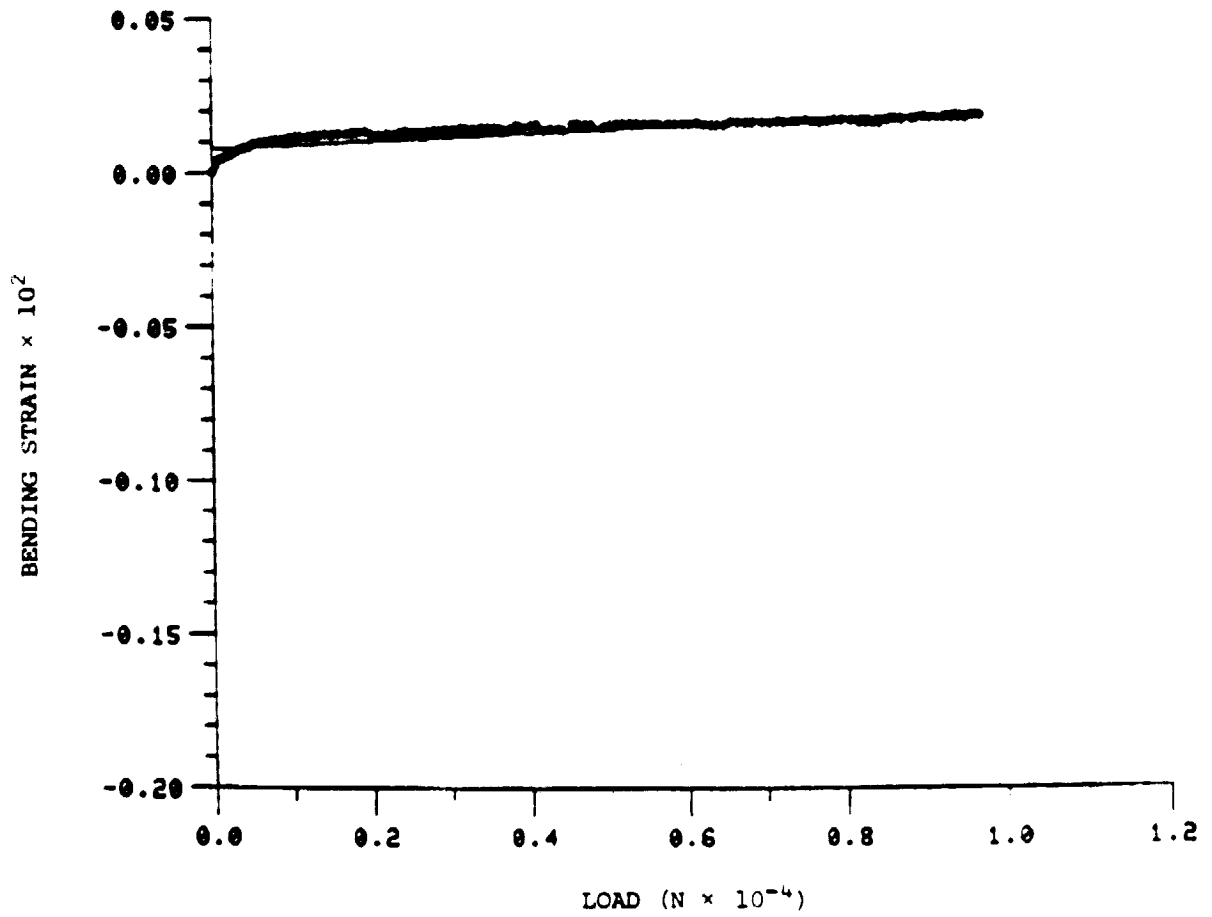
Figure 13. Load-bending strain response of short-block specimen DA (0°).
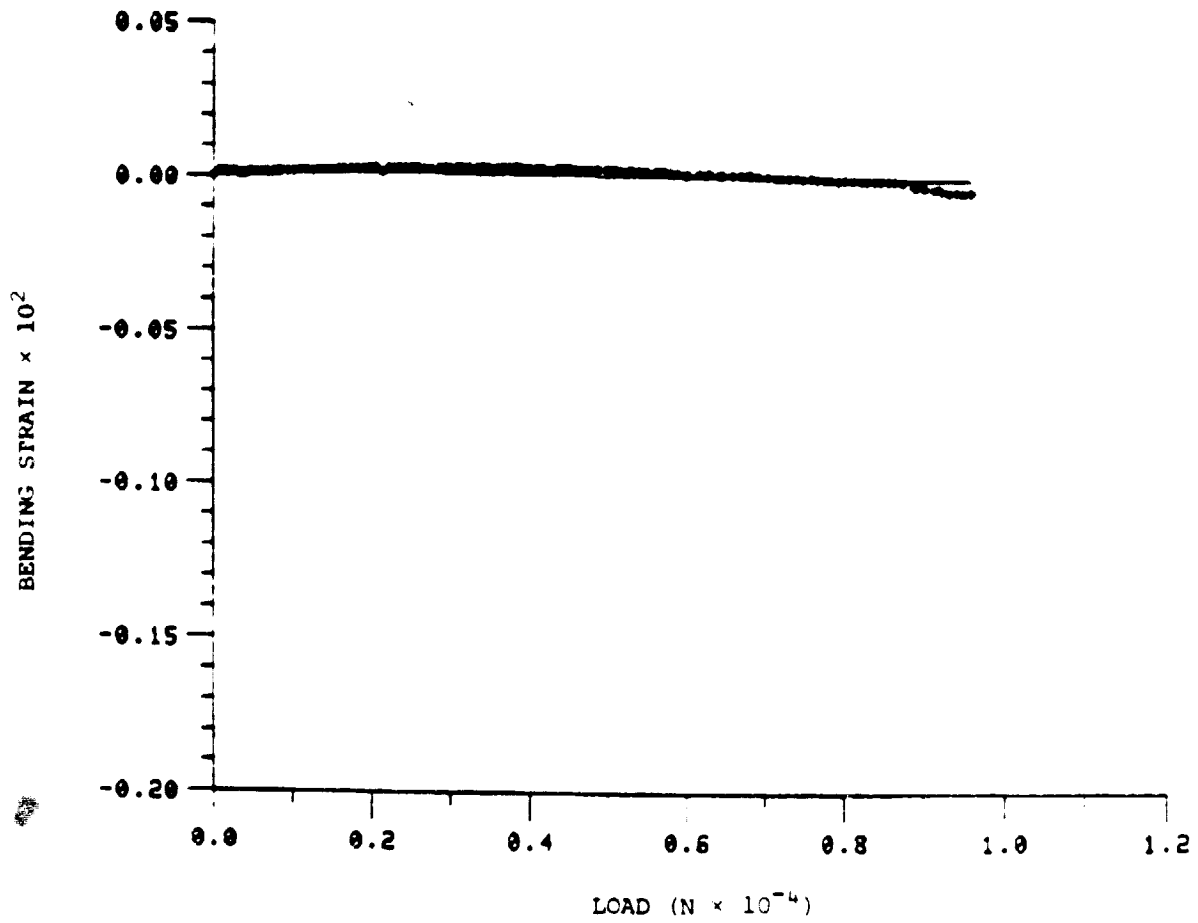
Figure 14. Load-bending strain response of short-block specimen DB (90°).
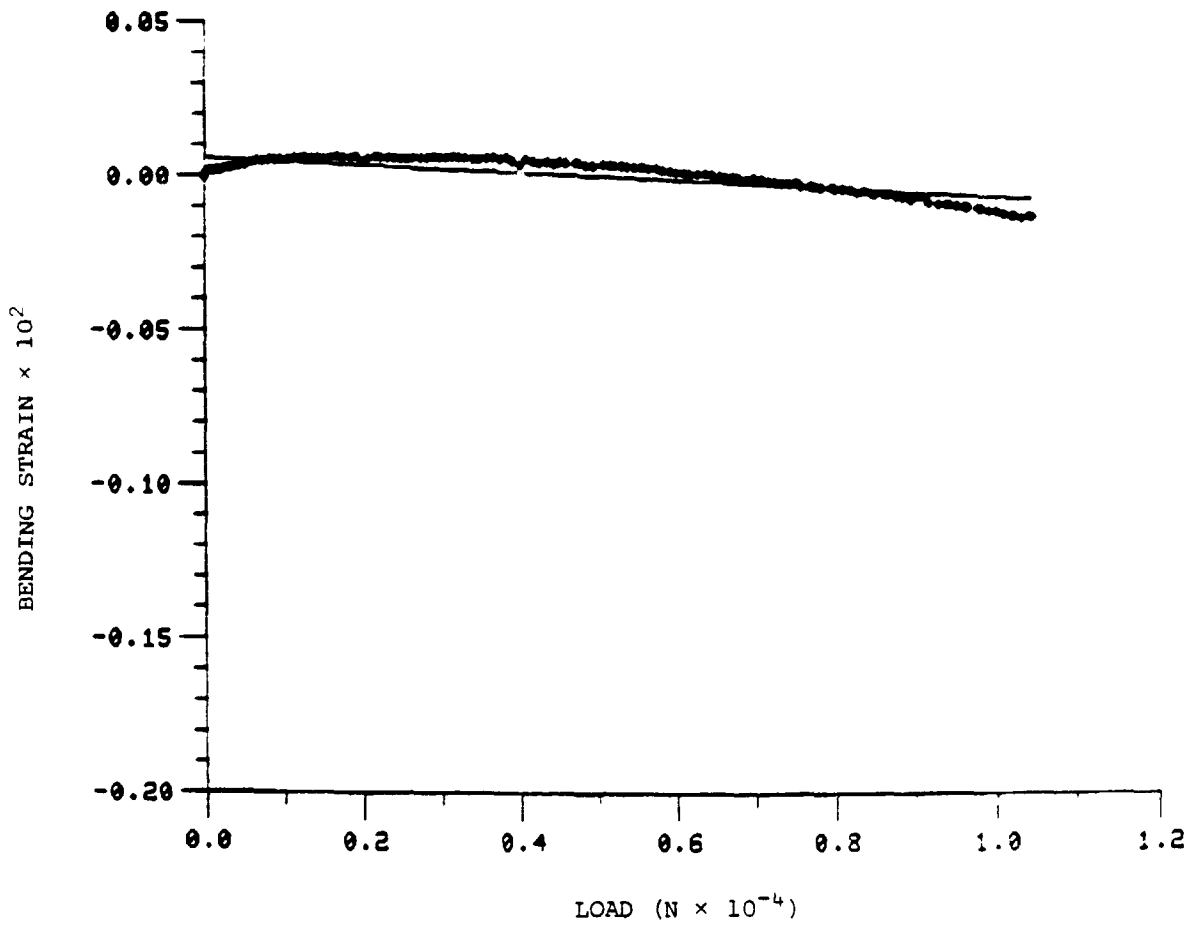
Figure 15. Load-bending strain response of short-block specimen DC (45°).
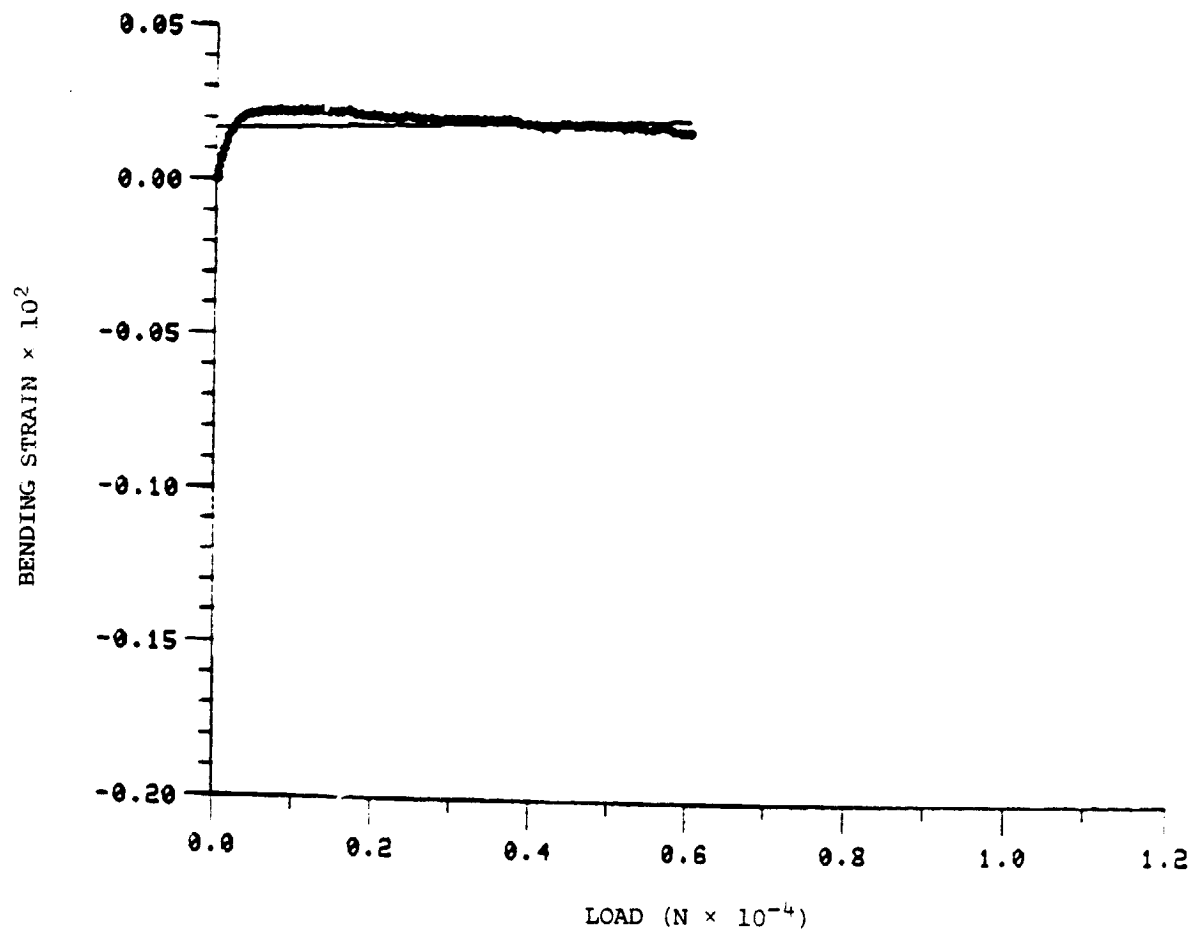
Figure 16. Load-bending strain response of short-block specimen DD (22.5°).
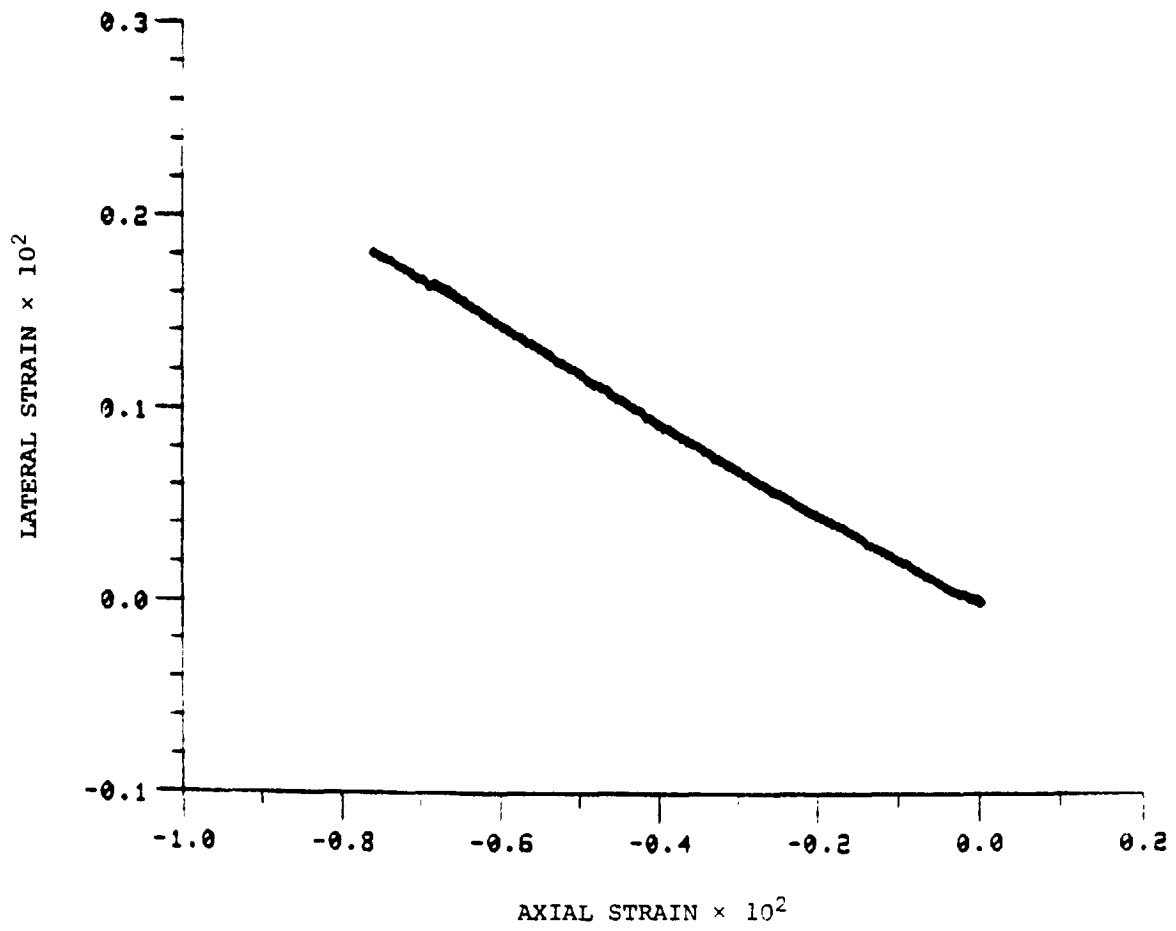
Figure 17. Lateral vs. axial strain response of short-block specimen DA (0°).
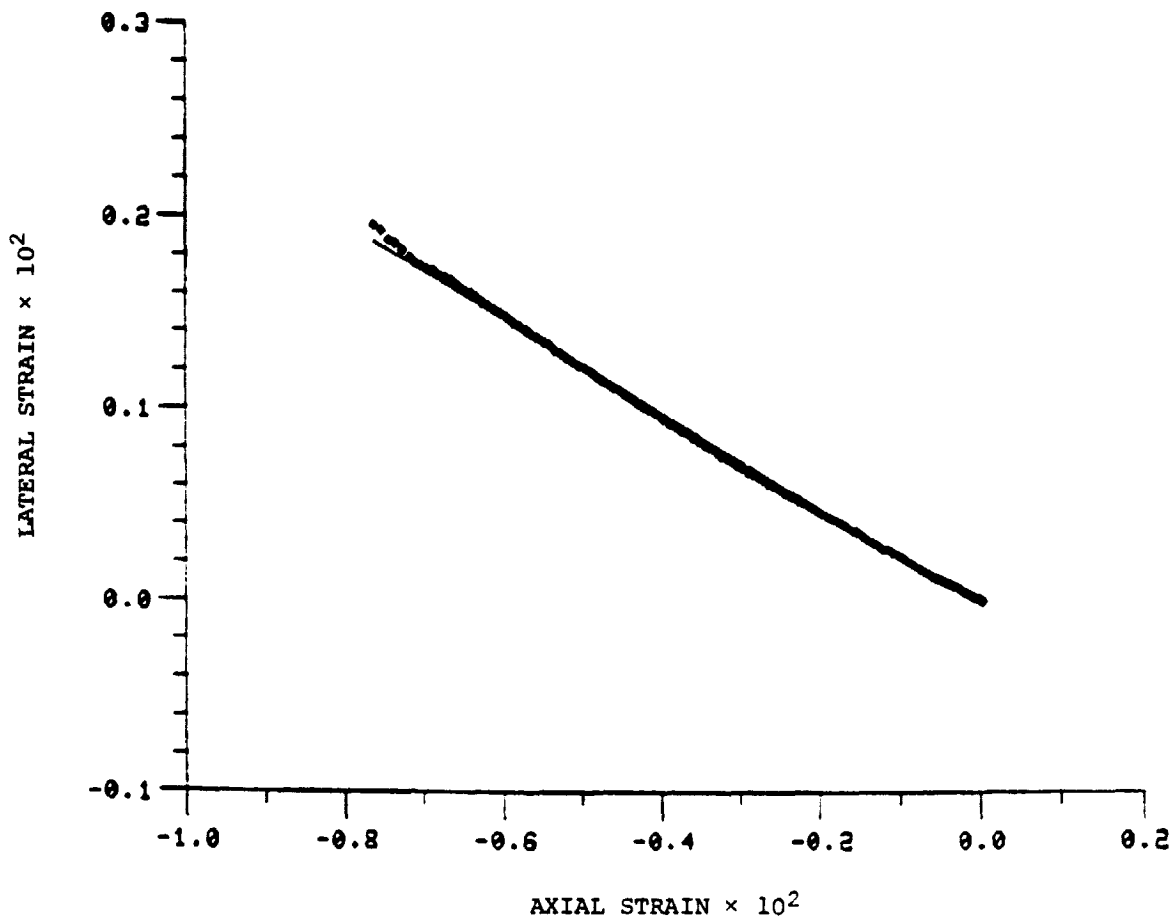
Figure 18.   Lateral vs. axial strain response of short-block specimen DB
              (90°).
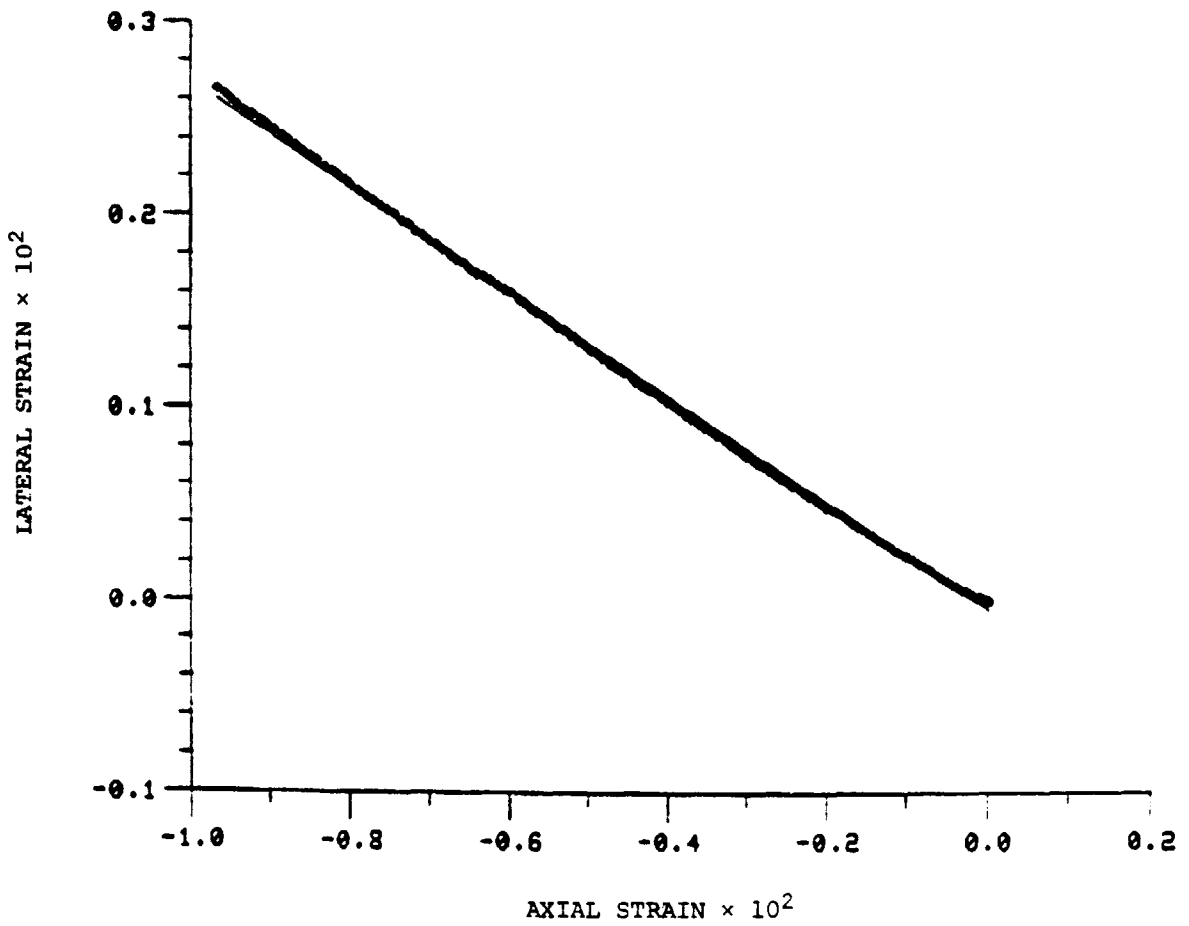
Figure 19. Lateral vs. axial strain response of short-block specimen DC (45°).
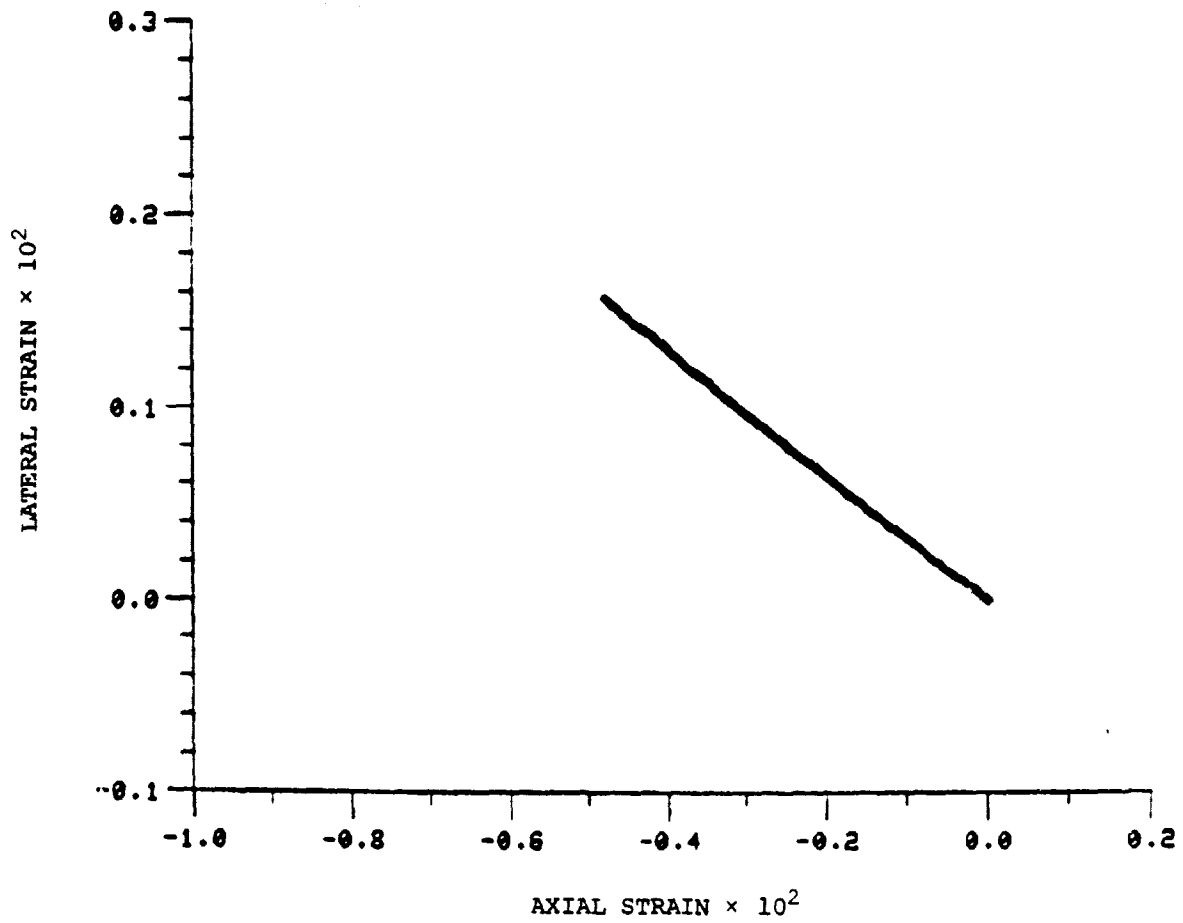
Figure 20. Lateral vs. axial strain response of short-block specimen DD (22.5°).

60
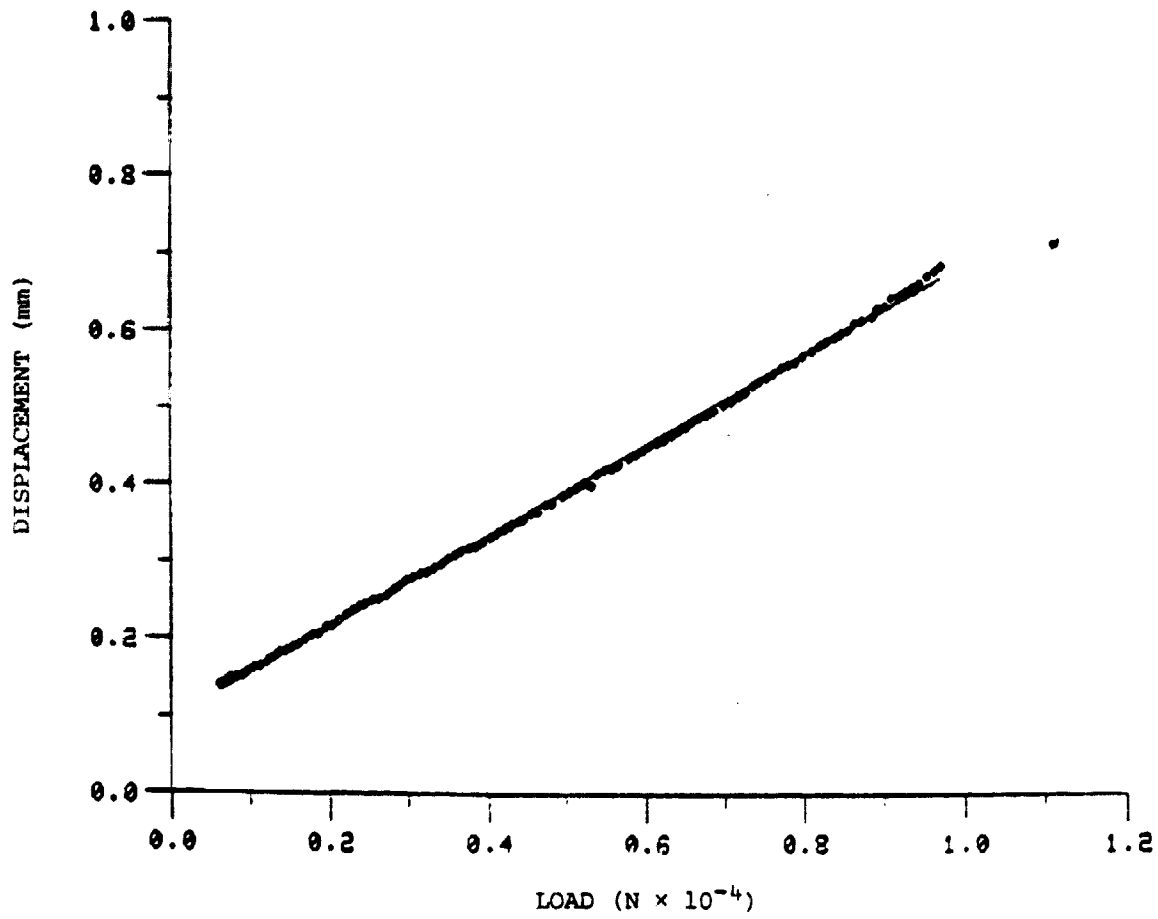
Figure 21. Load-axial displacement response of short-block specimen DA
(0°).
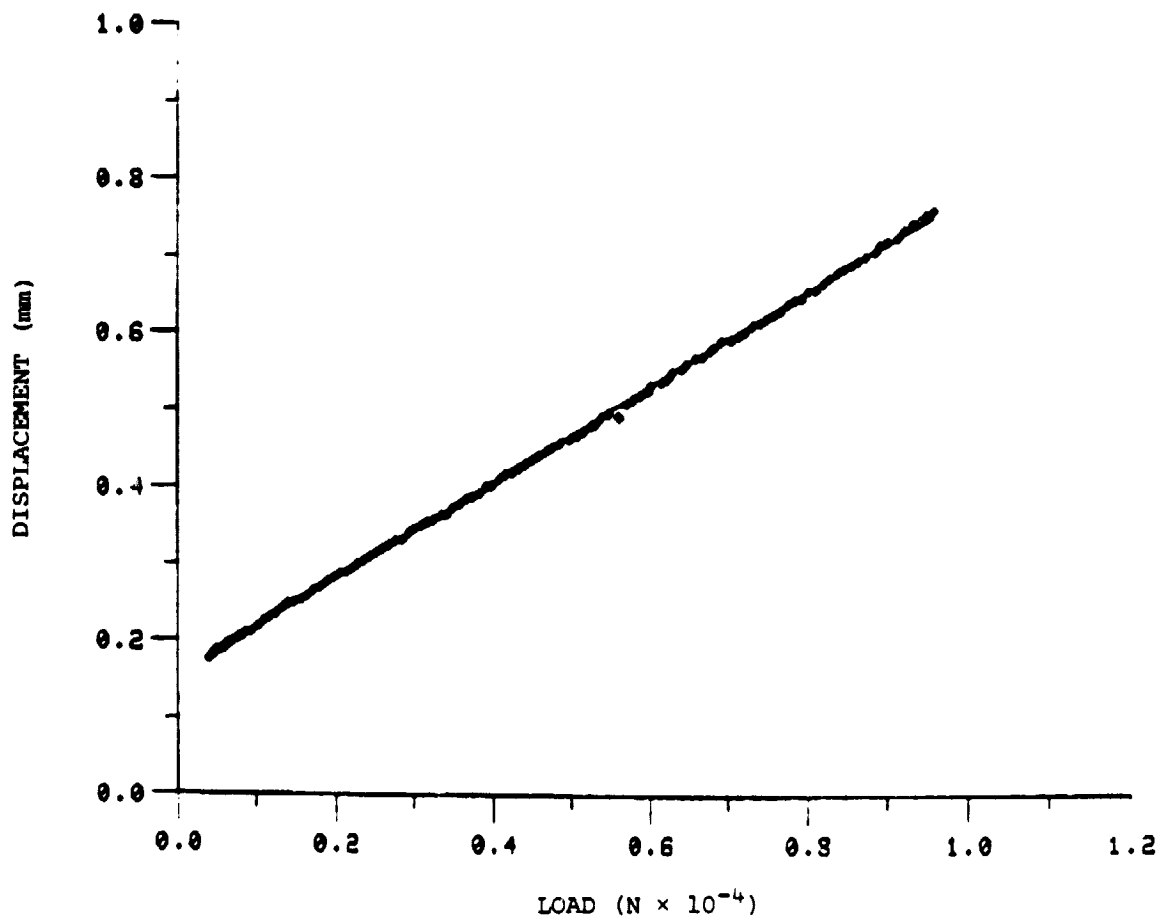
Figure 22.   Load-axial displacement response of short-block specimen DB
(90°).
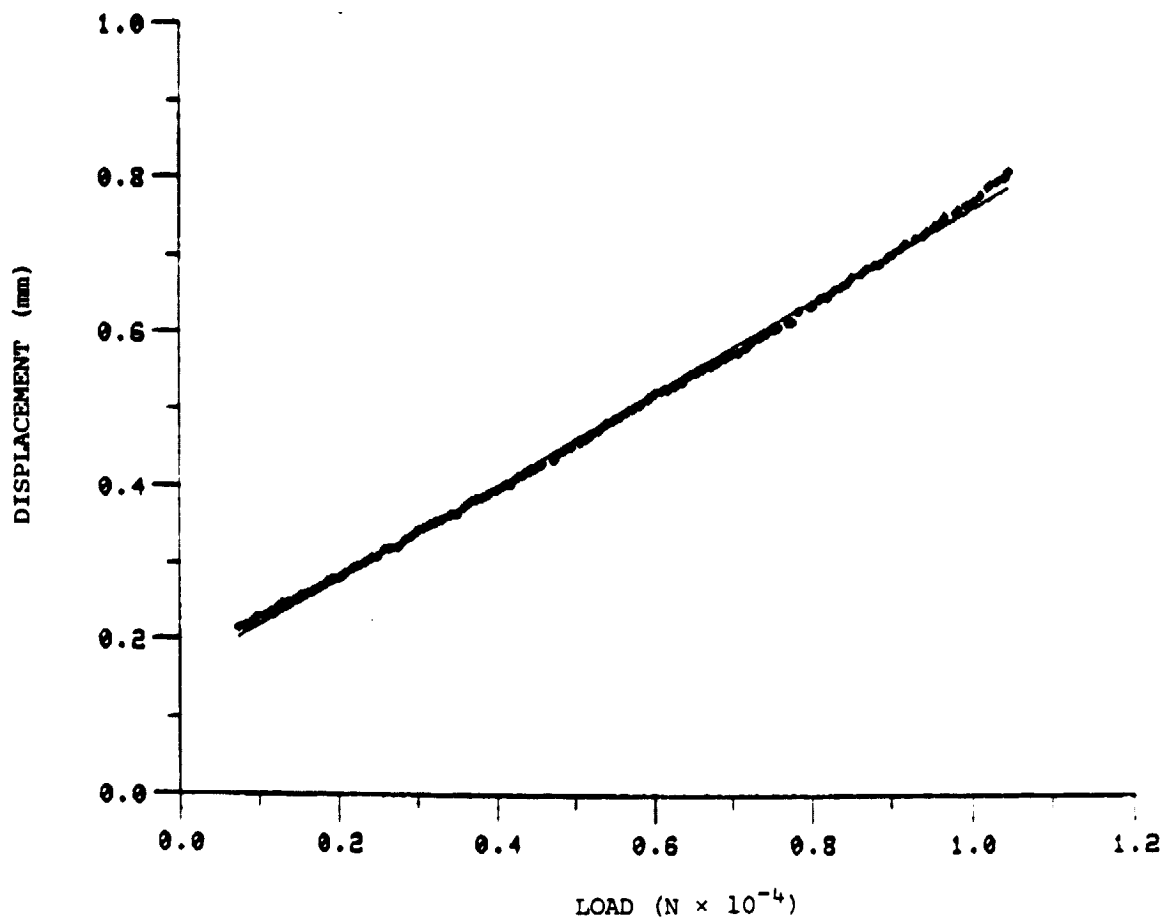
Figure 23. Load-axial displacement response of short-block specimen DC (45°).
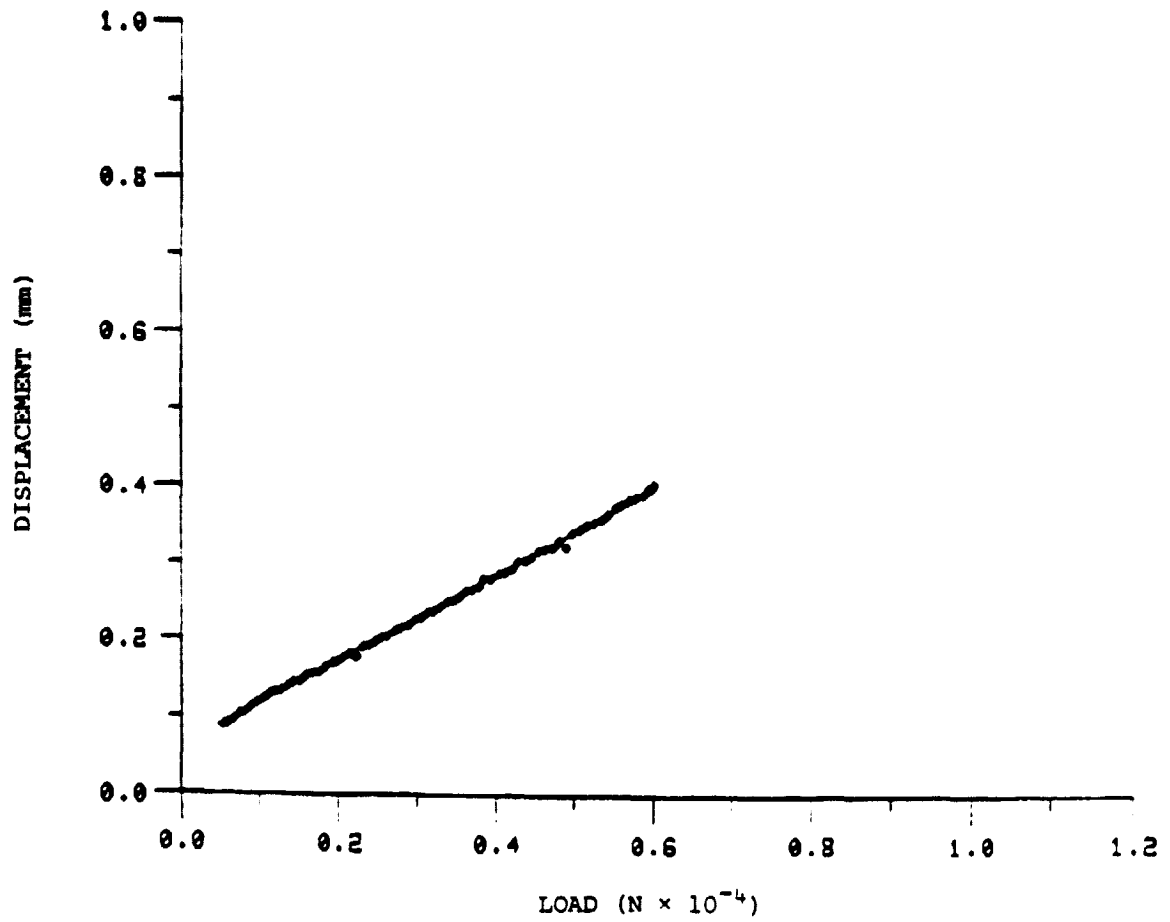
Figure 24. Load-axial displacement response of short-block specimen DD (22.5°).
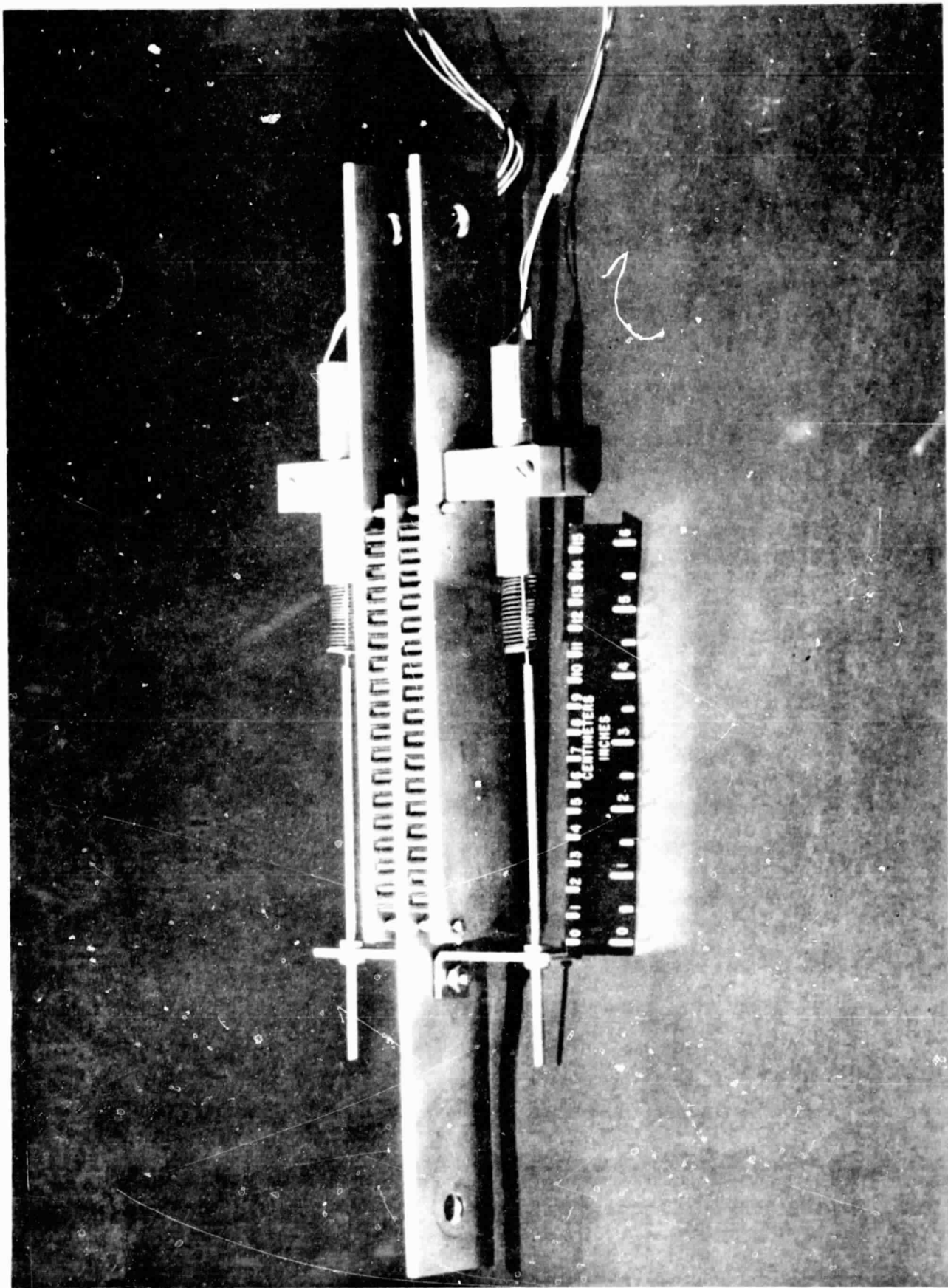
Figure 25. Fixture for measuring shear modulus of the core material.
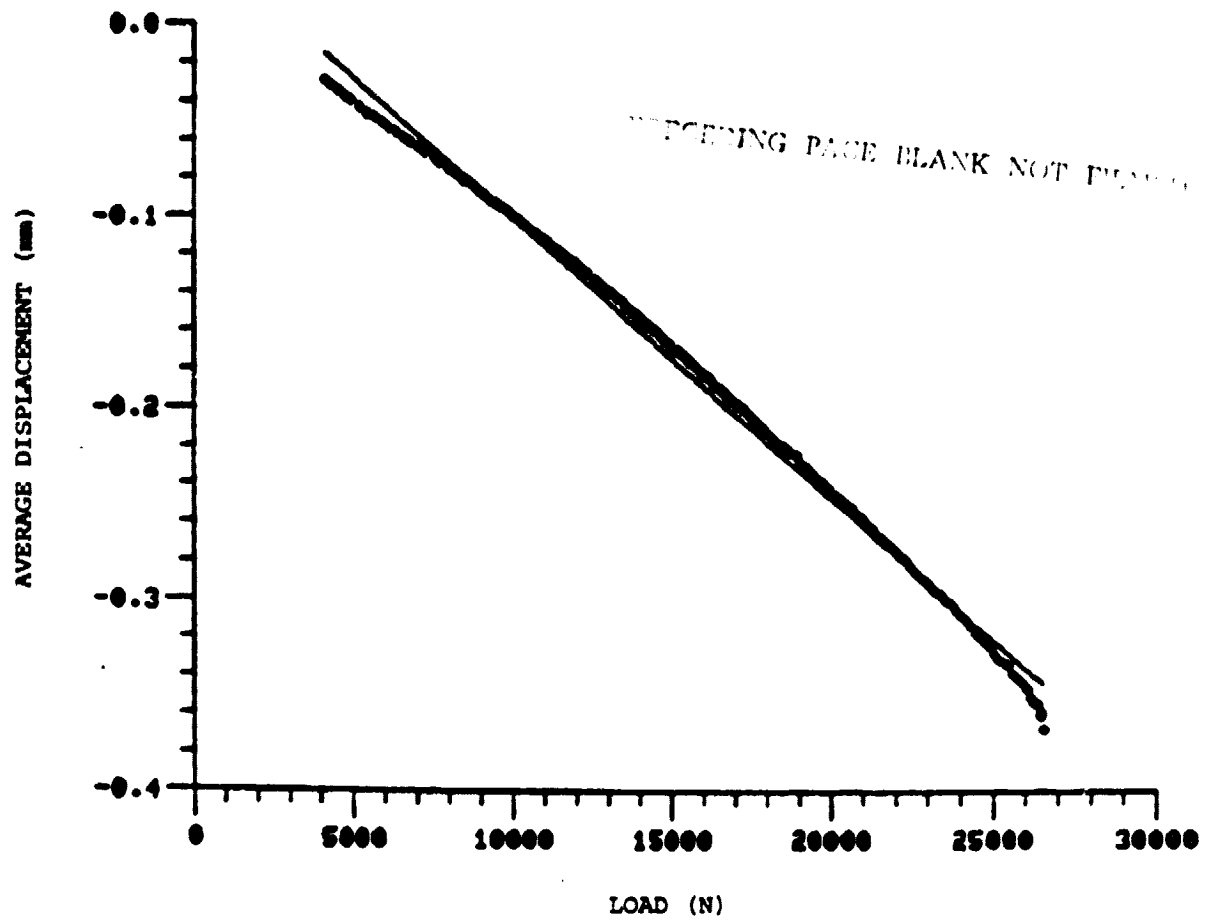
Figure 26. Force vs. average of right and left DCDT, core shear test.
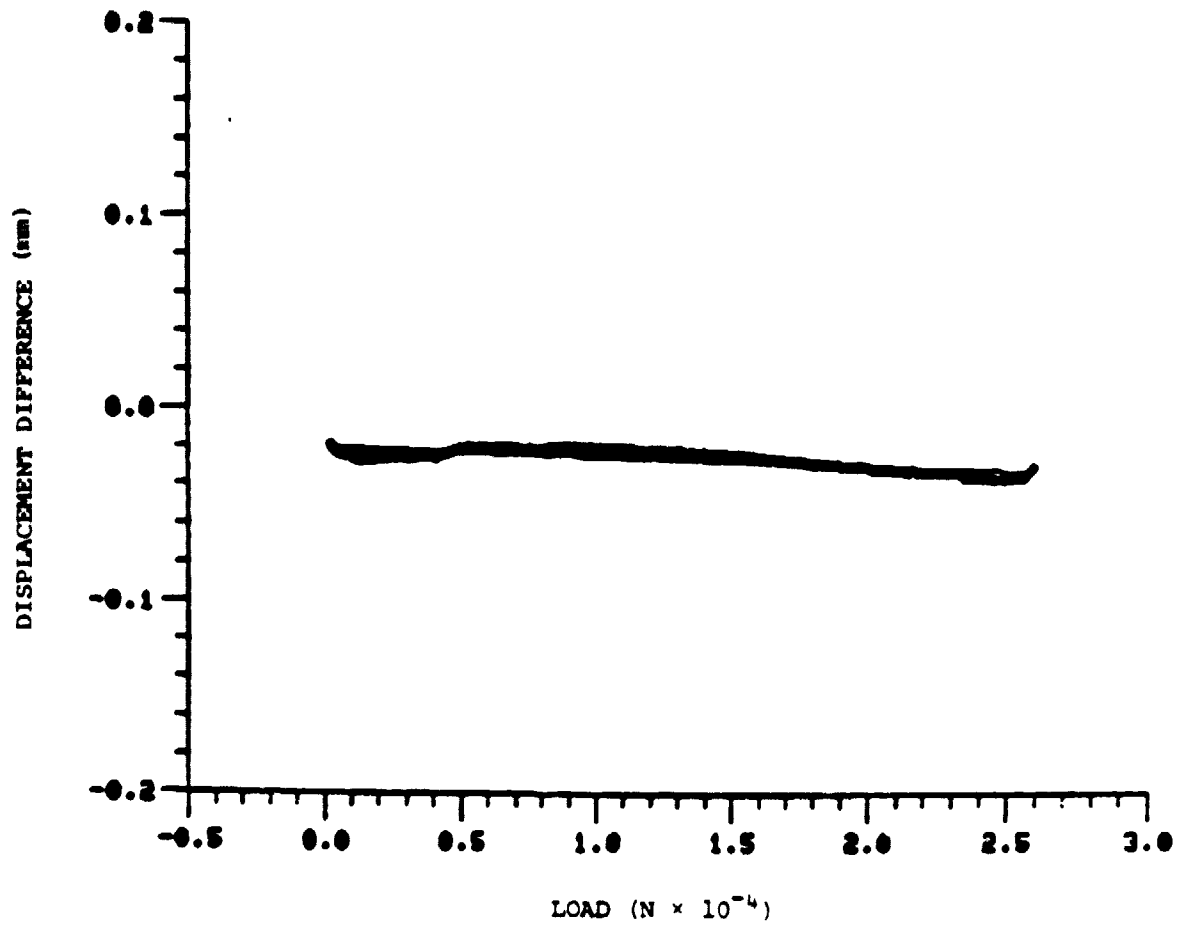
Figure 27. Force vs. difference of right and left DCDT displacements, core shear test.
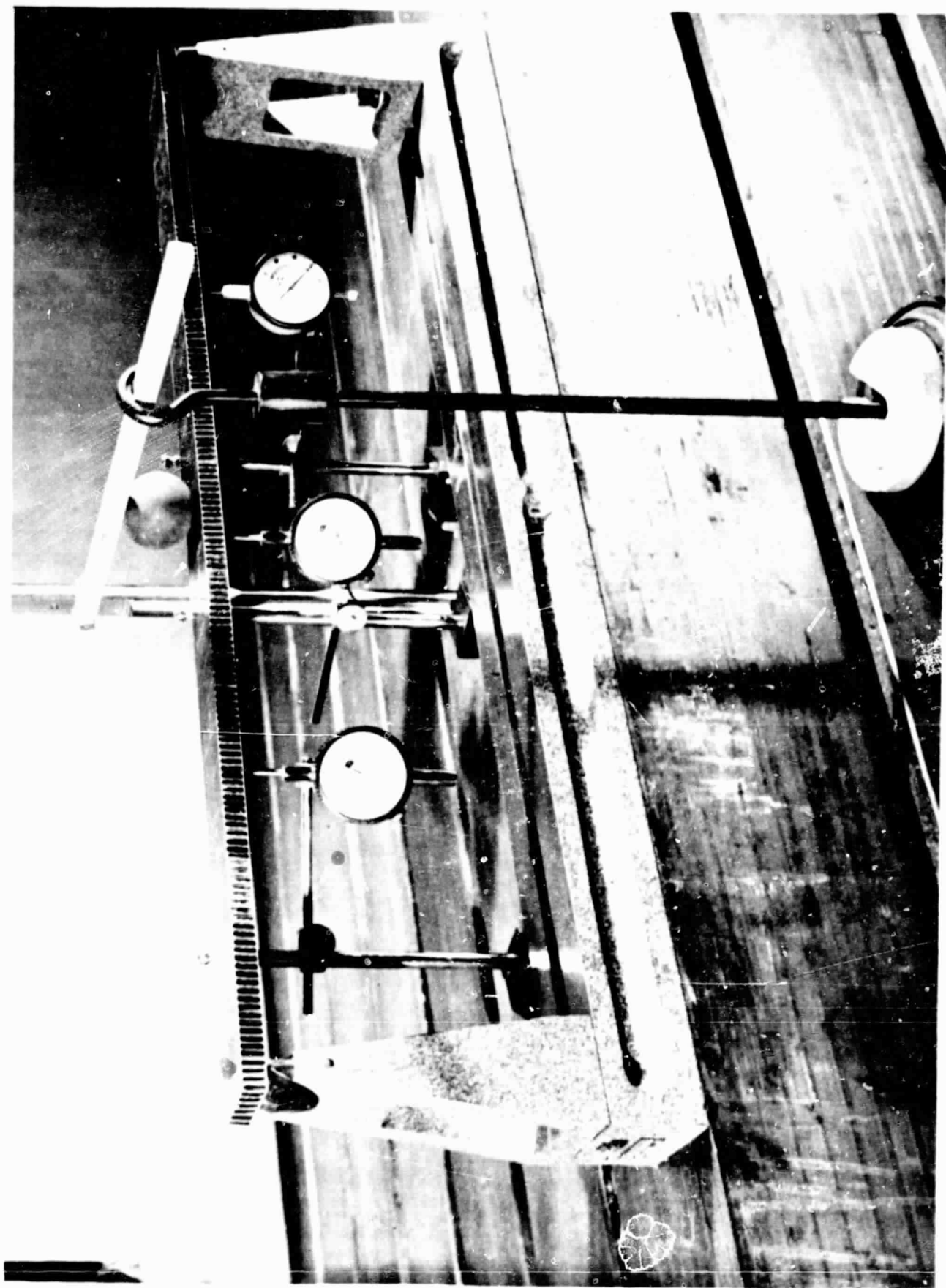
Figure 28. Three-point bending test setup.

P

L

P/2   P/2
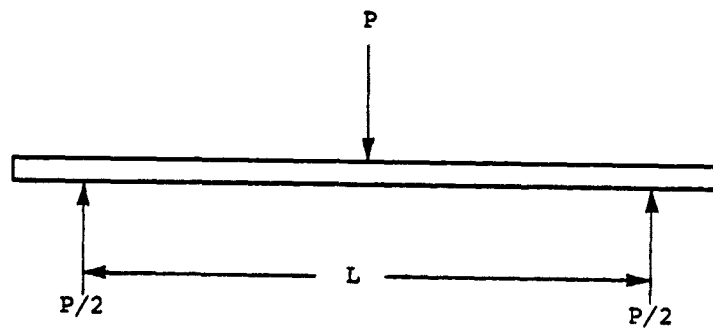
L = distance between supports

P = applied load

Figure 29. Three-point bending test configuration.
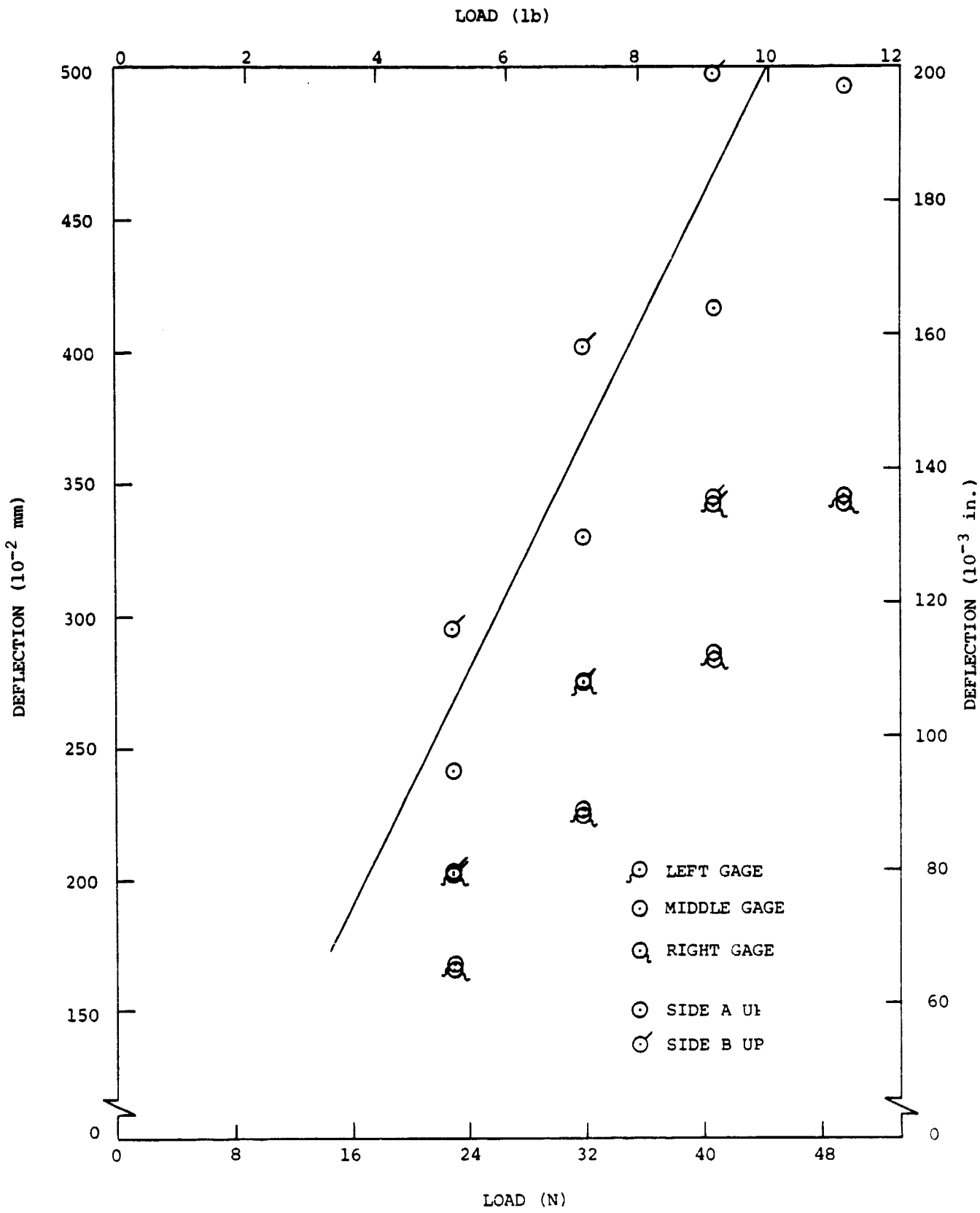
Figure 30.   Load-deflection characteristics for three-point bending test,
beam AA, L = 0.711 m (28 in.).
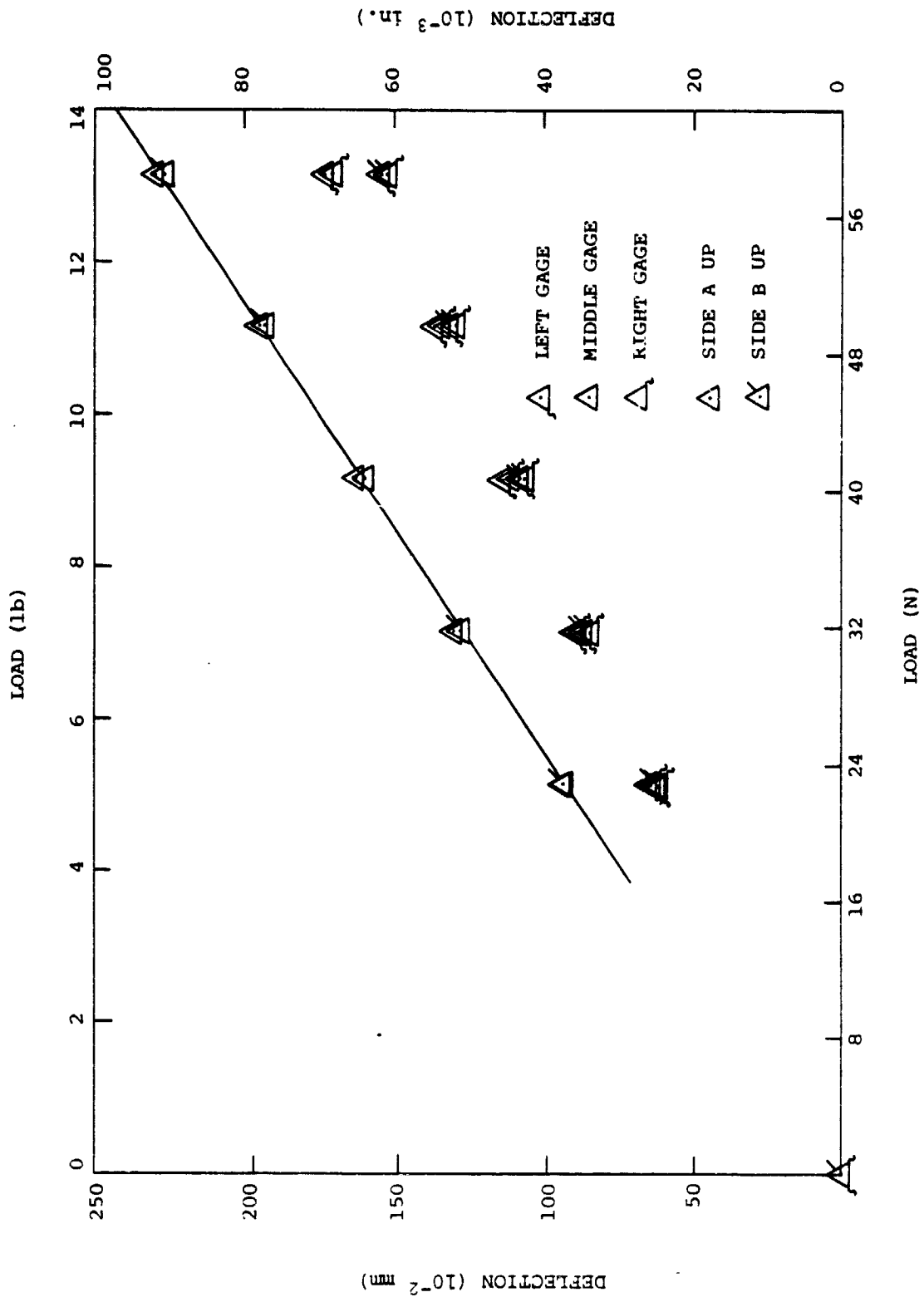
Figure 31. Load-deflection characteristics for three-point bending test, beam AC, L = 0.508 m (20.0 in.).

73
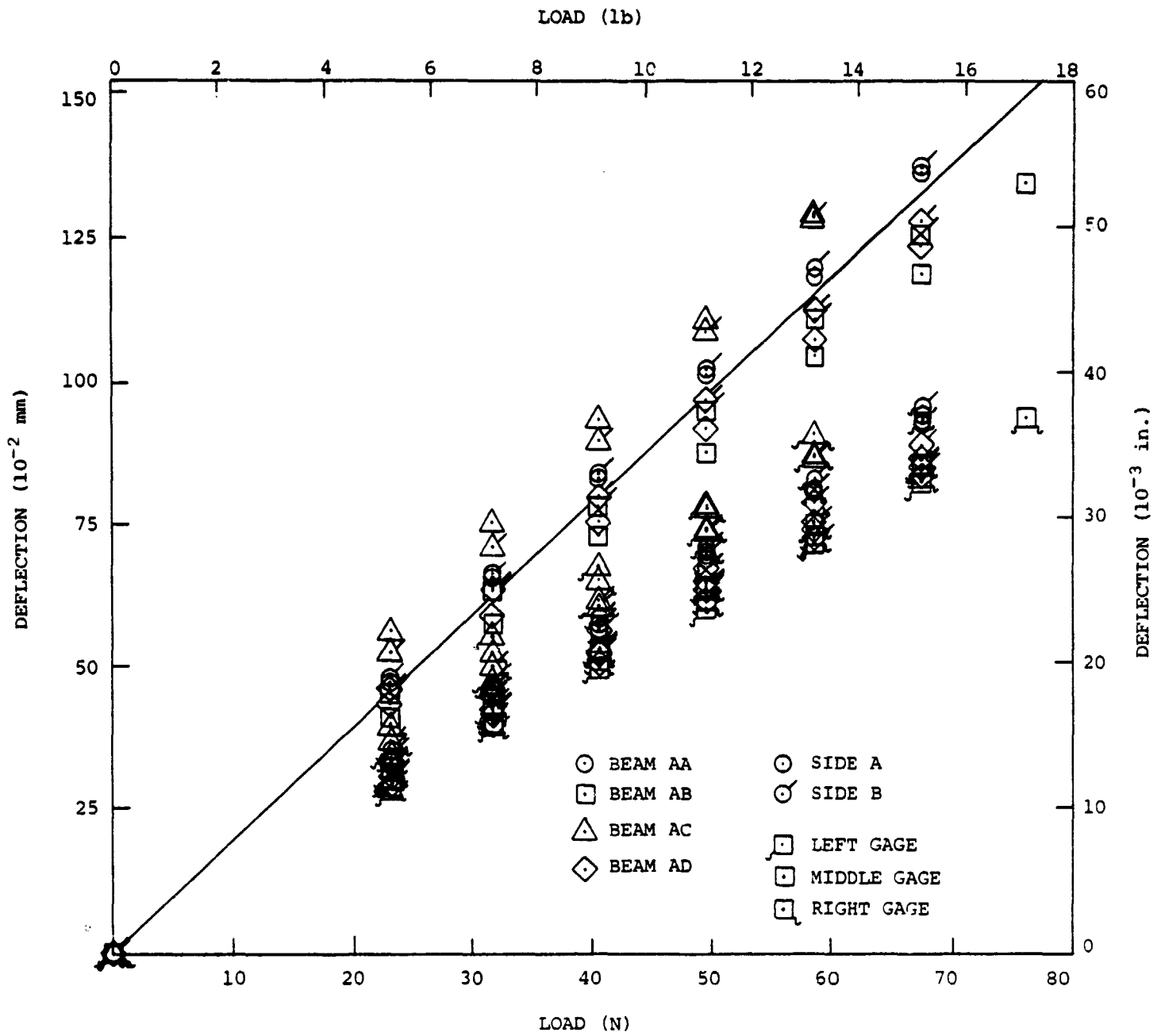
Figure 32. Load-deflection characteristics for three-point bending tests, all beams, L = 0.406 m (16.0 in.).
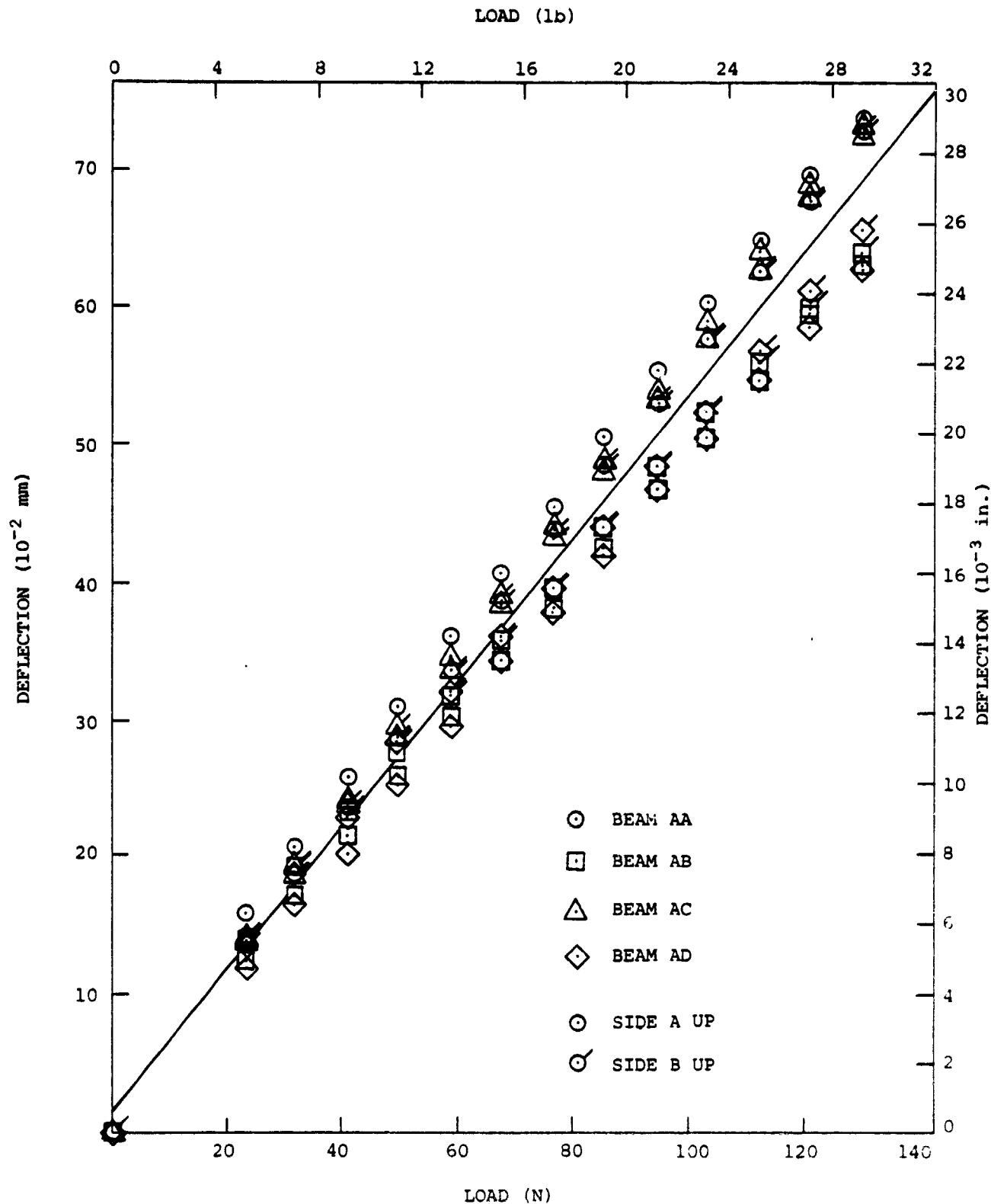
Figure 33. Load-deflection characteristics for three-point bending test, all beams, L = 0.254 m (10.0 in.).
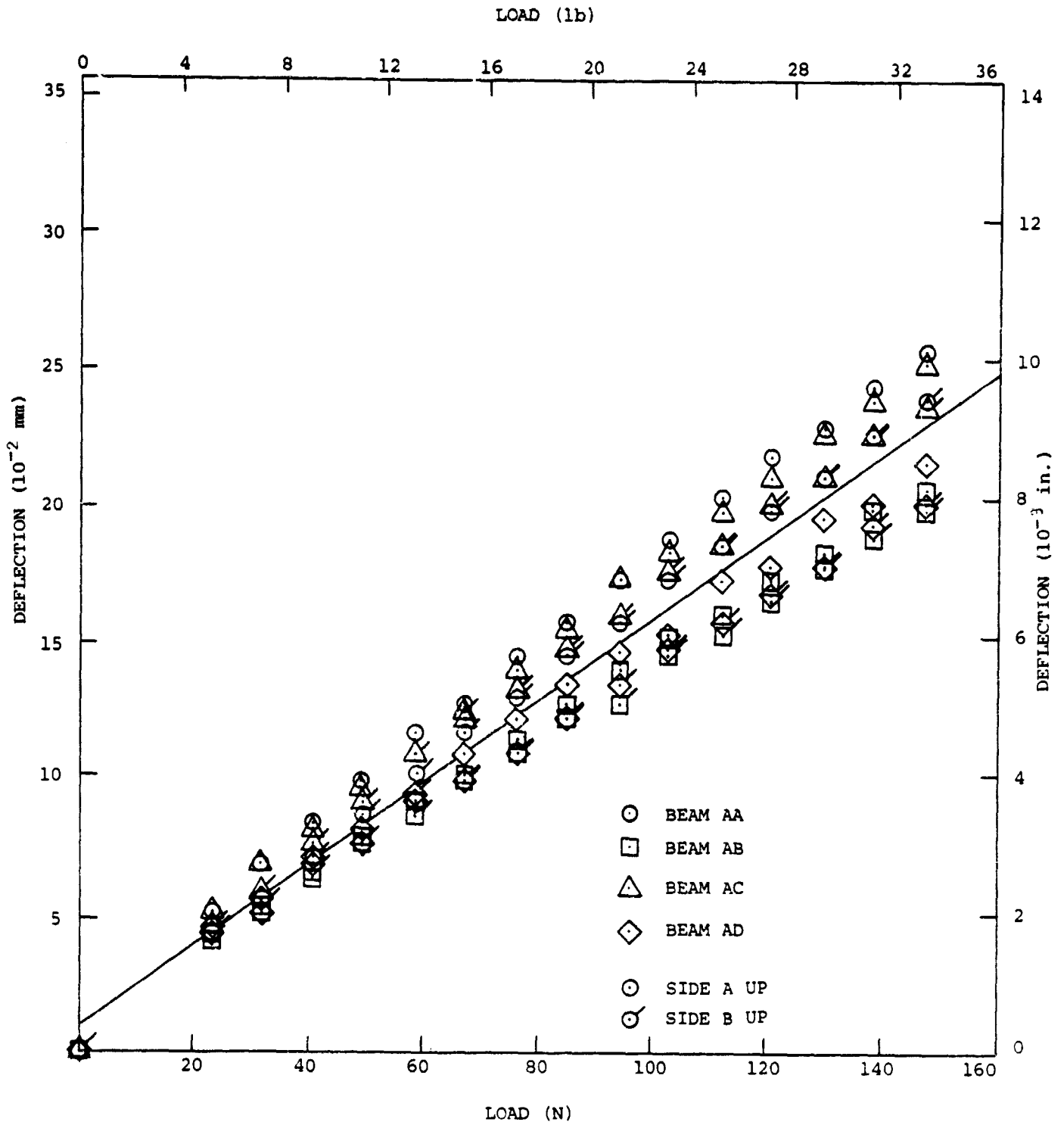
Figure 34. Load-deflection characteristics for three-point bending test, all beams, L = 0.152 m (6.00 in.)
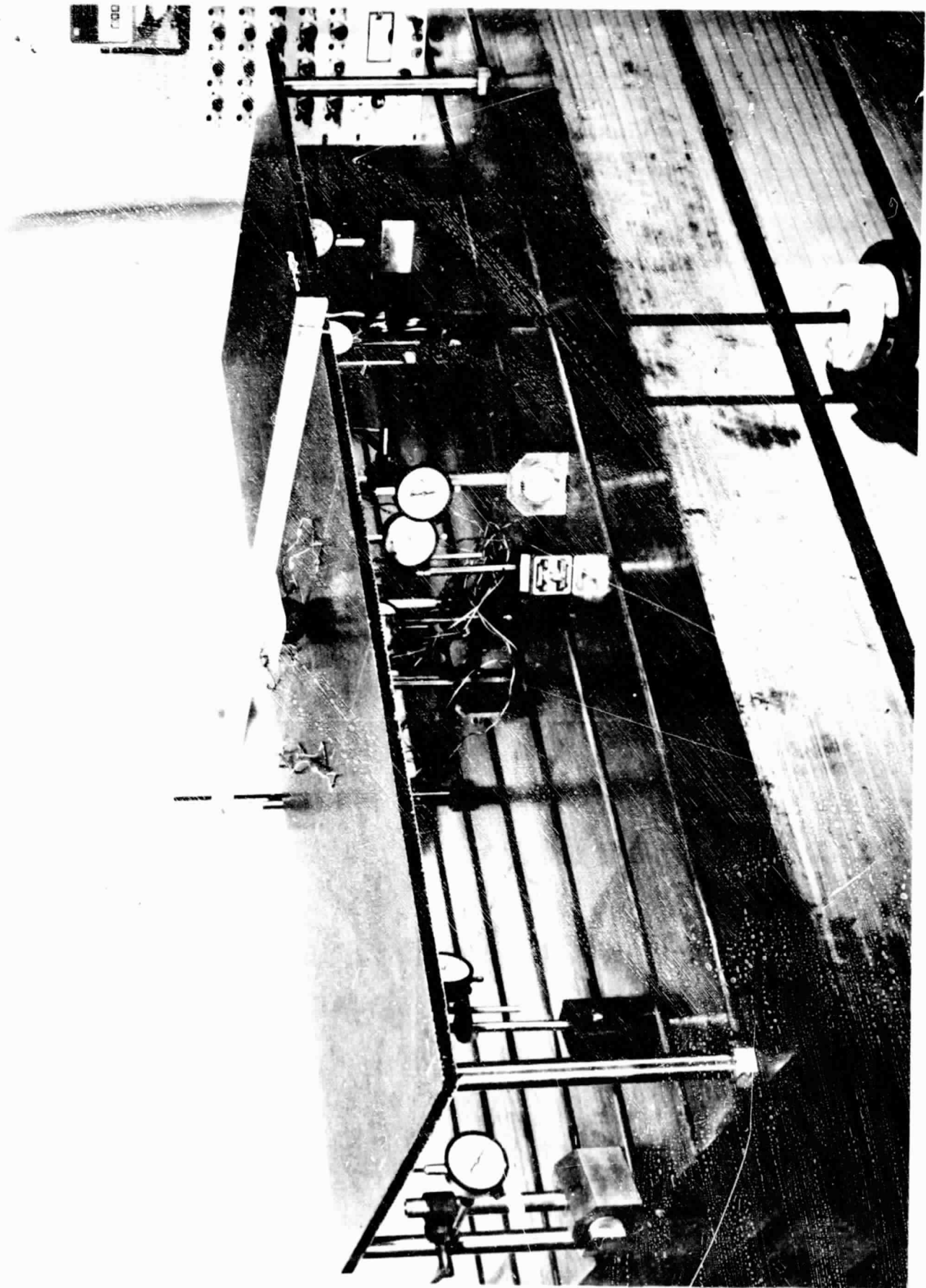
Figure 35. Plate bending test setup.

Distance between gage centerlines is 7.94 mm (0.312 in.) for gages
3 and 4, 7 and 8, 10 and 11, 14 and 15.

Distance between gage centerlines is 11.1 mm (0.438) for gages
1 and 2, 5 and 6, 12 and 13, 16 and 17.
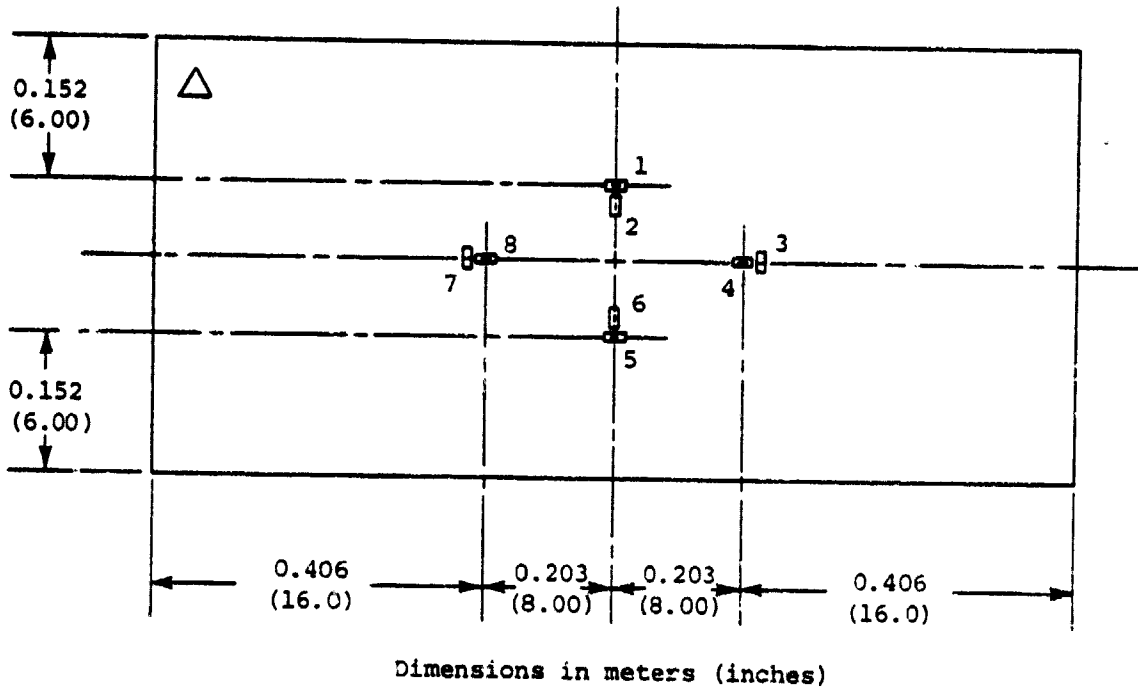
Dimensions in meters (inches)
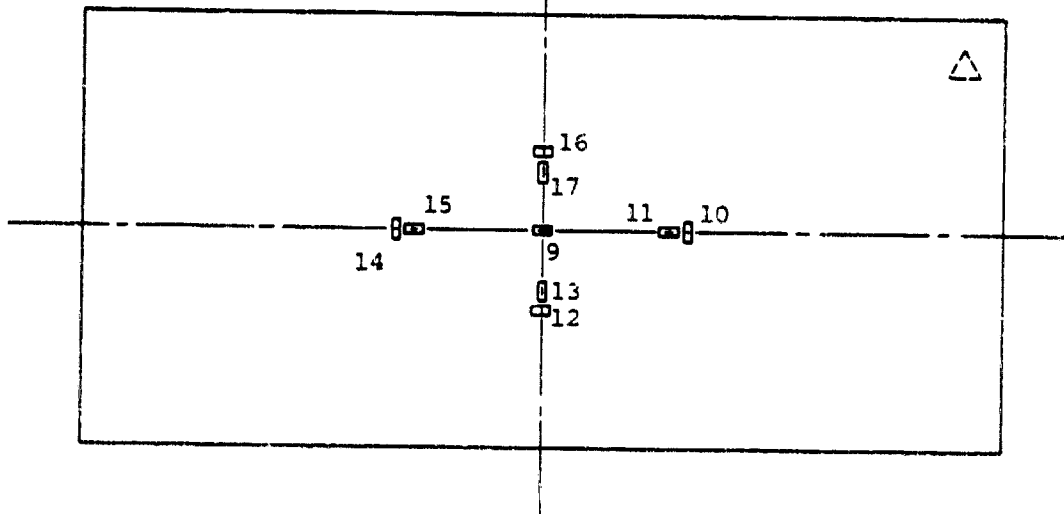
△ = guide to show panel orientation, coordinates with figure 37.

Figure 36. Strain gage locations and numbering for plate bending tests.
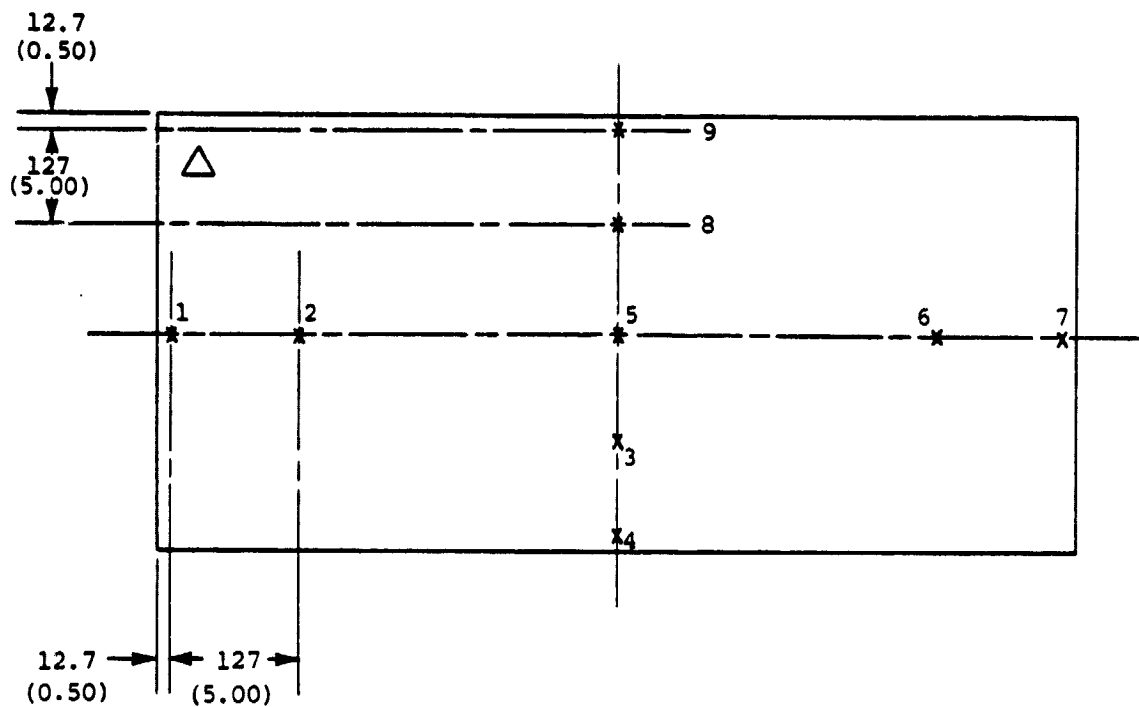
All dimensions in mm (inches)

△ = guide to show panel orientation, coordinates with figure 36.

Figure 37.   Dial gage locations and numbering for plate bending tests.

LOAD (lb)
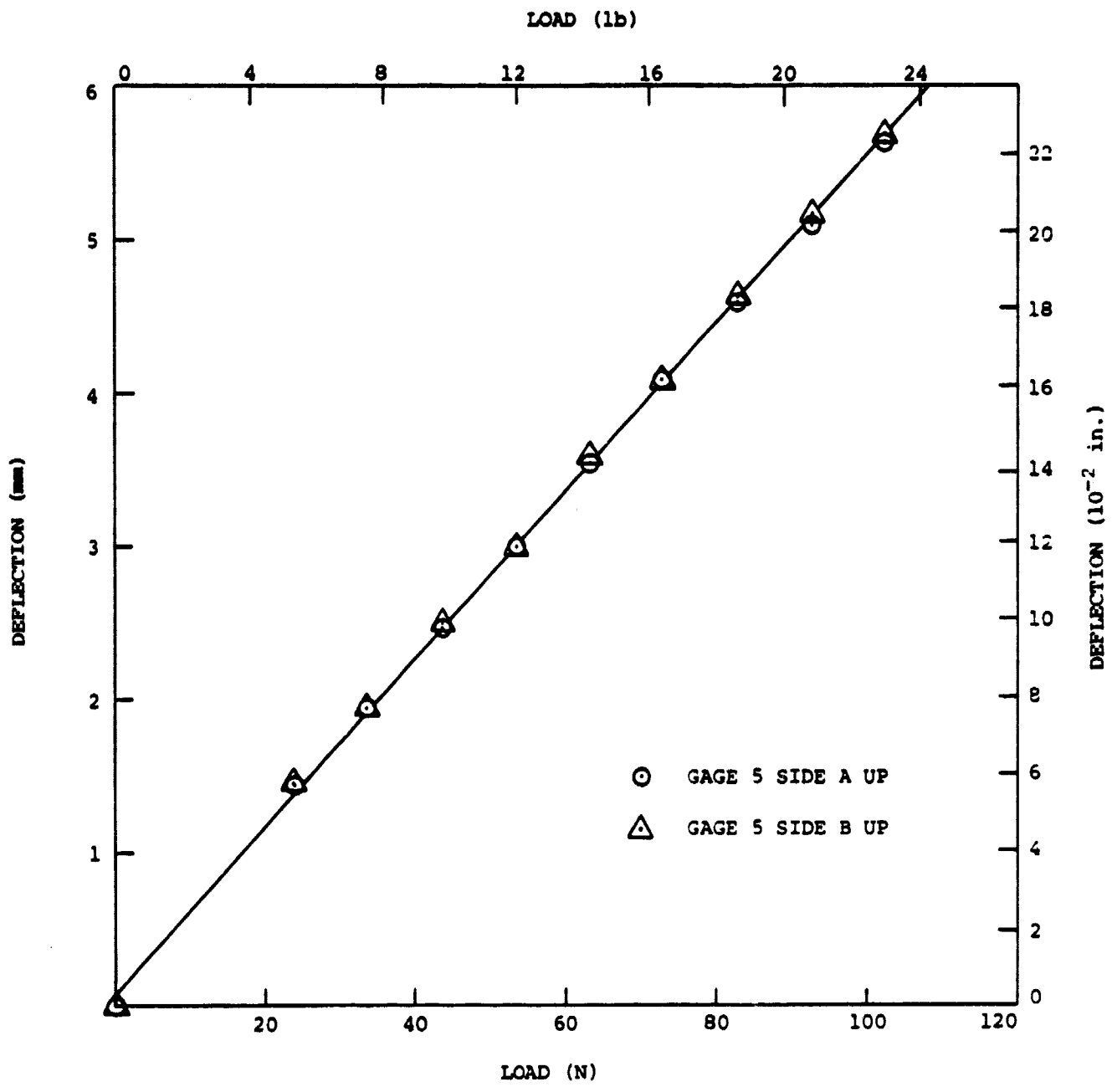
Figure 38. Load-midpanel (gage 5) deflection characteristics for
            plate bending test.
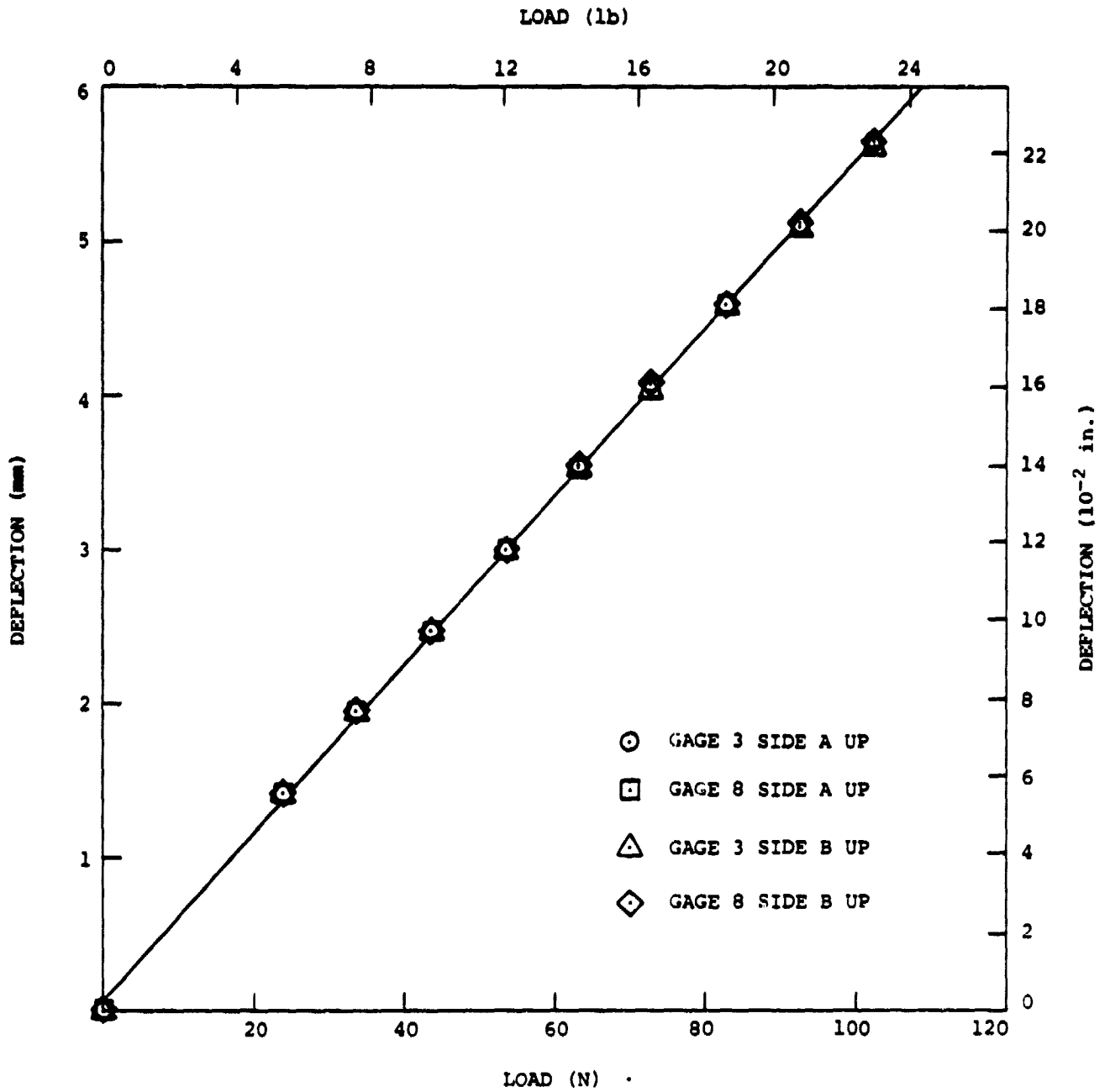
Figure 39. Load-deflection characteristics for plate bending test, gages 3 and 8.

LOAD (lb)
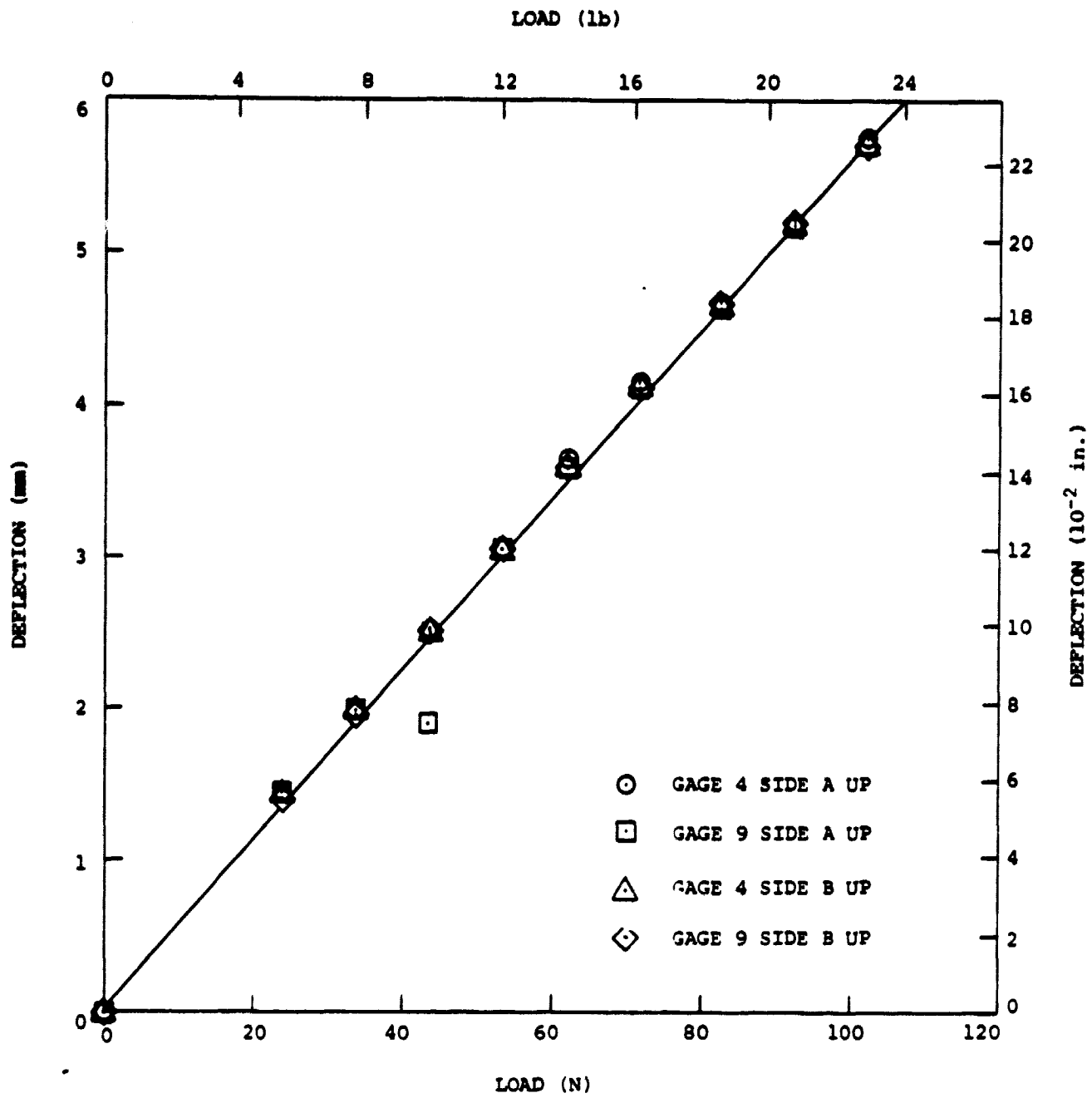
Figure 40. Load-deflection characteristics for plate bending test,
gages 4 and 9.

LOAD (lb)
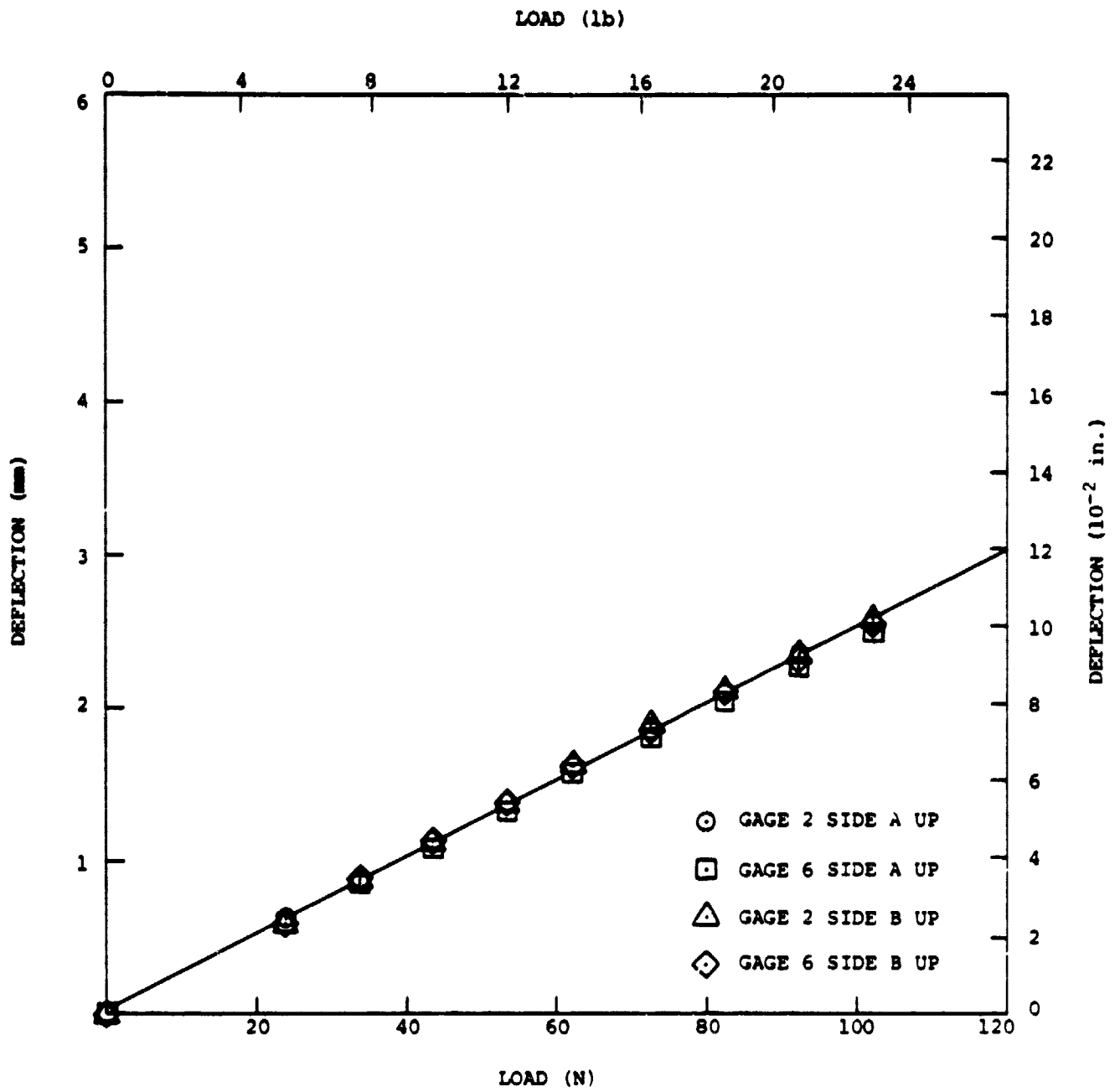
Figure 41. Load-deflection characteristics for plate bending test, gages 2 and 6.

LOAD (lb)
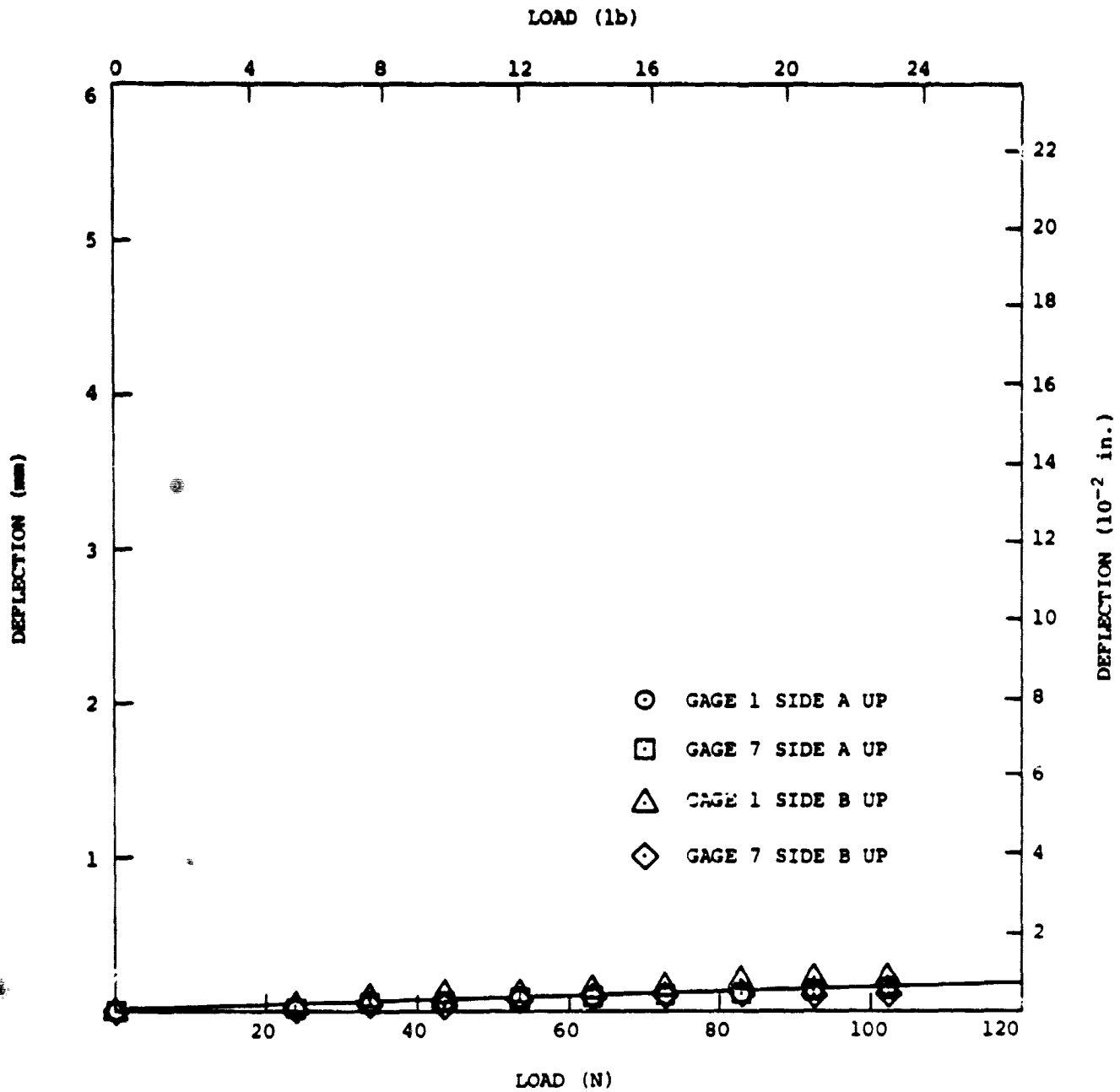
Figure 42. Load-deflection characteristics for plate bending test, gages 1 and 7.

LOAD (N)
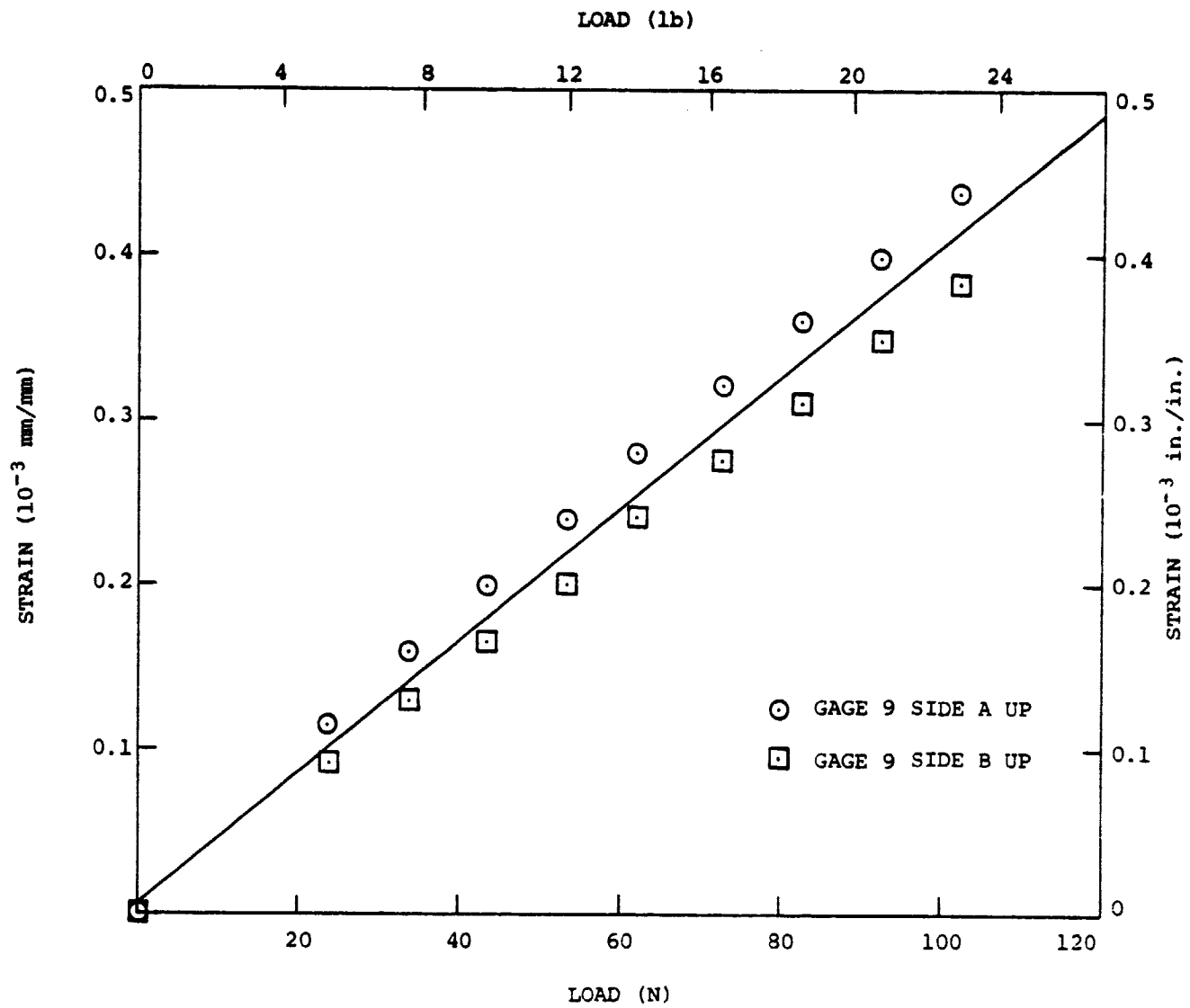
Figure 43. Load-bending strain characteristics for plate bending test, gage 9.
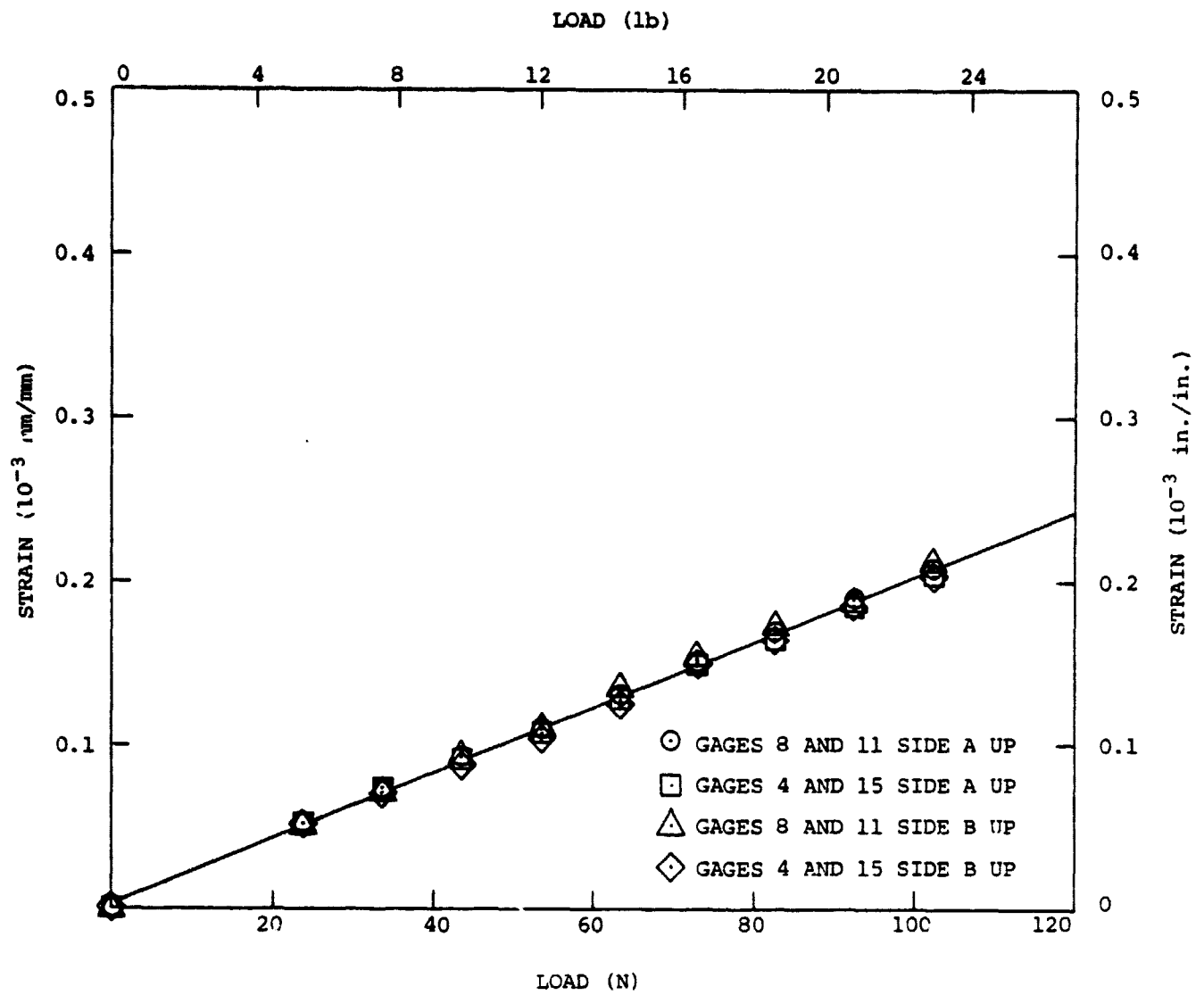
Figure 44. Load-bending strain characteristics for plate bending test, gages 4, 8, 11, and 15.

LOAD (lb)
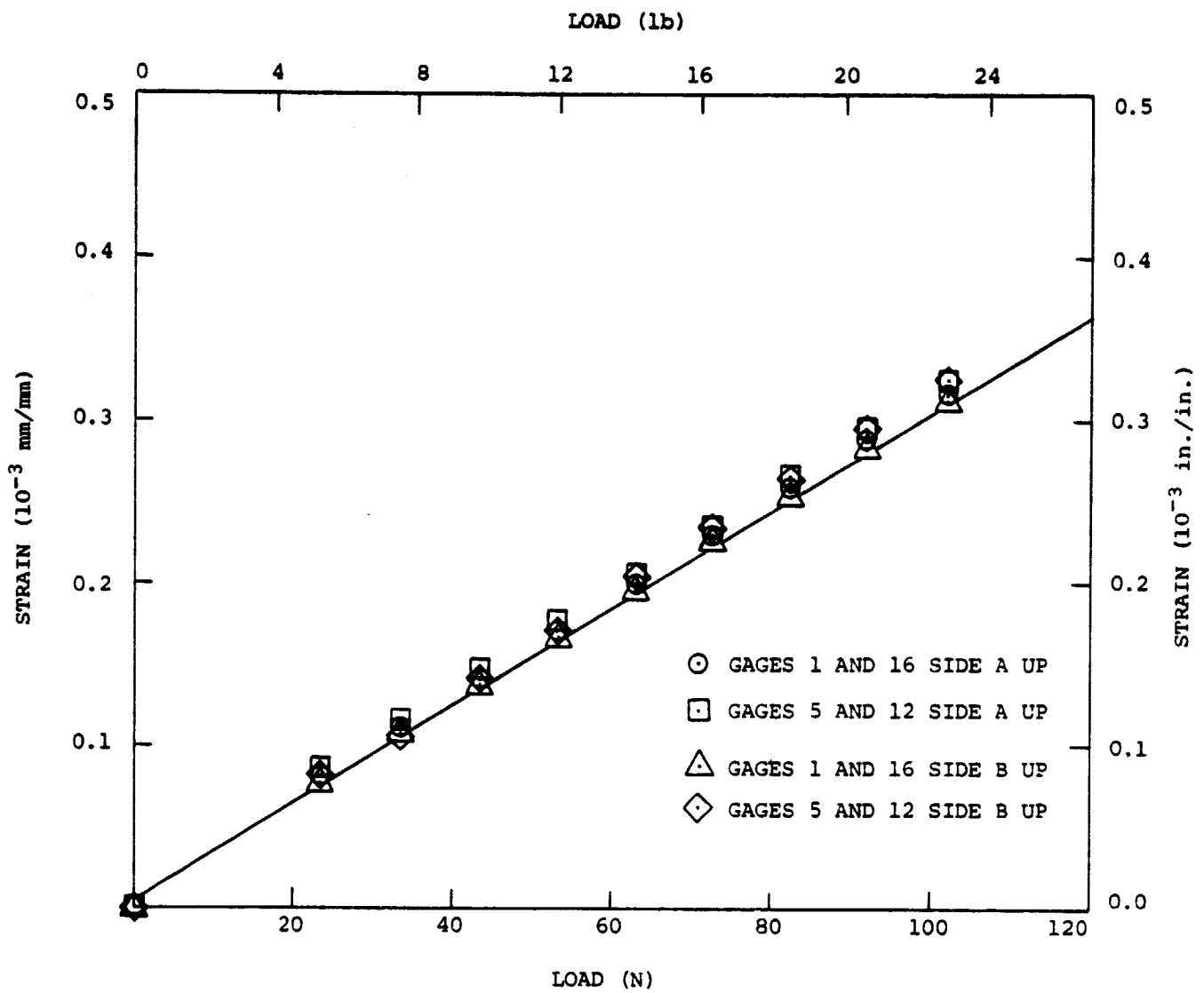
Figure 45. Load-bending strain characteristics for plate bending test, gages 1, 5, 12, and 16.
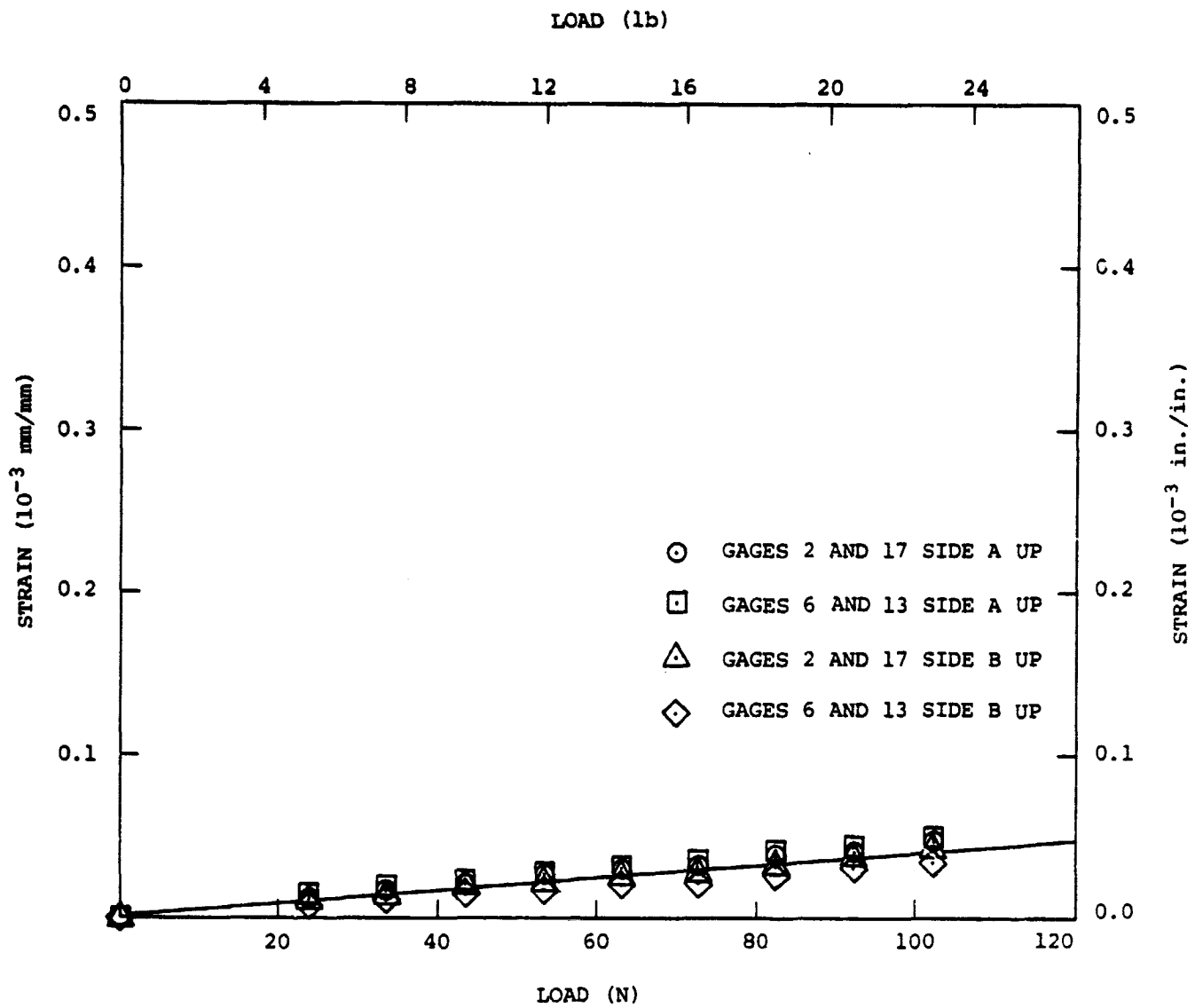
Figure 46. Load-bending strain characteristics for plate bending test, gages 2, 6, 13, and 17.
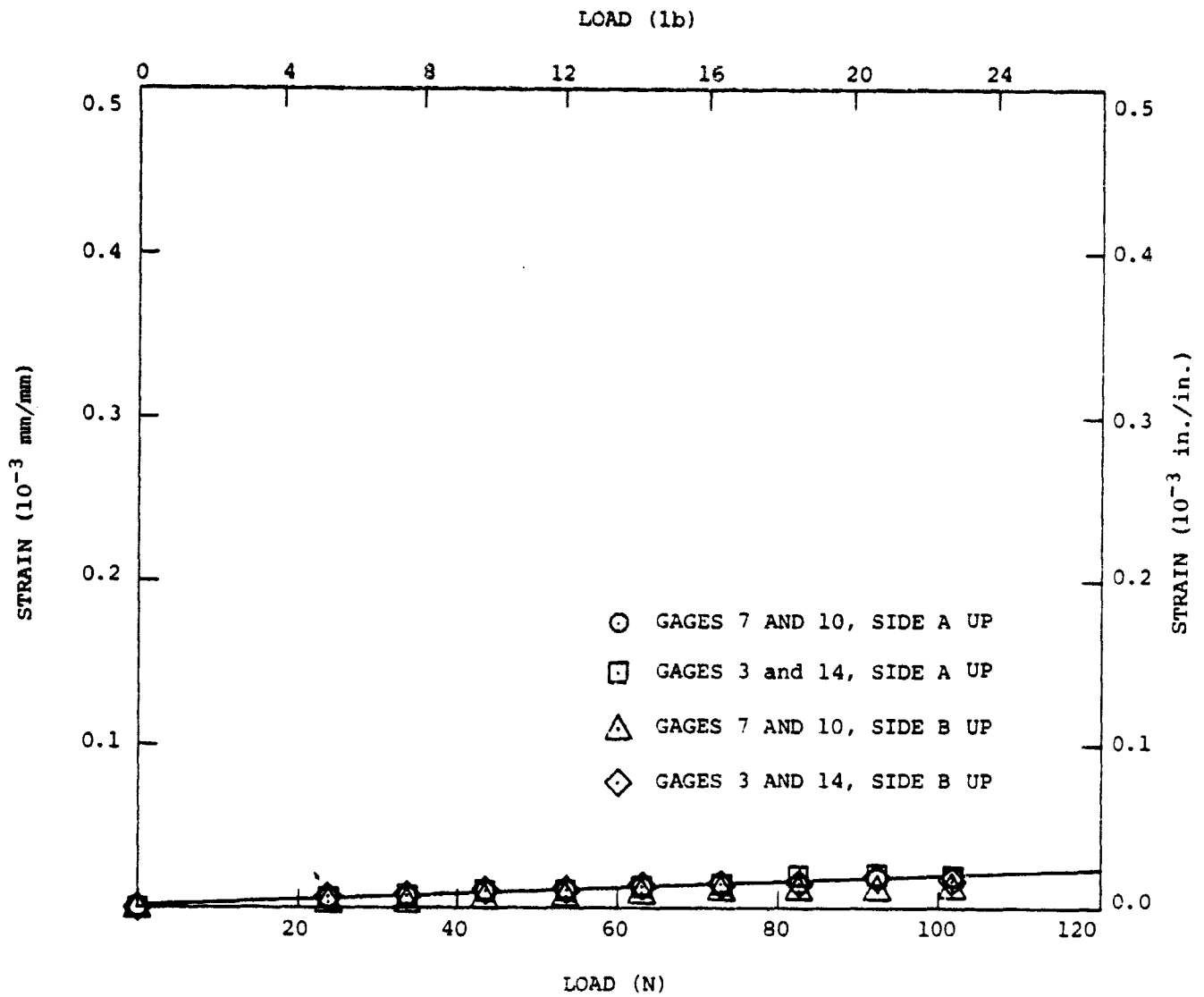
Figure 47. Load-bending strain characteristics for plate bending test,
gages 3, 7, 10, and 14.
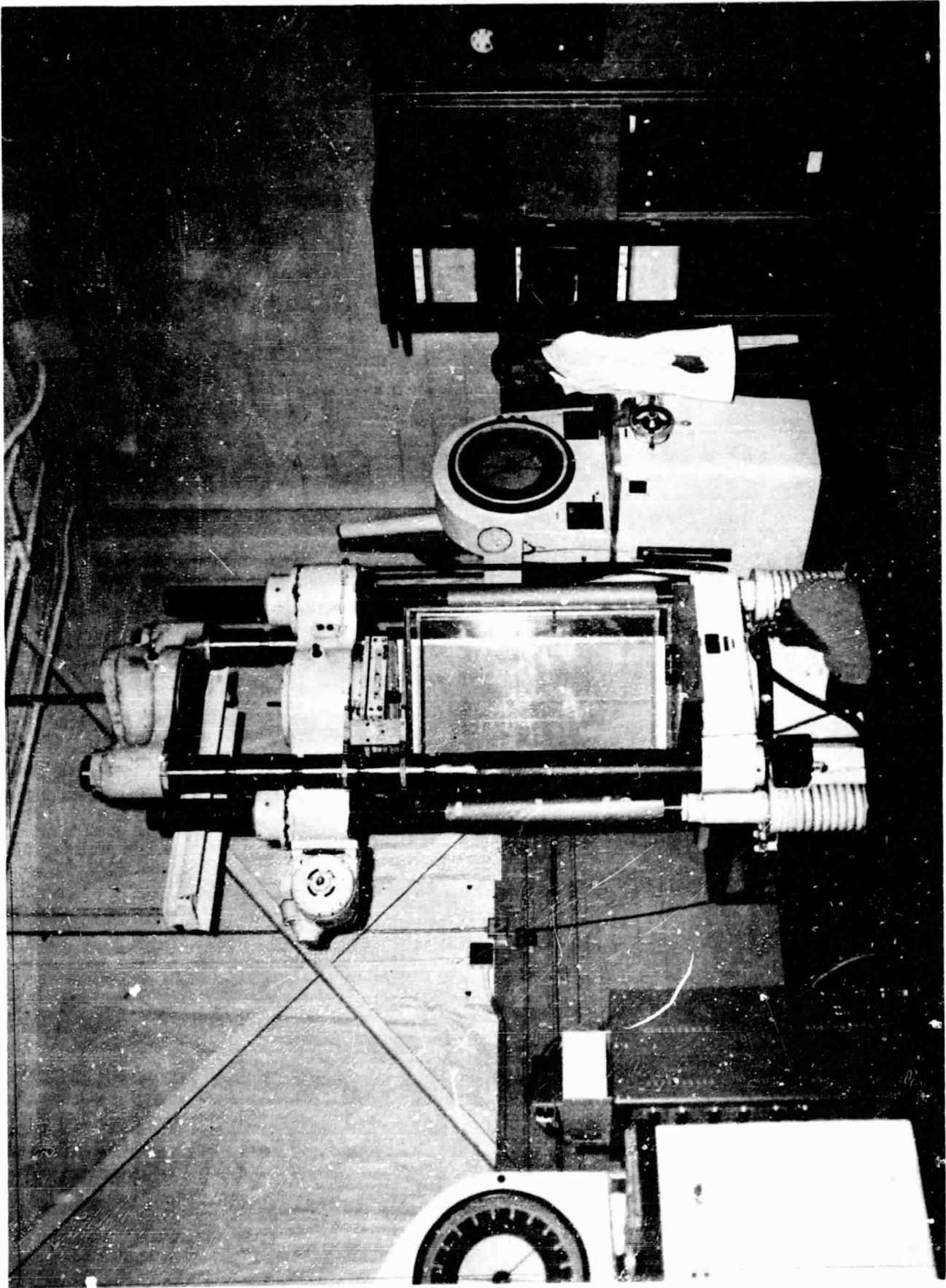
Figure 48. Panel stability test setup.
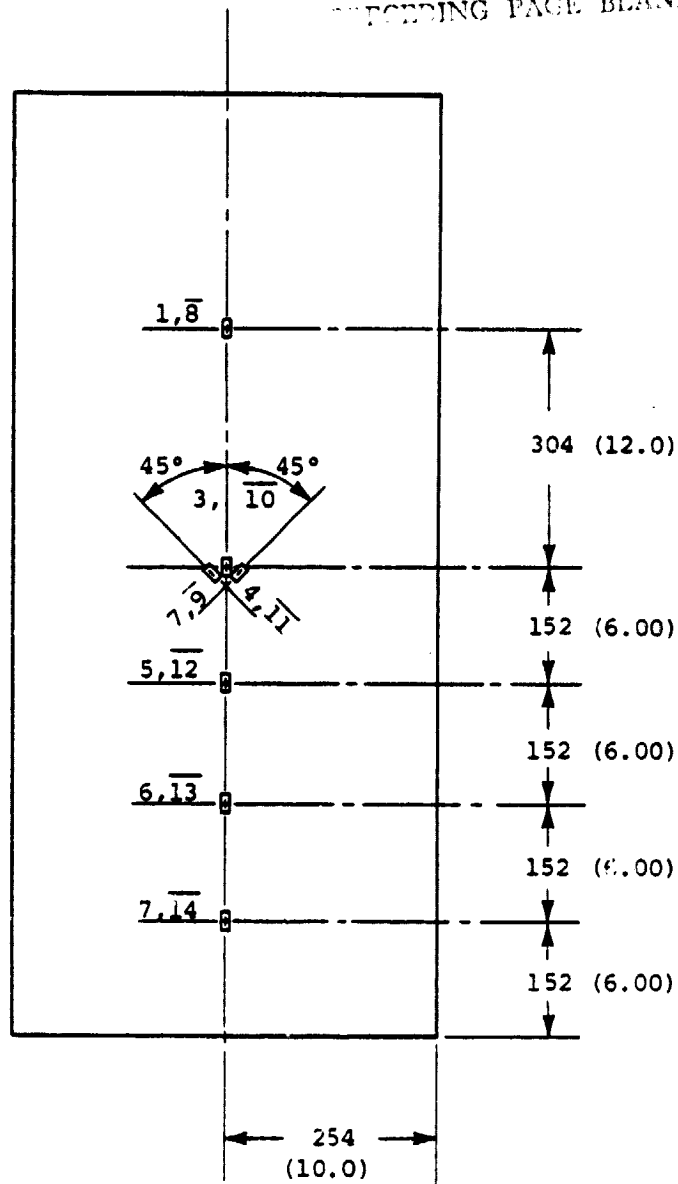
dimensions in mm (in.)

overbarred number means gage is on backside of panel

Figure 49.   Strain gage locations and numbering for
             panel stability tests.
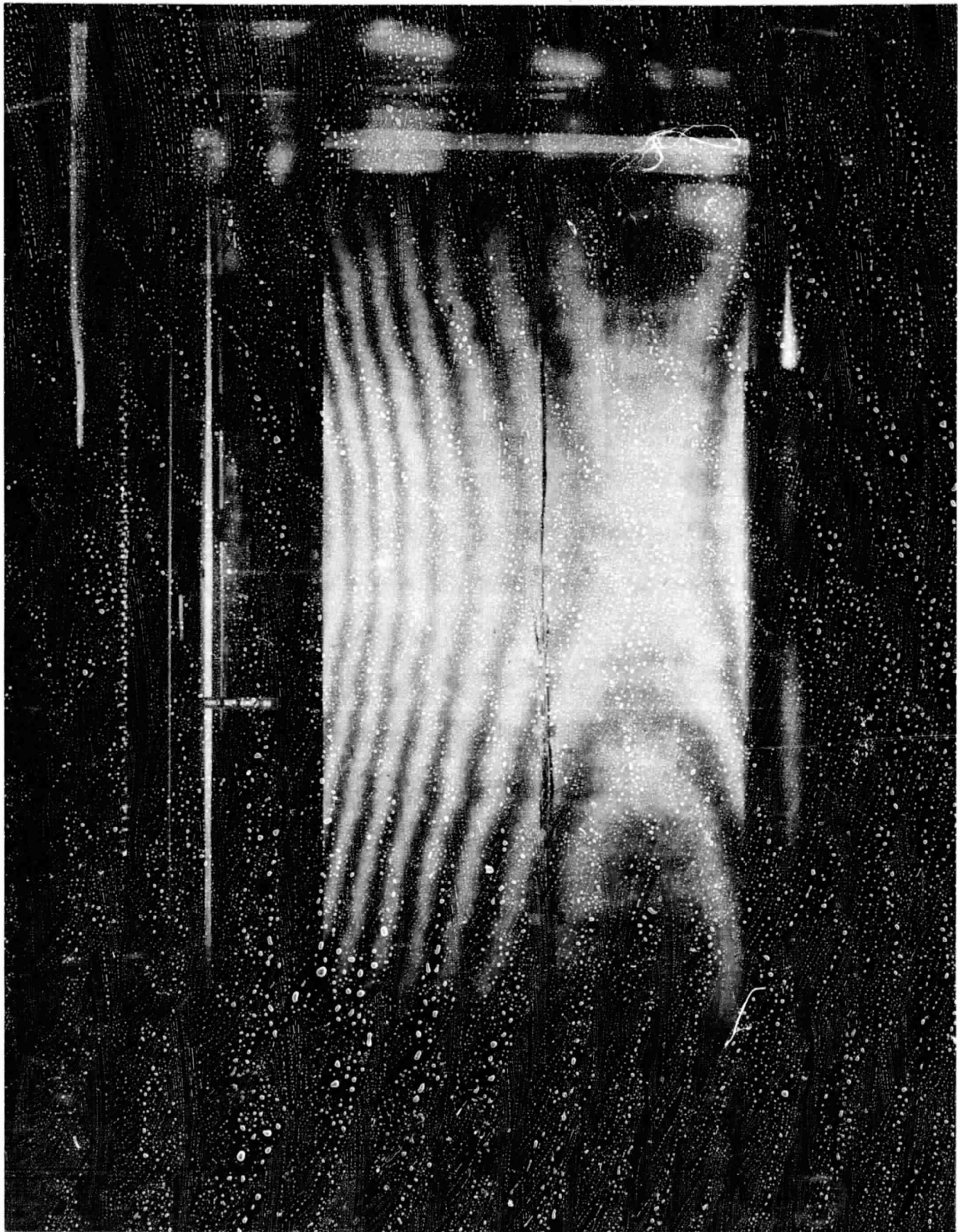
Figure 50. No-load shadow Moiré fringe pattern for
wide column panel.

OUT-OF-PLANE DISPLACEMENT, in.
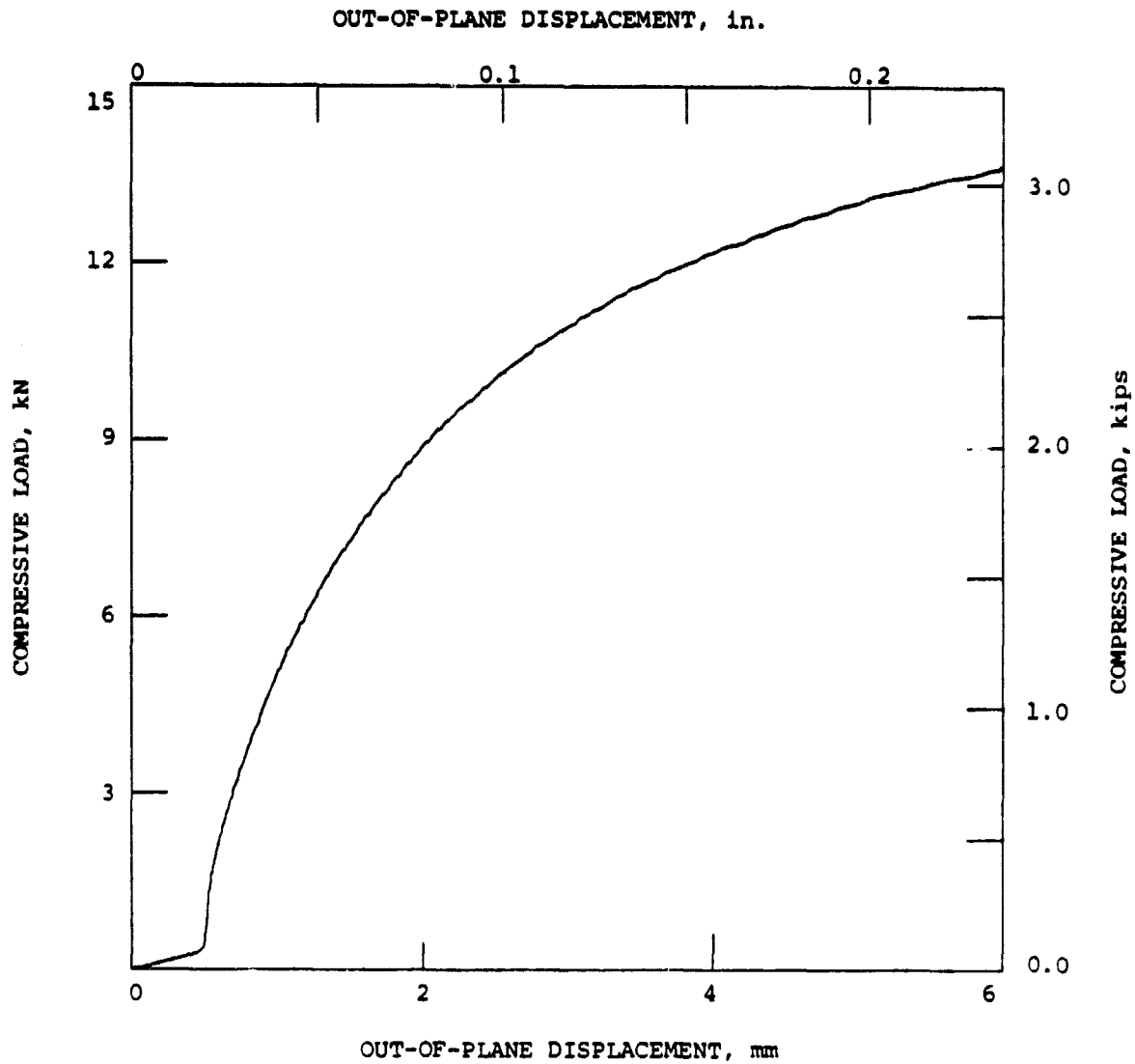
Figure 51.   Load-out-of-plane displacement characteristics,
            wide column panel.
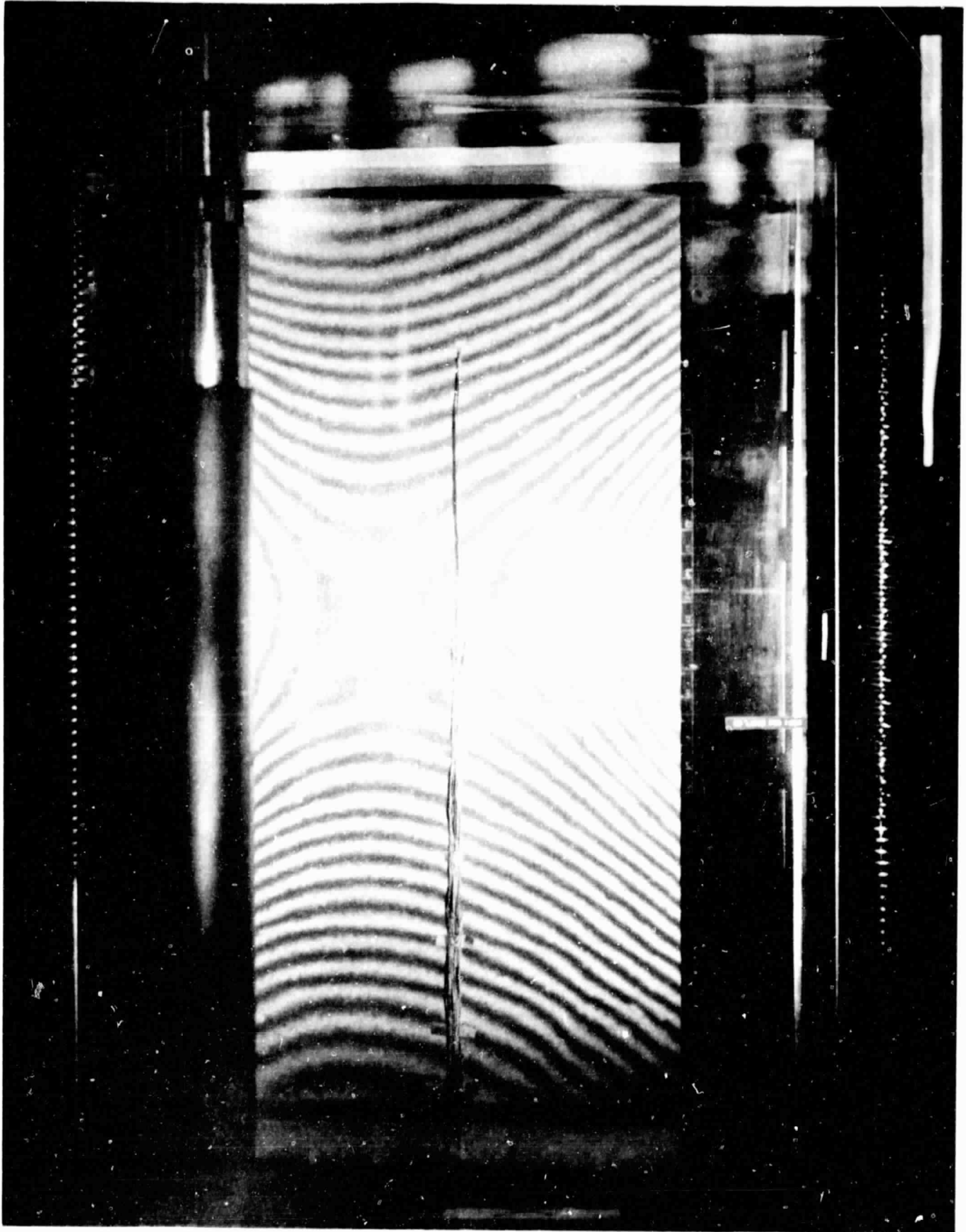
Figure 52.   Shadow Moiré fringe pattern for
wide column panel, maximum load.

99
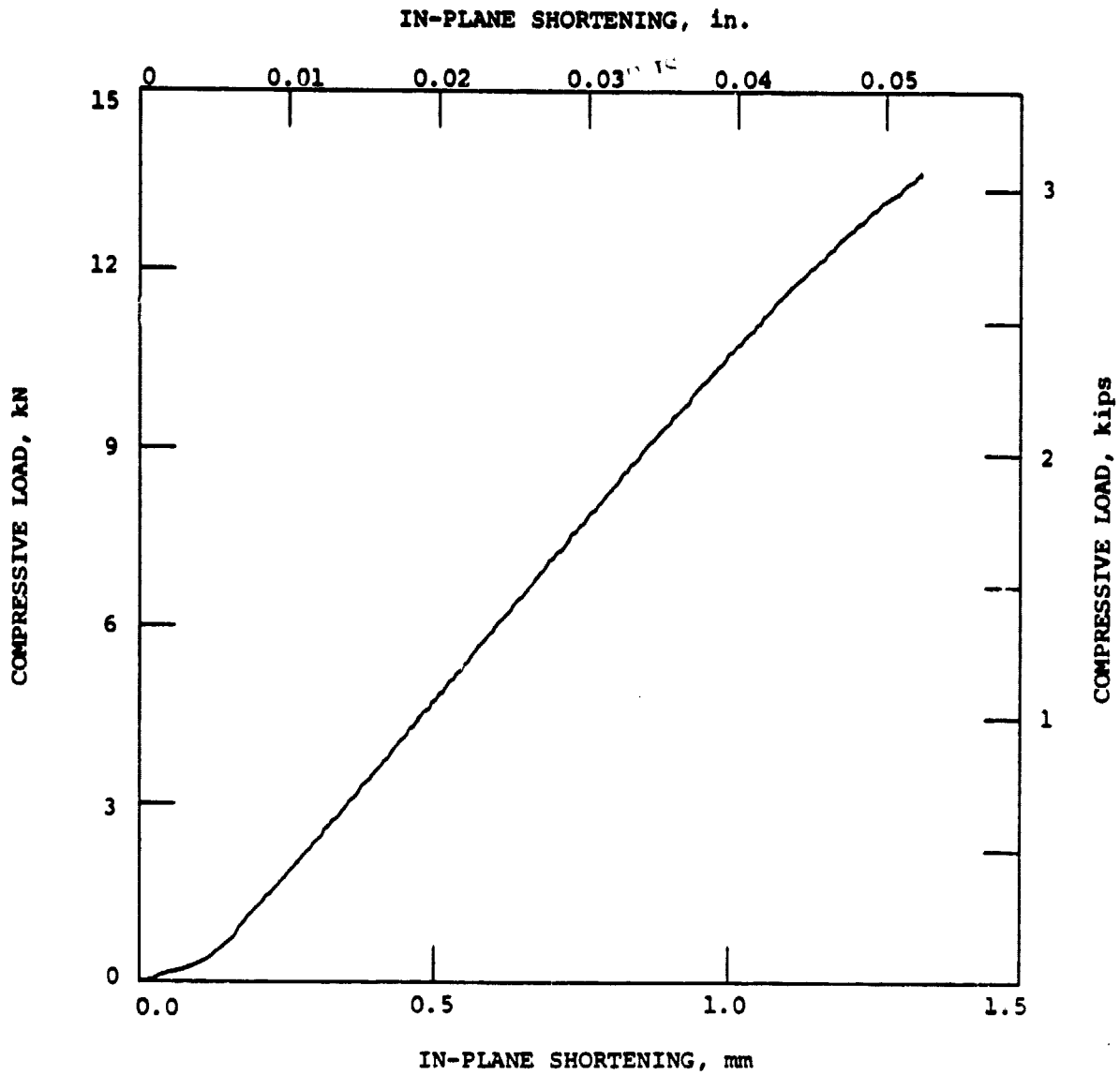
Figure 53. Load-in-plane displacement characteristics,
wide column panel.
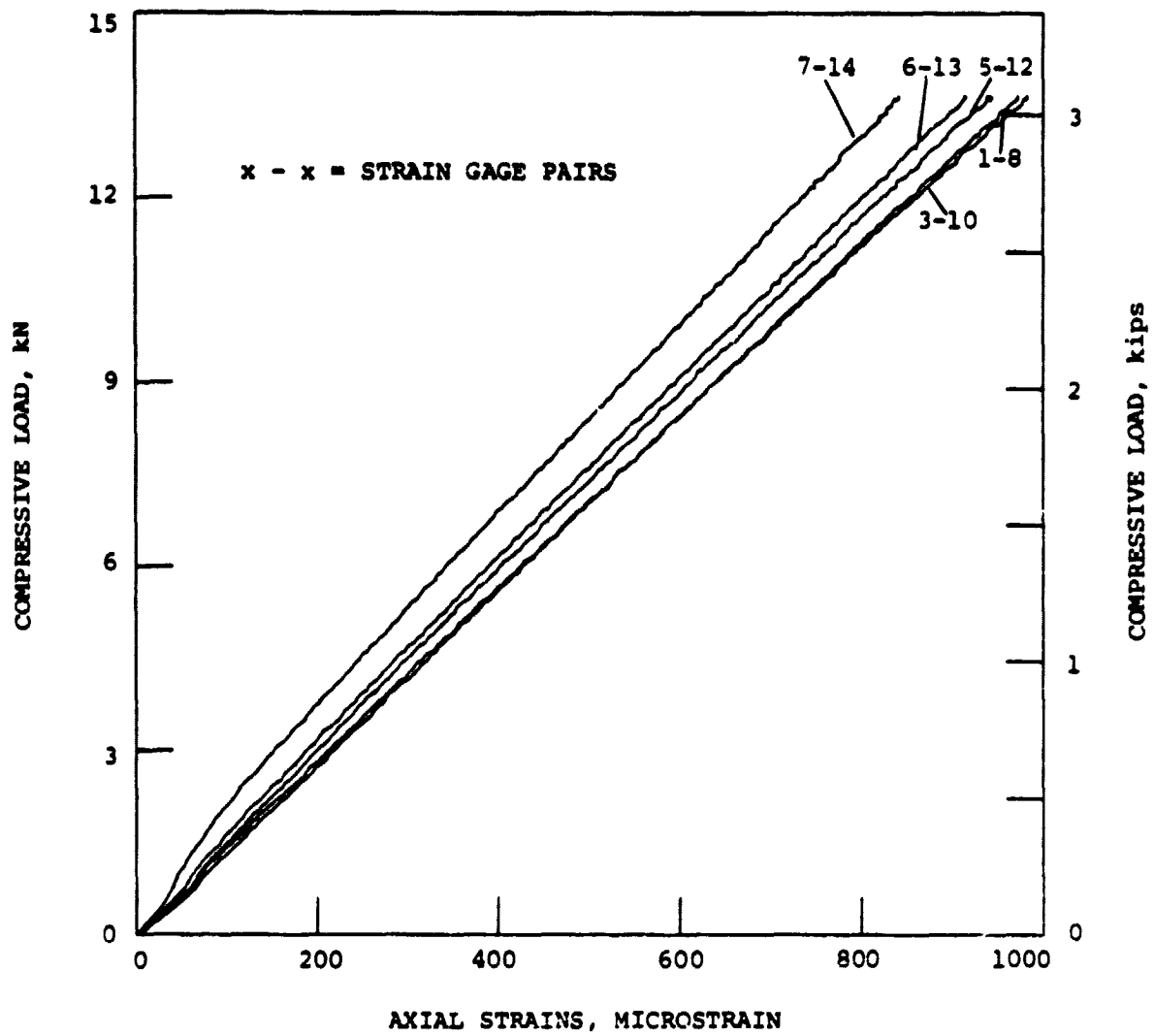
Figure 54. Load-in-plane axial strain characteristics,
wide column panel.
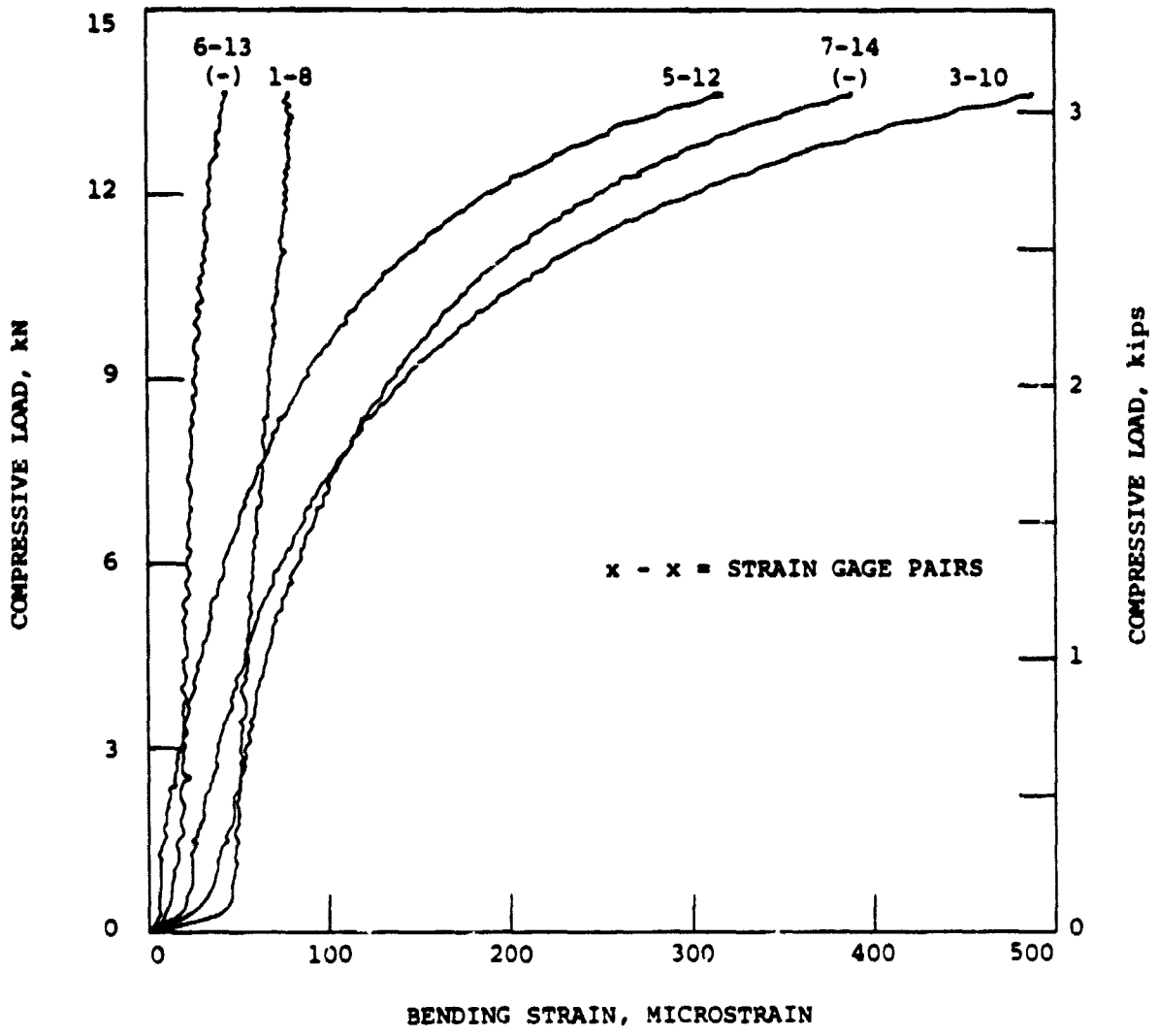
Figure 55.   Load-bending strain characteristics,
wide column panel.
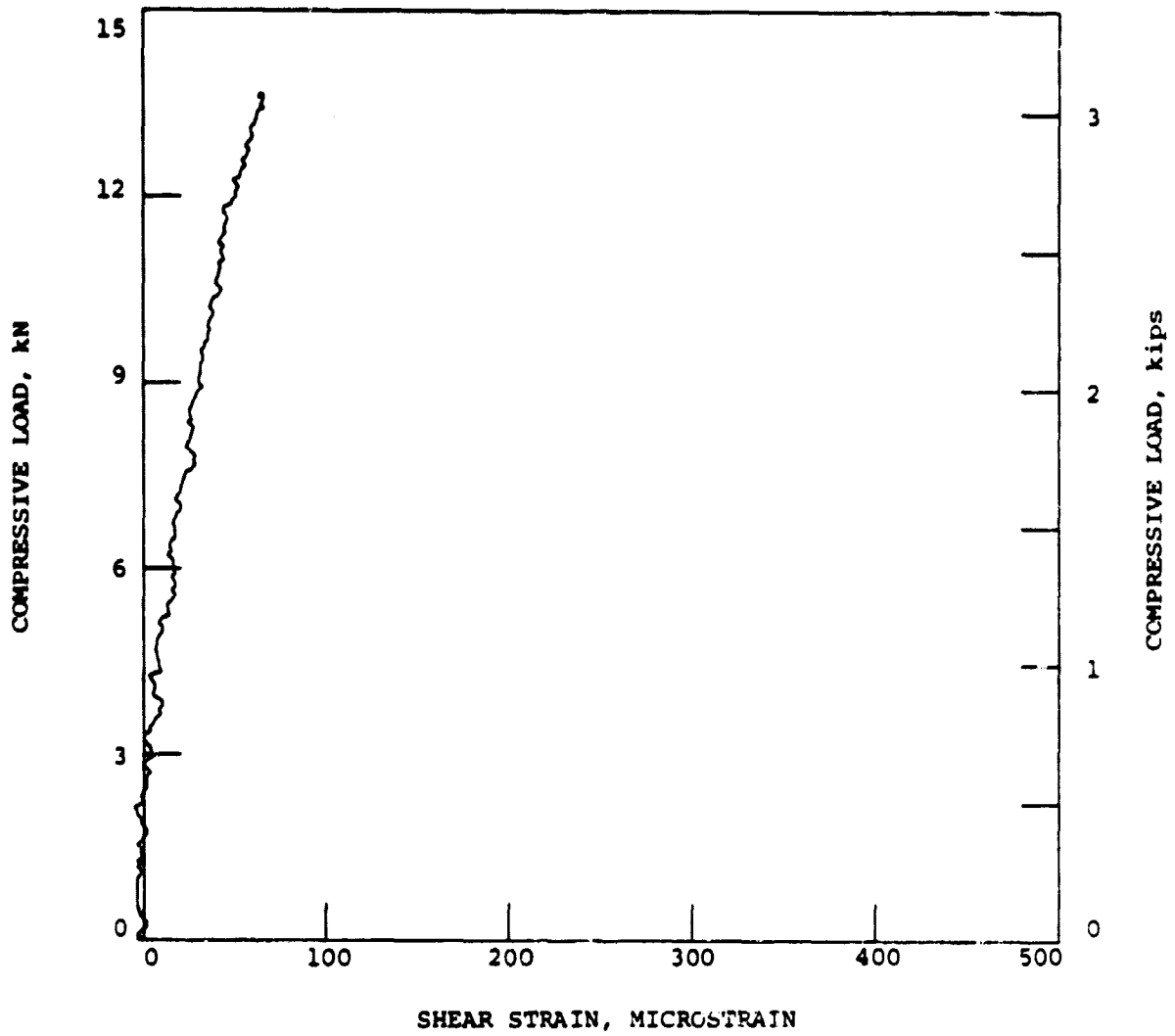
Figure 56.   Load-in-plane shear strain characteristics,
wide column panel.
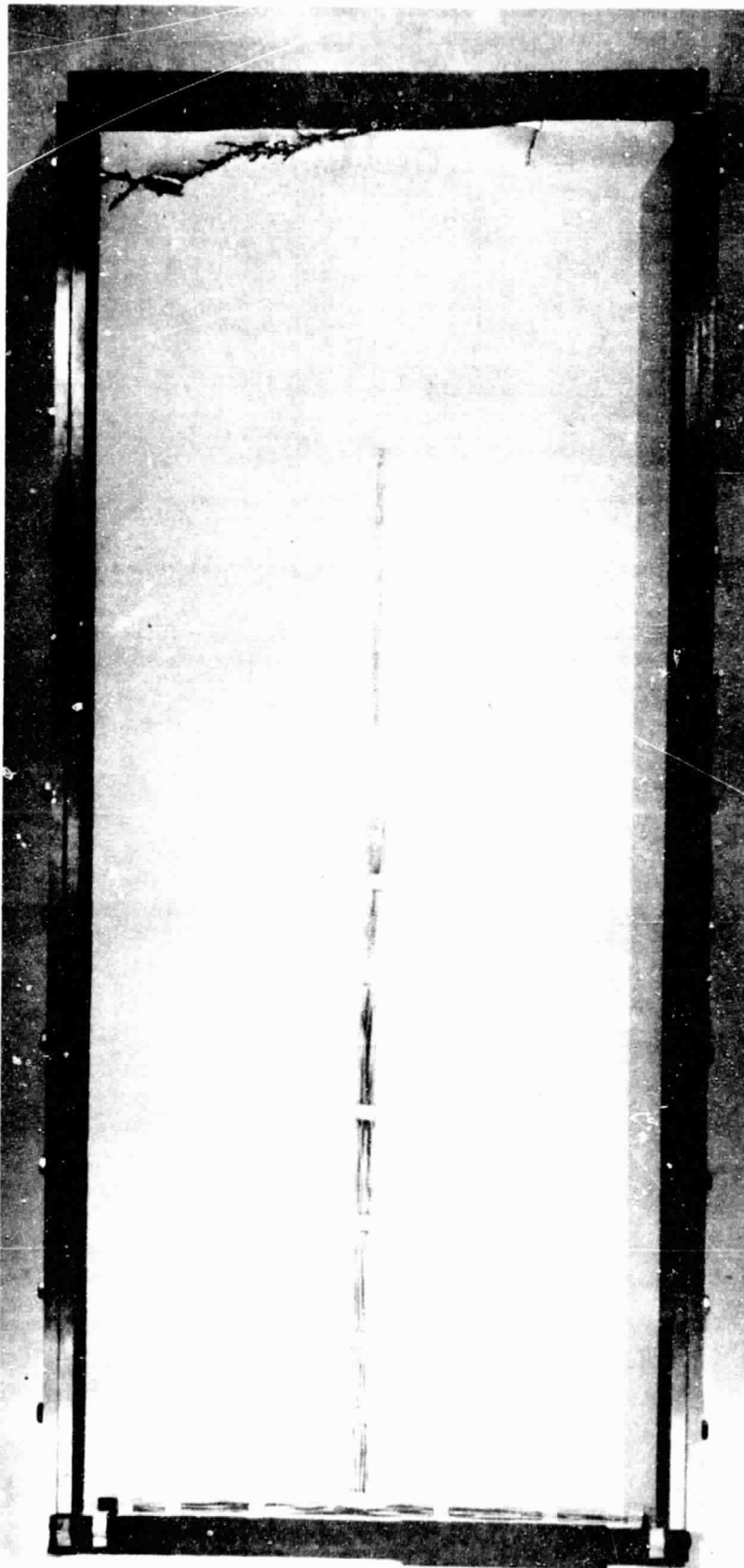
Figure 57. Failure of panel with supported edges, overall view.
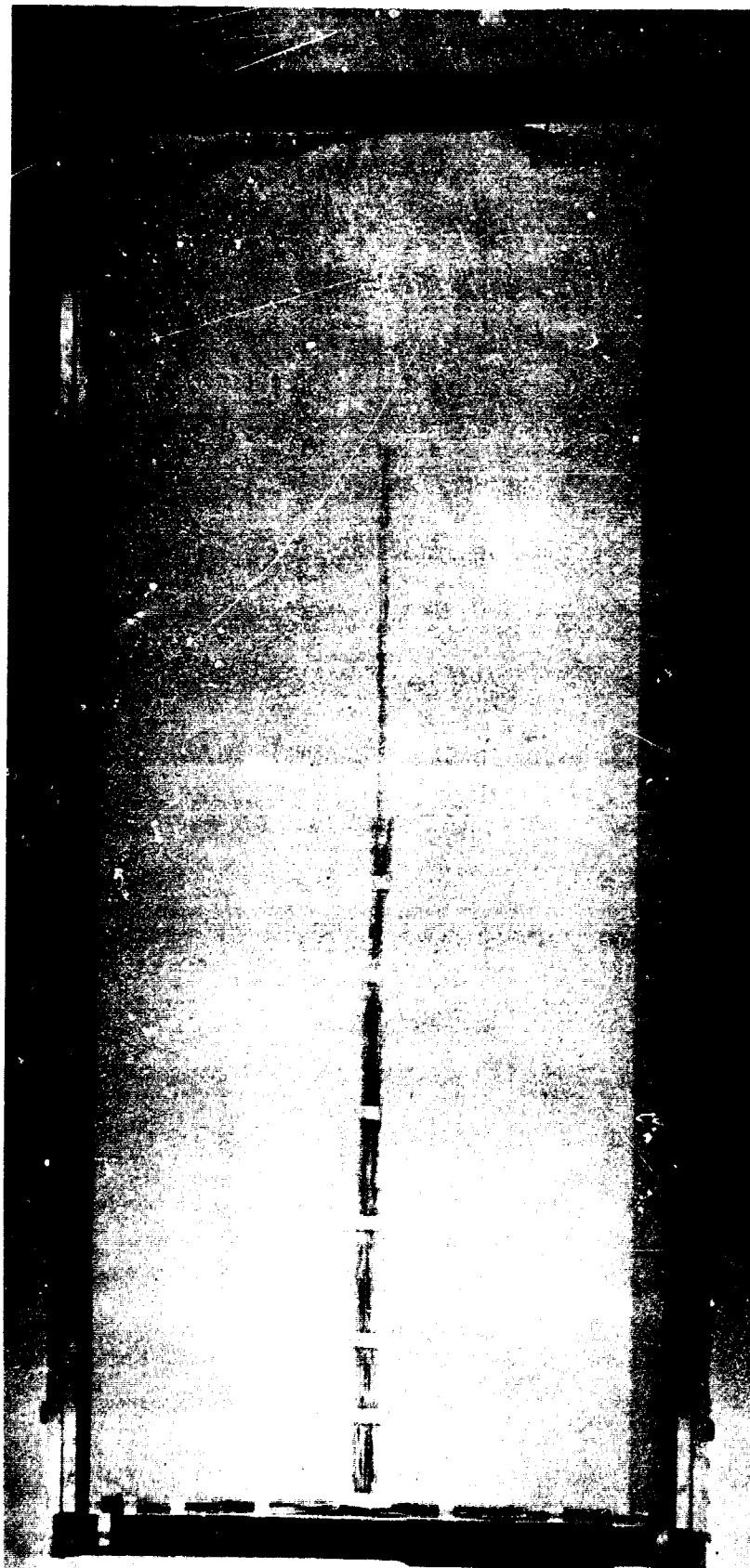
Figure 57. Failure of panel with supported edges, overall view.

Figure 58. Failure of panel with supported edges, closeup view.
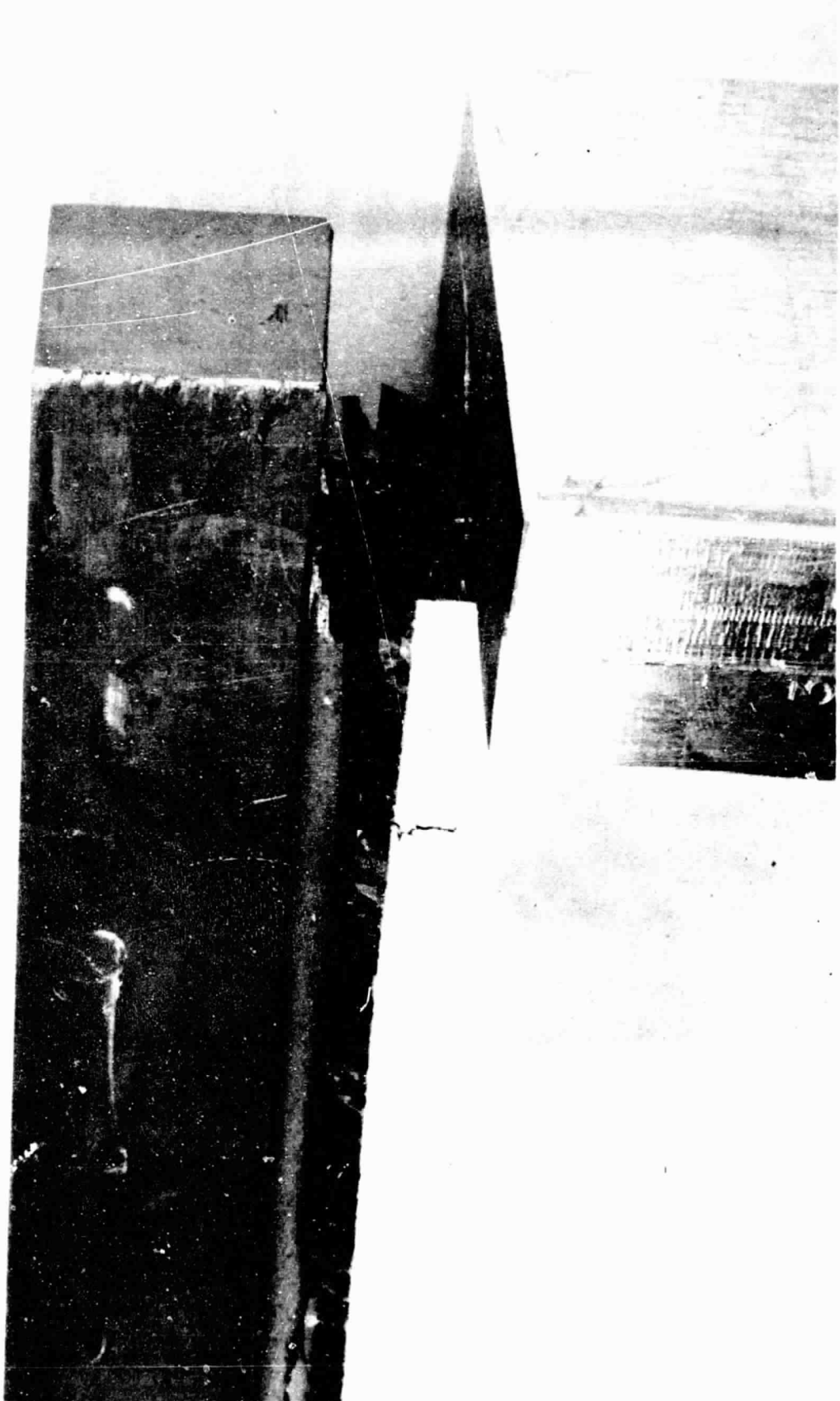
Figure 59. Failure of panel with supported edges, view of honeycomb damages.
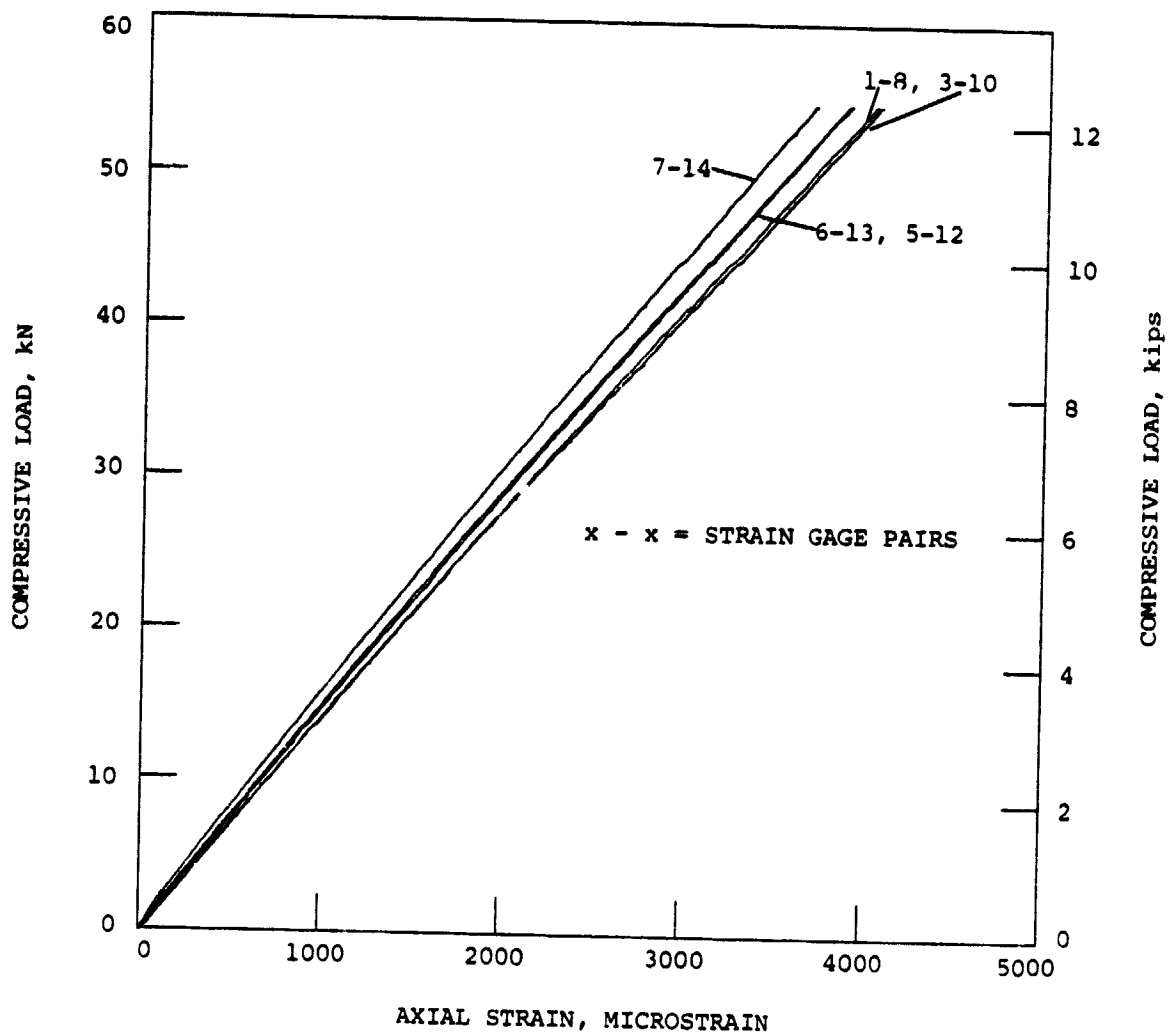
Figure 60. Load-in-plane axial strain characteristics,
            panel with supported edges.

IN-PLANE SHORTENING, in.
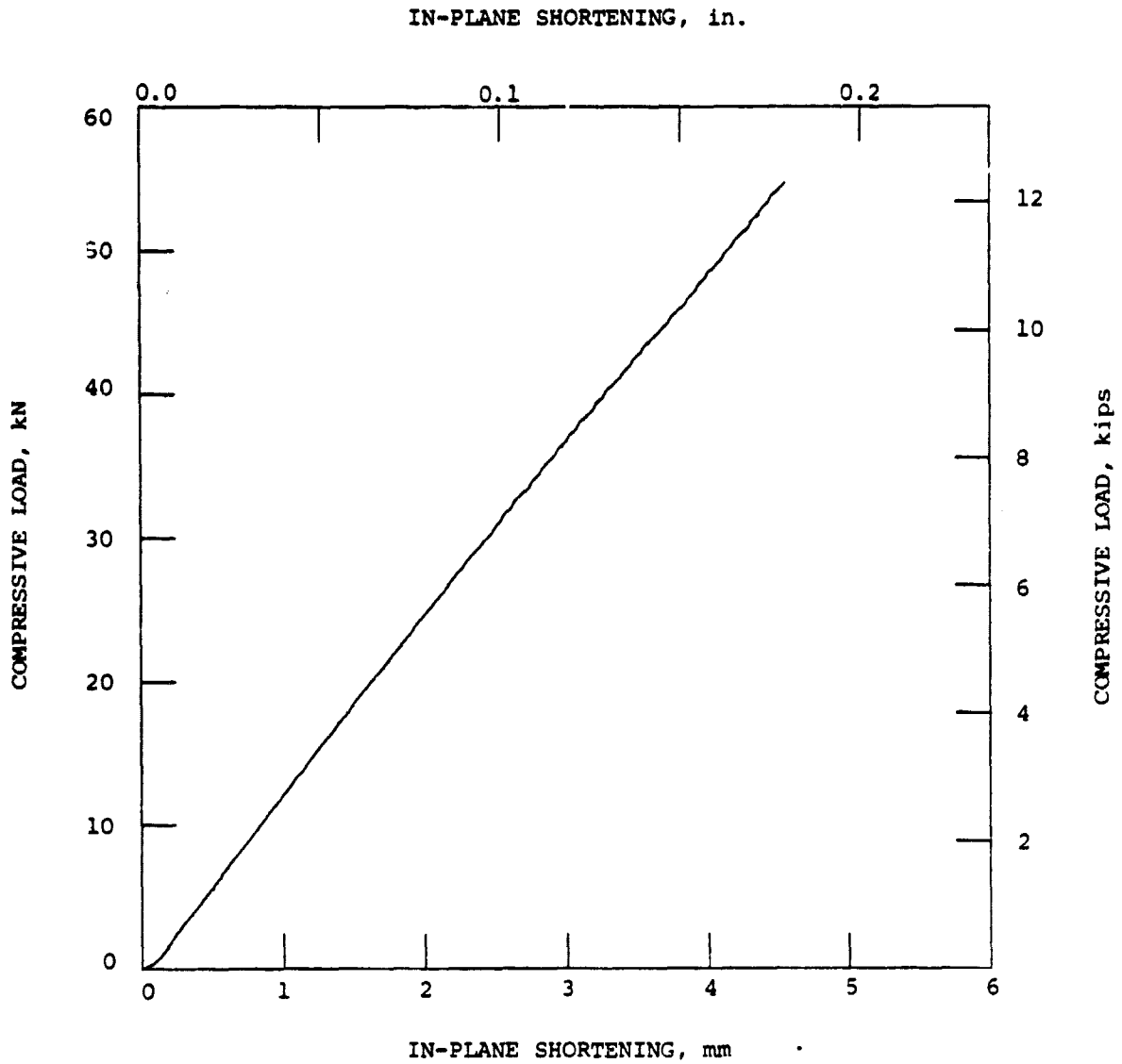
Figure 61. Load-in-plane displacement characteristics, panel with supported edges.

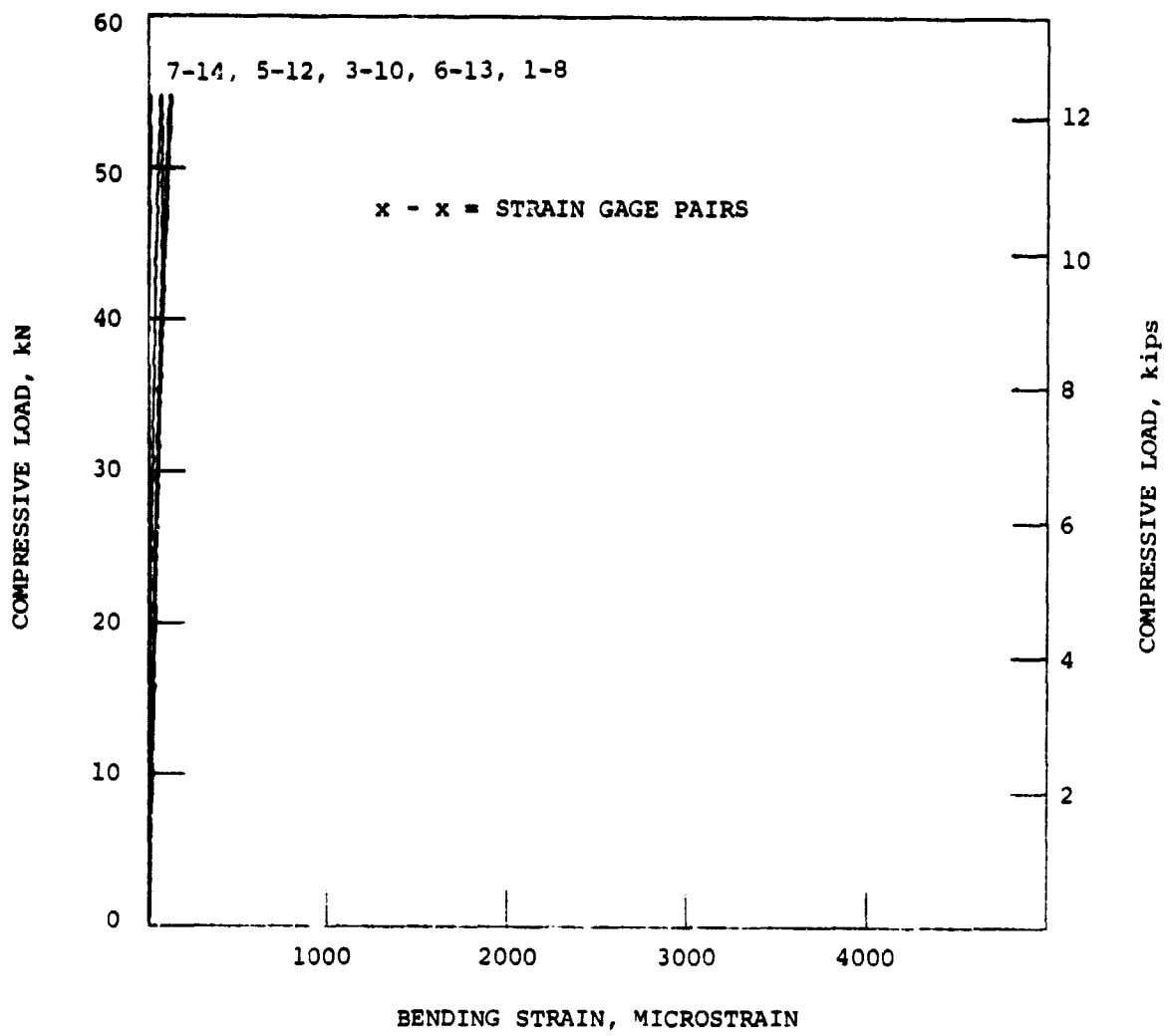Figure 62. Load-bending strain characteristics, panel with supported edges.

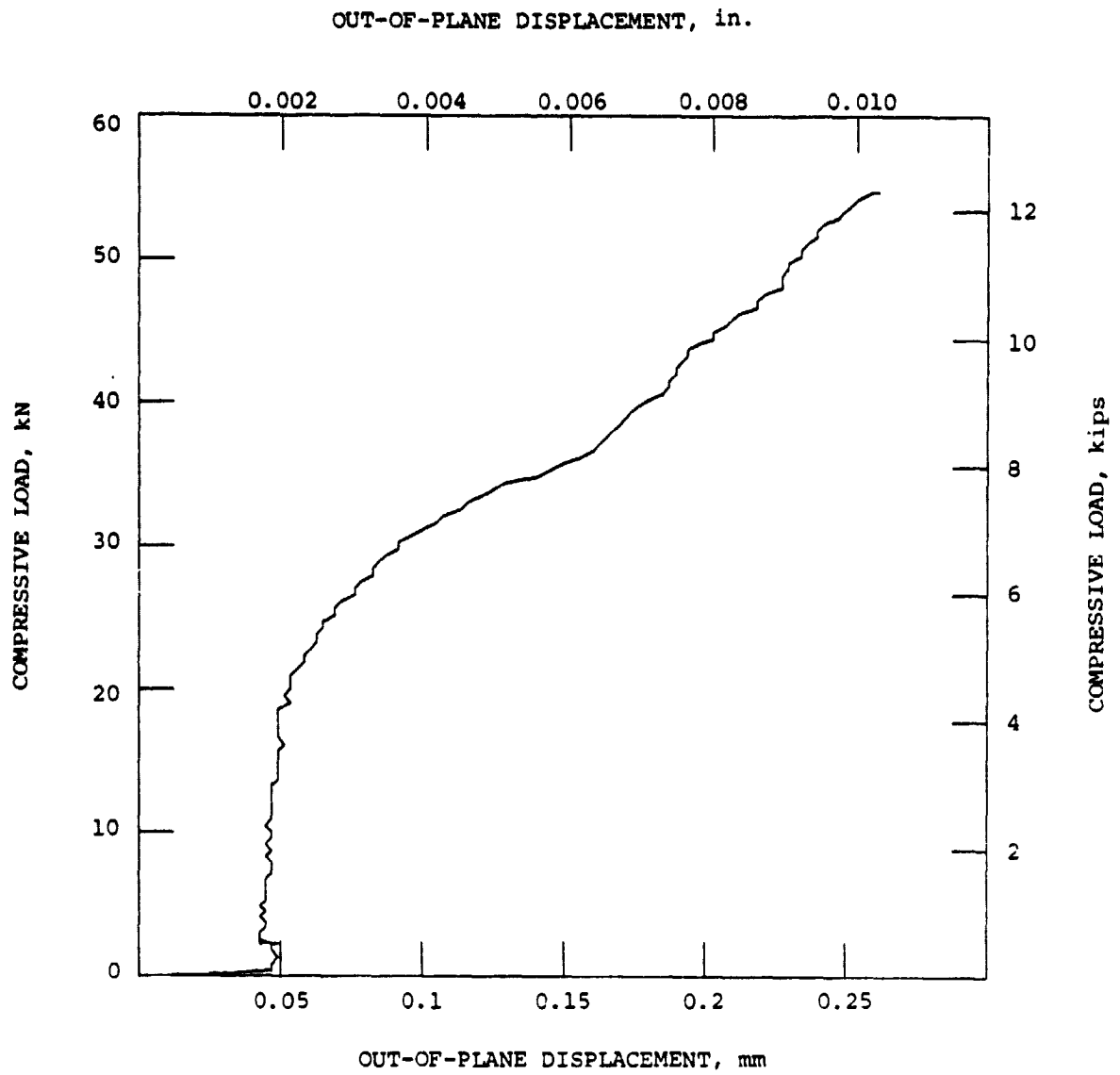OUT-OF-PLANE DISPLACEMENT, in.

Figure 63.   Load-out-of-plane displacement characteristics, panel with supported edges.
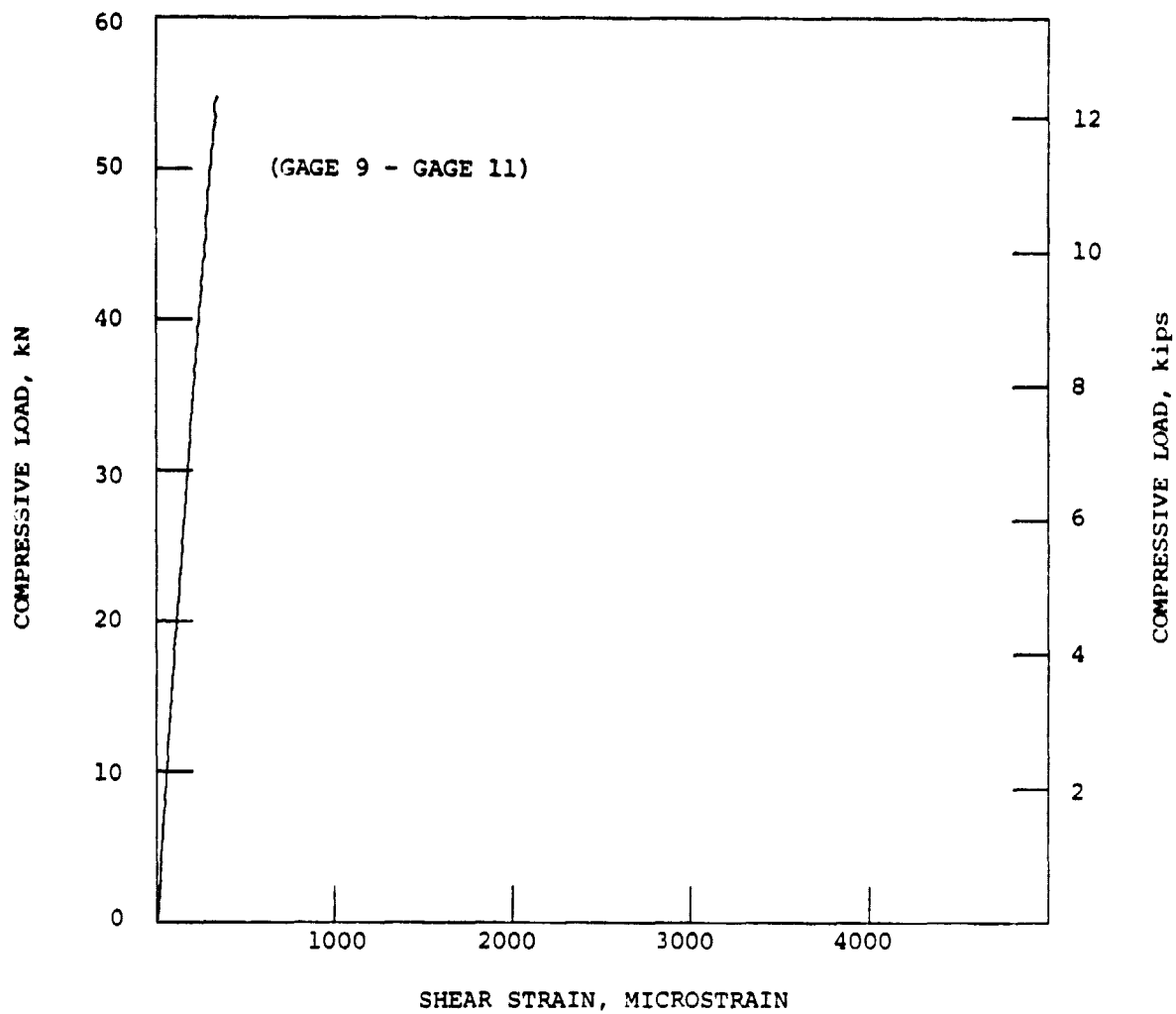
Figure 64.   Load-in-plane shear strain characteristics,
panel with supported edges.